Deliverable D2.3
Components of a new air interface - building blocks and performance

Project Number:	ICT-317669
Project Name:	Mobile and wireless communications Enablers for the Twenty-twenty Information Society

Document Number:	ICT-317669-METIS/D2.3
Document Title:	Components of a new air interface - building blocks and performance
Editor(s):	Frank Schaich (Alcatel-Lucent Bell Labs)
Author(s):	Petar Popovski, Cedomir Stefanovic, Hiroyuki Yomo, Nuno Pratas (Aalborg University), Frank Schaich, André Santos, Volker Braun, Mattia Bonomo (intern) (Alcatel-Lucent Bell Labs), David Gozalvez-Serrano (BMW Forschung und Technik GmbH), Erik Ström, Tommy Svensson, Wanlu Sun (Chalmers University of Technology), Mikael Sternad (Chalmers University of Technology/Uppsala University), Petra Weitkemper, Anass Benjebbour, Yuuya Saito, Yoshihisa Kishiyama, Marwa El Hefnawy (DOCOMO), Ning He (Ericsson AB), Hao Lin, Isabelle Siaud, Pierre Siohan (France Telecom – Orange), Malte Schellmann, Zhao Zhao, Martin Schubert (Huawei ERC), Eeva Lähetkangas, Jaakko Vihriälä, Kari Pajukoski (Nokia Solutions and Networks), Gerd Ascheid, Stefan Heinen, Arun Ashok, Aamir Ishaque, Volker Luecken (RWTH Aachen University), Armin Dekorsy, Carsten Bockelmann (University of Bremen), Fabian Quint, Raja Sattiraju (University of Kaiserslautern), Nandana Rajatheva, Pekka Pirinen, M. Fatih Bayramoglu (University of Oulu), Amer Baghdadi, Frederic Guilloud, Charbel Abdel Nour (Institut Mines-Télécom - Télécom Bretagne)
Dissemination Level:	PU
Contractual Date of Delivery:	30/04/2014
Status:	final
Version:	1
File Name:	METIS_D2.3_v1.docx

Abstract:

This document provides intermediate results of the concepts being developed in the radio link research of METIS. For each of the technology components (TeC) within the technology component clusters (TeCC), covering flexible air interface, new waveforms, modulation and coding techniques as well as multiple access, medium access control and enablers for radio resource management, key findings and conclusions collected so far are summarized in section 2. Continuative descriptions and research outcomes are given in the annex and referred publications.

The results presented here will be extended in the further progress of the project, and they will be used in the next phase of the project to develop and refine the overall METIS system concept instantiated by the horizontal topics. The suitability of the single technology components for the overall system design being able to meet the wide range of requirements for 5G will then be evaluated.

Keywords:

air interface, availability, dense deployment, coding, cost, coverage, energy efficiency, fading, faster than Nyquist, filter-bank multicarrier, flexibility, full-duplex, latency, link adaptation, machine-to-machine, medium access control, mobility, modulation, multiple access, non-orthogonal multiple access, orthogonal frequency division multiple access, overhead, power-domain multiplexing, radio resource management, reliability, research topic, signaling, spectrum efficiency, waveform

Executive summary

This document provides a detailed overview of the research results related to the Radio Link concepts being developed in METIS. In the deliverables prepared so far in the scope of METIS radio link research, the research activities of the partners have been grouped in so-called Research Topics (RTs). To align the naming within the whole project, the terminologies 'Technical Component (TeC)' and 'Technical Component Cluster (TeCC)' have been introduced with this deliverable. Starting within this deliverable, the term TeCC completely substitutes the former term RT in the METIS radio link research. More details about the TeCC structuring are given in the introduction.

Former deliverables covered the problem (D2.1, [MET13-D21]) and the solution (D2.2, [MET13-D22) space of the METIS radio link research based on a requirement analysis of the test cases identified at the beginning of the METIS project in D1.1 [MET13-D11]. This document provides first outcomes of the research activities being proposed in D2.2 [MET13-D22] to solve the problems and issues gathered in D2.1 [MET13-D21].

The main body of this document summarizes the key messages for each technology component investigated. Reading section 2 allows the reader to get a first tangible valuation of the basic characteristics of the technology components as well as their fundamental performance measures. Based on that, a first assessment of the added value the technology components can provide to an overall system concept can be enabled.

The focus areas are:

1. Flexible air interface
2. Waveforms, coding & modulation and transceiver design
3. Multiple access, MAC and RRM

For readers being interested in further details, the annex and related publications provide additional information on the solutions as well as additional evaluation results.

Working towards the next deliverable D2.4, radio link research will continue on the performance evaluation of the single TeCs, refining the proposed concepts and evaluating more clearly the different proposals in the light of an overall system concept to be presented in D6.6 at the end of the project. The most promising schemes will – in conjunction with existing radio access technologies and with schemes from other METIS work packages – be chosen as the METIS recommendation for the 5G air interface, suited to address the broad range of requirements the future communication landscape is requesting.

Contents

List of Figures

List of Tables

List of Abbreviations, Acronyms, and Definitions

2G	2nd Generation
3G	3rd Generation
3GPP	Third Generation Partnership Project
4G	4th Generation
AC	Access Class
ACK	Acknowledgement
AD	Analog to Digital
AMC	Adaptive Modulation and Coding
AP	Access Point
ARQ	Automatic Repeat reQuest
AV	Availability
AWGN	Additive White Gaussian Noise
B4G	Beyond 4G
BB	Baseband
BER	Bit Error Rate
BH	Backhaul
BLER	Block Error Rate
BLT	Balian-Low theorem
BOM	Bill-of-Materials
BPSK	Binary Phase Shift Keying
BR	Bandwidth Request
BS	Base Station
BW	Bandwidth
C2R	Complex to Real
CA	Collision Avoidance
CAPEX	Capital Expenditure
CCRS	Coordinated and Cooperative Relay Systems
CDF	Cumulative Distribution Function
CDMA	Code Division Multiple Access
CFO	Carrier Frequency Offset
CFR	Carrier Frequency Range
C-ITS	Cooperative Intelligent Transport Systems
COV	Coverage
C-plane	Control plane
CP	Cyclic Prefix
CP-OFDM	Cyclic-Prefix Orthogonal Frequency Division Multiplexing
CQI	Channel Quality Indicator
CPM	Constant Phase Modulation
CR	Cognitive Radio
CRAD	Cell Radius
CRC	Cyclic Redundancy Check
CRS	Common Reference Signal
CS	Compressive Sensing
CSI	Channel State Information
CSMA	Carrier Sense Multiple Access
C-TP	Cell Throughput

C-UE	Cellular UE
CW	Contention Window
D2D	Device-to-Device
DA	Digital to Analog
DCC	De-centralized Control Congestion
DCF	Distributed Coordinated Function
DeNB	Donor eNB
DFT	Discrete Fourier Transform
DI	Diffuse Scatterer
DIFS	Distributed Coordination Function Inter-Frame Spacing
DL	Downlink
DMRS	Demodulation Reference Signal
DRX	Discontinuous Reception
DS	Distribution System
DTX	Discontinuous Transmission
DVB	Digital Video Broadcast
DwPTS	DL Pilot Time Slot
ECON-AU	Energy consumption per area unit
ECON-B	Energy consumption per bit
EDCA	Enhanced Distributed Channel Access
EDGE	Enhanced Data Rates for GSM Evolution
EE	Energy Efficiency
eIMTA	enhanced Interference Management and Traffic Adaptation
eNB	Enhanced node B
EPDCCH	Enhanced PDCCH
ESS	Extended Service Set
ETSI	European Telecommunications Standards Institute
FAI	Flexible Air Interface
FAIR	Fairness
FBMC	Filter-Bank Multi-Carrier
FD	Full Duplex
FDR	Full Duplex Radio
FDD	Frequency Division Duplex
FDMA	Frequency Division Multiple Access
FEC	Forward Error Correction
FeICIC	Further enhancement of inter-cell interference coordination
FER	Frame Error Rate
FFT	Fast Fourier Transform
FIR	Finite Impulse Response
FMT	Filtered Multi-Tone
FSPA	Full Search Power Allocation

FTN	Faster Than Nyquist
FTPA	Fractional TPA
GBR	Guaranteed Bit Rate
GFDM	Generalized Frequency Division Multiple Access
GGMA	GR/GRM Mapping Approach
GI	Guard Interval
GLB	Green Link Budget
GOMP	Group Orthogonal Matching Pursuit
GP	Guard Period
GPRS	General Packet Radio Service
GPS	Global Positioning Service
GR	General Requirement
GRM	General Requirement Metric
GRT	General Requirement Tag
GSM	Global System for Mobile Communications
HARQ	Hybrid ARQ
HETNET	Heterogeneous Networks
HPA	High Power Amplifier
HSD	Hybrid Sparse/Diffuse
HSDPA	High Speed Downlink Packet Access
HSPA	High Speed Packet Access
HT	Horizontal Topic
HW	Hardware
ICI	Inter Carrier Interference
ID	Identifier
IEEE	Institute of Electrical and Electronics Engineers
IF	Intermediate Frequency
IFDMA	Interleaved FDMA
IFFT	Inverse Fast Fourier Transform
IM	Intermodulation
INTG	Integrity
IOTA	Isotropic Orthogonal Transform Algorithm
IP	Internet Protocol
IR	Incremental Redundancy
IRC	Interference Rejection Combining
IS	Interference Suppression
ISI	Inter Symbol Interference
ITS	Intelligent Transport Systems
KPI	Key Performance Indicator
L1	Layer 1
LA	Local Area
LAN	Local Area Network
LAT	Latency
LDPC	Low Density Parity Check
LDS	Low Density Signature
LFDMA	Localized FDMA
LLC	Logical Link Control

LNA	Low Noise Amplifier
LOLA	Low-Latency
LOS	Line of Sight
LSD	List Sphere Decoding
LSE	Link Spectral Efficiency
LTE	Long Term Evolution
LTE-A	LTE Advanced
M2M	Machine to Machine
MA	Multiple Access
MAC	Medium Access Control
MAI	Multiple Access Interference
MAP	Maximum A-Posteriori
MAX	Maximum
MBSFN	Multicast Broadcast Single Frequency Network
MC	Multi Carrier
MCM	MultiCarrier Modulations
MCS	Modulation Coding Scheme
MD	Moving Discrete Scatterer
MDFT	Modified Discrete Fourier Transform
MIM	Multiple Interface Management
MIMO	Multiple Input Multiple Output
MLD	Maximum Likelihood Detection
MMC	Massive Machine Communication
MMSE	Minimum Mean Square Error
mmW	Millimeter Wave
MN	Moving Networks
MPA	Message Passing Algorithm
MRE	Multi-rate equalizer
MSE	Mean-Square Error
MTC	Machine Type Communication
MTD	Machine Type Device
MTU	Maximum Transmission Unit
MU	Multi User
MUD	Multi User Detection
MU-MIMO	Multi User MIMO
MUPA	Multi User Power Allocation
NACK	Negative ACK
NLOS	Non Line of Sight
NOMA	Non-Orthogonal Multiple Access
NW	Network
OFDM	Orthogonal Frequency Division Multiplexing
OFDMA	Orthogonal Frequency Division Multiple Access
OFDP	Optimal Finite Duration Pulse
OMA	Orthogonal Multiple Access
OPEX	Operational expenditure
OQAM	Offset QAM

PAL	Protocol Adaptation Layers
PAM	Pulse Amplitude Modulation
PAPR	Peak-to-Average Power Ratio
PAR	Project Authorization Request
PBCH	Physical Broadcast CHannel
PDCCH	Physical Downlink Control Channel
PDCP	Packet Data Convergence Protocol
PER	Packet Error Rate
PHY	Physical
PMI	Precoder Matrix Indicator
PMP	Point to Multipoint
PRB	Physical Resource Block
ProSe	Proximity Service
PSS	Primary Synchronization Signal
PUCCH	Physical Uplink Control Channel
PUSCH	Physical Uplink Shared Channel
QAM	Quadrature Amplitude Modulation
QoE	Quality of Experience
QoS	Quality of Service
QPSK	Quadrature Phase Shift Keying
RA	Random Access
RAN	Radio Access Network
RAST	Random Access Schemes Throughput
RAT	Radio Access Technology
REL	Reliability
RF	Radio Frequency
RLC	Radio Link Control
RMS	Root Mean Square
RN	Relay Node
RRC	Root Raised Cosine
RRH	Remote Radio Head
RRM	Radio Resource Management
RS	Reference Signal
RT	Research Topic
RTG	RX/TX Transition Gap
RTT	Round Trip Time
Rx	Receiver
SA2	System Aspect, Work Group 2: 3GPP Architecture
SAW	Surface Acoustic Wave
SBW	Supported Bandwidth
SC	Subcarrier
SCMA	Sparse Code Multiple Access
SD	Static Discrete Scatterer
SDM	Spatial Division Multiplex
SE	Spectral Efficiency

SFO	Sampling Frequency Offset
SG	Scheduling Grant
SI	Study Item
SIC	Successive Interference Cancellation
SIFS	Short Interframe Spacing
SINR	Signal to Interference plus Noise Ratio
SISO	Single-Input Single Output
SLNR	Signal-to-Leakage and Noise Ratio
SMT	Staggered Multi-Tone
SNR	Signal to Noise Ratio
SotA	State of the Art
SR	Scheduling Request
SRS	Sounding Reference Signal
SSID	Service Set Identifier
SSS	Secondary Synchronization Signal
STA	Station
STBC	Space Time Block Code
STDMA	Self-organizing Time Division Multiple Access
SU	Single User
TA	Timing Advance
TC	Test Case
TCCA	TETRA + Critical Communications Association
TCP	Transmission Control Protocol
TDD	Time Division Duplex
TDM	Time Division Multiplexing
TDMA	Time Division Multiple Access
TETRA	Terrestrial Trunked Radio
TFL	Time Frequency Localization
TGad	Task Group ad (IEEE802.11ad)
TM	Transmission Mode
TP	Throughput
TPA	Transmit Power Allocation
TPC	Transmission Power Control
TTG	Tx/Rx Transition Gap
TTI	Transmission Time Interval
Tx	Transmitter
UDN	Ultra Dense Network
UE	User Equipment
UFMC	Universal Filtered MultiCarrier
UF-OFDM	Universal Filtered OFDM
UHF	Ultra High Frequency
UL	Uplink
UMTS	Universal Mobile Telecommunications System
U-plane	User plane
URC	Ultra Reliable Communications
V2D	Vehicle-to-Device

V2I	Vehicle-to-Infrastructure
V2V	Vehicle-to-Vehicle
V2X	Vehicle-to-X
VANET	Vehicular Ad Hoc Network
VHT	Very High Throughput
VoIP	Voice over IP
WA	Wide Area
WAVE	Wireless Access in Vehicular Environments
W-CDMA	Wideband CDMA
WI	Work Item
WiGig	Wireless Gigabit Alliance
WiMAX	Worldwide Interoperability for Microwave Access
WLAN	Wireless Local Area Network
WP	Work Package
WPAN	Wireless Personal Area Network
WSS-US	Wide-Sense Stationary Uncorrelated Scattering
XOR	Exclusive OR
ZF	Zero Forcing

1 Introduction

This document presents a first set of components for the 5G air interface together with corresponding performance evaluation results. It thus provides a first sketch of the potential building blocks for 5G air interface and allows for a first assessment of the achievable gains compared to current state of the art towards the METIS overall goals.

In deliverable D2.1, the radio link research has been structured into 14 research topics (RT). In this deliverable, this structure is refined further by introducing so called Technology Component Clusters (TeCCs). These TeCCs group technology components with similar research context and objectives and thus allow for a more detailed overview on the particular tracks of the METIS radio link research. To ensure consistency with the RT numbering in deliverables D2.1 and D2.2, the TeCCs are numbered using a two-level format, where the number on the first level represents the RT number, and the number on the second level specifies the cluster defined inside this RT (if applicable). Note that there are some RTs where no clusters have been defined; these are then lacking the second level number. Moreover, some of the original titles of the RTs have slightly been modified to make them more self-explanatory and illustrative. In this deliverable, the term TeCC completely substitutes the term RT introduced in D2.1. In the following, we will briefly describe the TeCCs defined for the radio link research, which are then studied in detail in the section 2, the main part of this document.

In deliverable D2.1 [MET13-D21], the problem space for the METIS radio link research has been defined, which covered the identification of the research challenges from the radio link perspective and an analysis how these are addressed by the different research topics. Deliverable D2.2 [MET13-D22] then described the solution space, elaborating more on the particular solutions studied and identifying clearly how these can serve as enablers for the METIS Horizontal Topics (HTs). As a compact summary of the output from both these preceding deliverables, we will illustrate here how the different TeCCs studied in the three tasks illuminate the problem space of the METIS radio link research, which is spanned by two dimensions: The METIS Horizontal Topics (x-axis of Figure 1-1) and the main challenges from the radio link perspective (y-axis). These main challenges are briefly described as follows:

- Machine type vs. human centric communication, exhibiting totally different traffic characteristics
- New device classes and service types, posing highly diverse requirements on the system
- High mobility support, which is particularly relevant in the context of V2x communication
- Provision of real-time services characterized by quick response times (i.e. very low latencies) and high reliability; enabling industrial control and traffic safety
- Spectrum sharing with other radio services, which implies efficient access to fragmented spectrum. This challenge also covers operation in different frequency spectra from low to very high frequencies up to and beyond 60 GHz.

Task T2.1: Flexible air interface design

The TeCCs in task T2.1 are aiming at a comprehensive air interface design for particular use cases. Hence, in Figure 1-1, most of these TeCCs have a clearly vertical or horizontal shape.

TeCC#1 Unified air interface design for dense deployments

Given that a broad range of frequencies may be used in UDN targeting extreme mobile broadband service in the order of multiple gigabit per second end-user bit rate with ultra-dense deployment, a scalable frame structure allows adapting framing times and symbol durations, which facilitates a common baseband design meeting low cost constraints.

TeCC#2 Optimized signalling for low-cost MMC devices

Optimized signalling structures are developed meeting the main requirements of machine type communications, i.e., low cost andlow power, and targeting rather small data packets.

TeCC#3 Air interface supporting dynamic spectrum usage

To enable efficient spectrum sharing and dynamic spectrum use, a radio frequency (RF) architecture is developed for frequency-agile front-ends.

TeCC#4 Multiple air interface management

A set of different configurations for different modes of operation is provided, allowing the air interface to be individually configured according to actual system conditions and service requests.

TeCC#5 Advanced signalling concepts

Signalling aspects for novel multiple access schemes (like non- and quasi-orthogonal multiple access investigated in TeCC#11.1) and new waveforms.

TeCC#6 Air interface for moving networks

Air interface design takes into account the requirements for vehicular based (V2x) communications, including road safety applications, meeting strict reliability constraints.

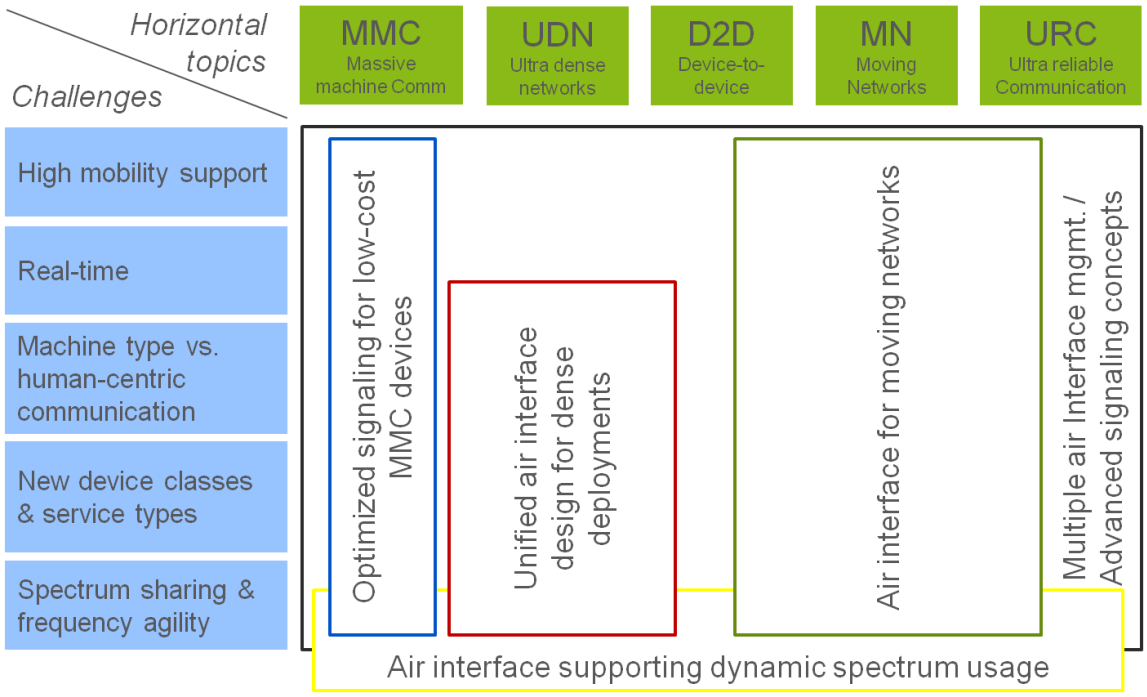

Figure 1-1: TeCCs in task T2.1 - Flexible air interface design

Task T2.2: Waveforms, coding & modulation and transceiver design

Challenges and HTs addressed by the TeCCs in T2.2 are illustrated in Figure 1-2.

TeCC#7 Faster than Nyquist (FTN)

FTN enables to boost the data rate by transmitting symbols faster than the Nyquist rate.

TeCC#8 Filtered and filterbank based multi-carrier

The use of filters with good energy localization in frequency domain enables partitioning the spectrum into independent bands that can be independently configured and support relaxed synchronization requirements. Thus, these waveforms are promising enablers for efficient spectrum sharing, in particular for the access to fragmented bands.

TeCC#8.1: FBMC based waveform & transceiver design

TeCC#8.2: Universal filtered multi-carrier (UFMC)

TeCC#9 Modulation & coding and new channel coding concept

TeCC#9.1: Constrained Envelope Coded Modulation is an energy efficient transmission scheme providing high robustness to non-linear power amplifiers, which renders it favourable for the application in low-cost transceivers.

TeCC#9.2: Advanced coding and decoding schemes aim to improve the coding delay and to enable a faster link adaptation.

TeCC#10 Advanced transceiver design

TeCC#10.1: Full duplex communications are investigated, where a node can transmit and receive in the same band simultaneously.

TeCC#10.2: Multi-rate equalizer for single carrier communications enables achieving the throughput of the trellis based equalizer with complexity of linear equalizers. Single carrier communications is gaining new interest for facilitating low cost transceiver solutions.

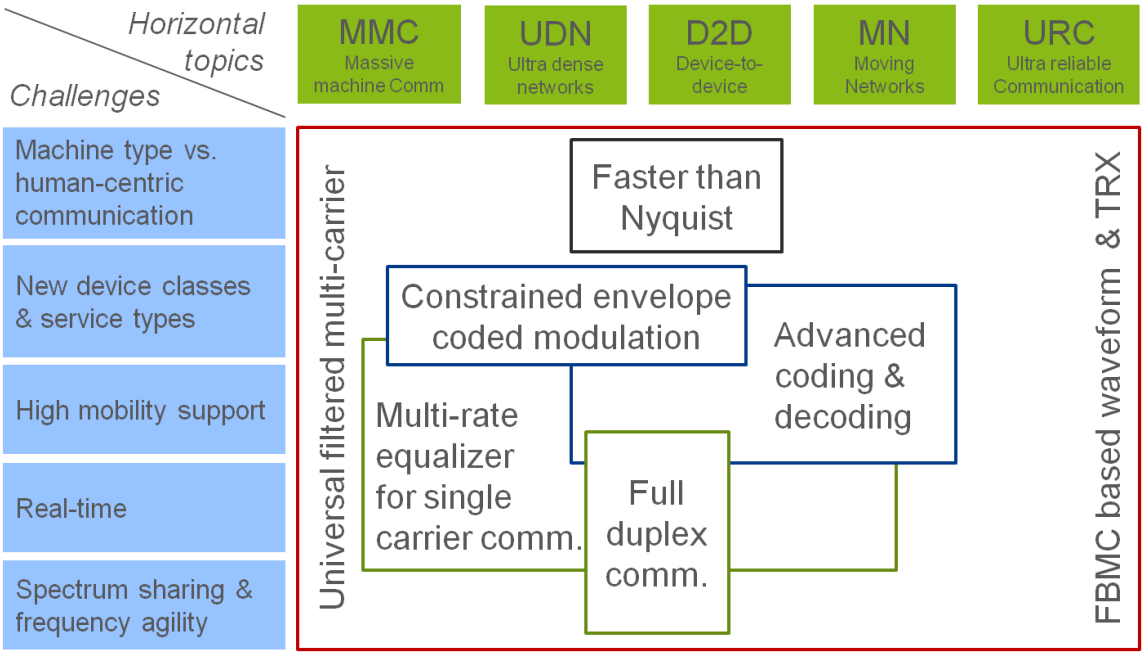

Figure 1-2: TeCCs in Task T2.2 - Waveforms, coding & modulation and transceiver design

Task T2.3: Multiple Access, MAC & RRM

Challenges and HTs addressed by the TeCCs in T2.3 are illustrated in Figure 1-3.

TeCC#11 Multiple Access (MA)

TeCC#11.1: Non- and quasi-orthogonal MA schemes relax the constraint of the number of users to be served simultaneously being limited to the set of orthogonal resources. Thus enable spectrum overloading with smooth performance degradation.

TeCC#11.2: FBMC based MA and Cognitive Radio focus on novel schemes for MA in spectrum sharing environments. An architecture based on the frequency-agile frontends from TeCC#3 is studied for adaptive reconfigurability under TDD / FDD modes.

TeCC#12 Medium Access Control (MAC)

TeCC#12.1: *Contention based massive access* proposes MAC approaches for contention or reservation based access of a large number of devices with low overhead.

TeCC#12.2: *Distributed network synchronization* addresses synchronization of a large number of nodes when reference clocks are available or are absent.

TeCC#12.3: *MAC for UDN and mmW* investigates the benefits of a hybrid MAC approach that leverages the advantages of scheduled and contention based protocols.

TeCC#13 Hybrid automatic repeat request (HARQ)

Research on deadline-driven HARQ processes and on enablers for reliability-based HARQ is carried out, aiming at reducing the end-to-end (E2E) latency as well as improving the spectral and energy efficiency.

TeCC#14 Radio link enablers for radio resource management (RRM)

Radio link enablers for RRM take into account the impact of the large diversity of new device classes, QoS requirements and traffic characteristics.

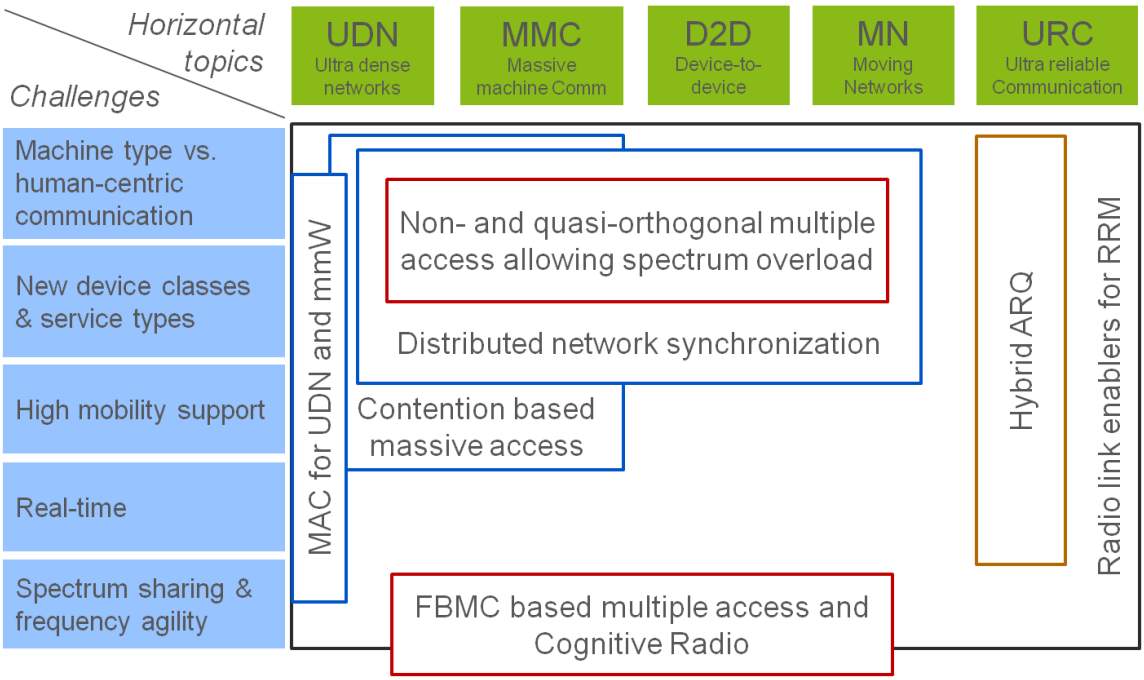

Figure 1-3: Task T2.3 - Multiple Access, MAC & RRM

Each of the TeCC comprises one or several Technology Components (TeCs), which represent a particular solution for a given problem. All TeCs presented in this document are summarized in the Table 1-1. TeCs have been numbered using a format that reflects the TeCC they belong to. For each of the TeCs, the addressed scenarios and test cases as defined in deliverable D1.1 [MET13-D11] are briefly listed, and the expected gains towards the METIS overall goals are qualitatively assessed. Quantitative gains were given where already available. Note that many TeCs in the radio link research will provide enablers for a more efficient use of system resources, and their true potential may be unleashed in the interplay with other higher layer solutions when being evaluated on system-level. Expected quantitative gains obtained solely

from evaluations on radio link level, however, may still be far away from the ambitious METIS overall goals and may thus sound not too impressive at first glance.

Table 1-1: List of Technology Components investigated in the document

No.	TeC	Scenario(s) covered	Expected gains
1.1	UDN TDD frame numerology	Virtual reality office Dense urban information society Massive machine access	>50x discovery capacity 10-100x higher typical user data rate 7-40x longer battery life Reduced E2E latency due to shorter TTIs
1.2	METIS UDN optimized frame structure		
1.3	Flexible TTI for efficient energy saving and high-speed transfer		
2.1	MMC type D2D links	Massive machine access	Higher number of connected devices Longer battery life
3.1	RF architecture for dynamic spectrum access	Blind spots Emergency comm.	Reduced infrastructure cost
4.1	Multi-RAT PHY layer design & multi-band processing	Service in a crowd Traffic efficiency and safety	Higher data volume and user data rate Increased energy efficiency
4.2	Software configurable air interface	Service in a crowd Massive machine access	Improved efficiency of system and energy
5.1	Signaling for non-orthog. multiple access	See NOMA (11.1.1)	See NOMA (11.1.1)
6.1	Framework for URC	Traffic efficiency and safety	Reduced E2E latency
6.2	URC Framework for modeling and predicting the reliability of a link		
6.3	Channel estimation for V2V links	Traffic efficiency and safety	Higher typical user data rate
6.4	Channel prediction for the backhaul link	Real-time remote computing Traffic eff. and safety	Higher data volume and user data rate
7	Faster than Nyquist	Virtual reality office Dense urban inf. soc.	Higher user data rate
8.1	FBMC based waveform & transceiver design	Service in a crowd Massive machine access Traffic efficiency and safety	Higher number of connected devices Higher user data rate Relaxed sync. requirem. support longer battery life and reduced E2E latency
8.2	Universal filtered multi-carrier (UFMC)		
9.1	Constrained envelope coded modulation	Massive machine access	Longer battery life
9.2.1	Adaptive complexity flexible baseband	Blind spots Real time remote computing	Higher user data rate
9.2.2	Practical lattice codes		Higher user data rate Reduced E2E latency

10.1	Full duplex TRX	Service in a crowd	Higher user data rate
10.2	Multi-rate equalizers for single-carrier comm.	Blind spots Massive machine access	Longer battery life
11.1.1	Non-orthogonal multiple access (NOMA)	Service in a crowd Traffic efficiency and safety	~30% higher system throughput vs. LTE-A Up to 2x higher number of connected devices Better mobility support
11.1.3	UL SCMA random access	Massive machine access	Higher number of connected devices Longer battery life Reduced E2E latency
11.2.1	Precoding & RX processing for MA MIMO FBMC	Service in a crowd	Higher data volume and user data rate Increased number of connected devices
11.2.2	MA using cognitive radio	Blind spots Emergency comm.	Reduced infrastructure cost
12.1.1	Coded random access	Massive machine access Teleprotection in smart grid network	Higher number of connected devices Longer battery life
12.1.2	Coded access reservation		
12.1.3	Advanced PHY processing for enh. MAC		
12.2	Distributed network sync	Networks out of coverage of BS	Higher number of connected devices
12.3	MAC for UDN and mmW	Service in a crowd Virtual reality office	Higher data volume and user data rate Higher number of connected devices
13.1	Incremental Redundancy with backtrack retransmission	Virtual reality office Dense urban information society Service in a crowd	Higher user data rate Reduced E2E latency
13.2	Multi-level ACK/NACK for reliability based HARQ		
14	Radio link enablers for RRM	Service in a crowd	Higher number of connected devices

Structure of the document

The document is structured as follows: in section 2, the main part of the document, first evaluation results are presented for each of the technology components in the clusters, clearly highlighting the expected gains compared to known solutions from state of the art towards the METIS goals. The single technology components are highlighted by using **bold face underlined headings**. In section 2, emphasis was put on a very compact description; further details on the evaluation of each component can be found in the annex (chapter 5) as well as in external publications referenced in the text. Chapter 3 draws some conclusions and give some hints on future work.

2 Radio Link Technology Components

This section highlights the key outcomes elaborated so far within the radio link research. Relevant building blocks are described and surveyed in the light of their integration into an overall air interface. Degree of detail is restricted to extended abstract level. Detailed performance evaluation results can be found in the annex (chapter 5) and in related publications.

2.1 Unified air interface design for dense deployments

The air interface design for dense deployment is an important part of the METIS ultra-dense networks (UDN) horizontal topic, targeting multi-Gbps end-user data rates with flexibility in design for different user cases and large range of frequency and in deployment, simple and low cost devices, energy efficiency with shorter wireless links and with low power consumption when not active etc. Below is a summary of the concept and main results obtained so far, with focus on frame structure design and multi-antenna aspect. Please see annex 5.1 for some more details. The unified air interface design covers a large operating frequency range from 3 GHz up to mmW bands of 100 GHz, for which MAC layer design is challenging topic, which is addressed in the technical component medium access control. See 2.12.3 for details of the topic.

Flexible OFDM-based waveform

OFDM can easily be manipulated to achieve flexibility for a diversity of use cases without adding significant complexity. E.g. SC-FDM, as well as zero-tail DFT-S-OFDM [BTS+13] can be obtained as a straightforward add-on over basic OFDM. While these methods can fully co-exist with CP-OFDM, they can be utilized to achieve better spectral containment, lower PAPR and to enable link specific CP lengths or flexible guard times that can be used for example for extending the cell/link coverage. With this approach it is also possible to enable link direction (transmission ↔ reception) or antenna switching on OFDM symbol level, enabling extremely high flexibility in terms of link direction even inside a frame. This property could further be utilized for example to generate efficient D2D discovery patterns.

UDN TDD frame numerology:

Preliminary UDN TDD time numerology: The UDN environment properties together with small transmission powers and evolved component technology aspects, such as improved switching time, enable the usage of UDN optimized OFDM and TDD guard times. The following initial rough estimates, including guard times required for radio channel and for hardware and corresponding to ~10-100 m cell radius with ~10-100 ns delay spreads respectively, are given here in order to provide a high level view about the matter [LPB+13][LPT+13]:

- Guard period length: $T_{GP} \approx 0.1 - 0.55\ \mu s < 0.6 \mu s$
- Cyclic prefix length: $T_{CP} \approx 0.1 - 1.0\ \mu s$ (compensates also timing and synchronization errors)

Preliminary UDN frequency numerology: Oscillator's phase noise is critical for OFDM systems, because it destroys the orthogonality of sub-carriers and increases with carrier frequency f_c. Thus, the sub-carrier spacing needs to be increased for higher carrier frequencies. It can be assumed that the amount of available bandwidth will increase when the carrier frequency f_c is increased (we have noticeably more spectrum available at mmW), allowing the FFT block size to be kept roughly constant when f_c is increased.

The digital signal processing (DSP) performance may be assumed to increase according to Moore's law [BC11] within METIS timeframe, enabling more than tenfold increase in the execution speed of fast Fourier transform compared to the current component benchmarking values. This enables still relatively low SC spacing even with large METIS bandwidths.

Harmonized OFDM: The cost and the complexity of the baseband are minimized if the same baseband design is reused for multiple carrier frequencies and bandwidths. The sampling rate should be selected in such a way that the same base clock can be used for different parts of the spectrum. Thus, when increasing f_c (towards mmW), it is proposed simultaneously to increase the used bandwidth and SC spacing, while keeping the FFT size also within a small number of quantized values (and by using clock rate of integer multiples of e.g. the LTE-A base clock = 30.72 Mchips/s). Similar scaling can be done in time domain numerology, meaning that e.g. the delay spread and the related frame numerology may further be variable according to f_c. This concept is referred here as "harmonized OFDM" (see annex 5.1 for more clarification and illustration on high level).

UDN optimized frame structure

The UDN optimized TDD numerology introduced above enables the usage of shorter frame length and a physical frame structure design fully optimized for TDD with fast and fully flexible switching between transmission and reception. A TDD optimized physical frame structure [LPT+13] for a UDN system is given in Figure 2-1. Only one TDD type is presented here, in the other TDD mode the transmission (TX) and reception (RX) phases are in the opposite order. The frame structure consists of a bi-directional (including both RX and TX resources) control part embedded to the beginning of each frame and time-separated from data plane. Control symbols are located before data symbols in order to allow fast and cost efficient pipeline processing in the receiver. In order to achieve low complexity, the data part in one frame (including DMRS) contains only transmitting or receiving possibility for data symbols. More detailed explanation is provided in annex 5.1.

It can be shown that the proposed UDN optimized physical frame structure allows usage of low TTI lengths, such as 0.25 ms when assuming 60 kHz SC spacing, with reasonable overhead and with sufficient resources for control and RS. [LPT+13] The frame length can be even shorter when moving to higher frequencies.

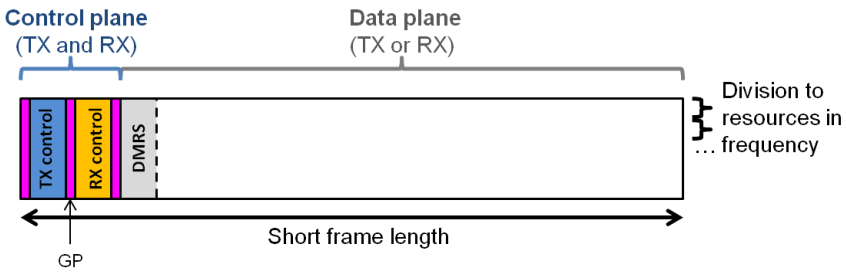

Figure 2-1: A UDN optimized frame structure.

The UDN optimized physical frame structure enables e.g. the following properties:

Flexibility and increased spectral efficiency: Possibility to allocate data part of the frame either for TX or RX enables fully flexible UL/DL ratio switching for data transmission. The decreased guard overheads, such as GP and CP, together with flexibility in UL/DL ratio improve the maximum achievable link spectral efficiency (LSE) per link direction compared to LTE-A.

Fast network synchronization: It is possible to embed a synchronization signal (e.g. by eNB or AP) to the control part of each frame, further enabling really fast network synchronization (to

this DL synchronization signal) by the network devices. This is a useful property when considering also D2D and MMC scenarios.

Reduced control signalling latency: The proposed frame structure allows fast and robust control signalling and handshakes, such as related to UE initiated data transmission.

Clean HARQ structure & reduced latency: The simplified control plane and its presence in each frame enables a clean TDD HARQ scheme with HARQ timing not dependent on the UL/DL ratio. HARQ timing can be fixed and counted in frames, which remarkably reduces TDD HARQ complexity and decreases the related HARQ latency. It can be shown that the total HARQ RTT enabled by the proposed frame structure is ≤~1ms, which is a clear improvement compared e.g. to LTE-A (minimum 8 ms). [LPT+13] A reduced HARQ latency further enables usage of fewer HARQ processes, reducing also memory consumption and device cost since less receiver HARQ buffers are required. Since every frame has control in both directions, control signalling of HARQ can be made independent of the direction of the data part. Asynchronous HARQ is supported. The enabled HARQ arrangement is therefore also well-suited for multi-hop scenarios.

Decreased energy consumption: Utilizing the enabled fast network synchronization and reduced control and data plane latency, it is possible to enable quick transitions between device's sleep and active modes, further reducing total energy consumption. A simplified theoretical analysis about battery life time as a function of transmissions rate with different reception opportunities is shown in Figure 2-2 [LPV+14]. ~7-40 times lower energy consumption can be achieved with the proposed frame structure when compared to MTC (machine type communication) optimized LTE-A [TLS+12].

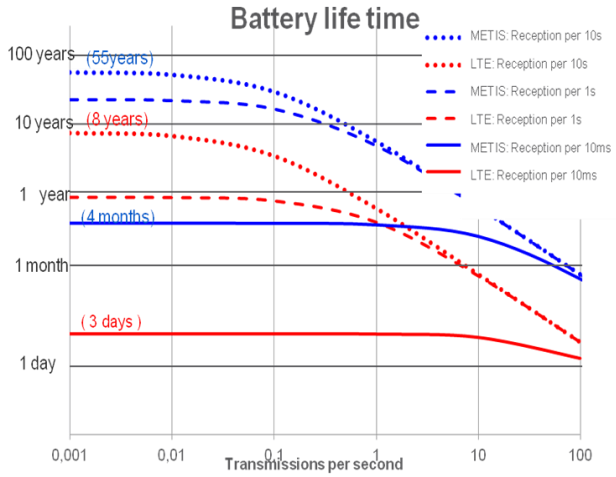

Figure 2-2: Battery life time comparison between LTE and proposed frame structure.

Cross-link interference mitigation: -The frame structure allows (UL/DL) symmetric DMRS design. Since the DMRS symbols between link directions are fully aligned, it is possible to design cross-link orthogonal reference signals. Thus, the proposed frame structure contains inbuilt support for cross-link interference mitigation, further enabling usage of advanced receivers.

Extension to D2D and efficient device discovery: Flexible OFDM-based waveforms, such as zero-tail DFT-S-OFDM, can be applied for D2D communication in order to mitigate asynchronous in-band interference between D2D and cellular communications. By utilizing the flexible OFDM-based waveforms enabling link direction switching on OFDM symbol level together with advanced TX/RX patterns [TRL+13] and with the enabled fast network synchronization time, the frame structure can be extended to support very short discovery

activity time (leading to lower energy consumption) for high number of devices, for which more than 50 times increase can be achieved compared to what is achievable with LTE-A frame structure. This property is essential in e.g. D2D scenarios (and also for MMC).

Flexible TTI for efficient energy saving and extreme high-speed transfer

The physical layer parameters define the granularity of the available resources, which serve as the basis of scheduling transmissions with a minimum unit called atomic scheduling unit. Please note that the numerology below is an example and will be compared to frame structure shown in Figure 2-1 and to be further studied and harmonised in the coming period of the project.

Atomic scheduling unit (ASU): A minimally allocable spectral resource is defined as a "product" of bandwidth and time units. For example for mmW frequency bands, the UDN concept assumes a peak operation bandwidth of 2 GHz. However, the bandwidth unit of 100 MHz is a reasonable scheduling granularity in frequency to support simpler, band-limited devices. In the time domain, 12.5 µs (the length of a subframe) is the candidate choice for the minimum scheduling time unit. Already at a modest spectral efficiency, e.g. 1 bps/Hz, the ASU defined by these bandwidth and time units is a good compromise in transport block size (156 Bytes), so a single ASU can host small IP packets and signalling messages, while only a few concatenated ASUs are needed to carry the typical wireline IP packets.

Flexible vs. fix TTI concept: In the fix Transmit Time Interval (TTI) concept, the UE wakes up at each TTI and checks for scheduled data. The basic idea of Flexible TTI is that the UE listens to scheduling information at tuneable periodicity. Moreover, a scheduling assignment can involve multiple ASUs, which can start later in a frame and even continue in the following frames. Flexibly long scheduling units (group of ASUs) could carry full-size and aggregated IP packets thus avoiding segmentation of packets speeding up MAC and simplifying retransmissions (needed for high TCP throughput). This scheme allows UEs to sleep in subframes between transmissions; hence the scheduled transmissions can virtually go over frame boundaries. Furthermore, sleeping UEs do not need to monitor each paging slot; a wake-up period can be dynamically and individually negotiated for each UE.

Performance evaluation: Our study indicates that transmitting scheduling information in every 10^{th} subframe (i.e. the scheduling period is a frame) is a good compromise between latency and active time of UE needed to monitor scheduling information. Simulations of a heavily loaded system verified the expectation that Flexible TTI introduces an extra delay of half a frame (60 µs in case of 125 µs frame length) compared to sending scheduling information in every subframe. In the same comparison, Flexible TTI requires 20% less resources and 49% less active time from access nodes, while 78% less active time from UEs. This corresponds to energy savings of 40% at identical user activity. See annex 5.1 for more details.

Multi-antenna techniques

For UDNs to be deployed in high frequency bands, where radio wavelengths are substantially smaller than those in conventional cellular networks, a considerable number of antenna elements can be implemented even in nodes with small physical dimensions.

A UDN is expected to primarily rely on beamforming to meet the link budget at high frequencies. Using polarization diversity, two layers can be multiplexed even for LOS links. The minimum assumption for one UE is to receive two spatial layers. Using differently reflected links, higher-layer spatial multiplexing can be implemented. Typical numbers under study are in the order of 64 antenna elements in the access nodes and 16 antenna elements in the UEs per spatial layer, at least for up to two layers.

We assume MIMO with spatial multiplexing or beamforming for the lower frequencies.

2.2 Optimized signalling for low-cost MMC devices

MMC-Type D2D Links:

Wireless cellular networks feature two emerging technological trends: direct Device-to-Device (D2D) communications and Machine-Type Communications (MTC). MTC devices (MTDs) pose new challenges to the cellular network, such as low transmission power and massive access that can lead to overload of the radio interface. In this research track we explore the opportunity opened by D2D links for supporting Low-rate Low-power MTDs that are connected to a nearby device, such as an on-body MTD connected to a mobile phone that acts as a relay towards a Base Station. In Figure 2-3, we depict a simplified version of this scenario, where in the same resource in frequency and time, a MTD M1 transmits to the cellular device U1, while the Base Station B transmits to the cellular user U2. The M1-U1 transmission is interfered by the B's transmission, while the transmission B-U2 is interfered by M1's transmission. A detailed analysis of this scenario is provided in [PP14].

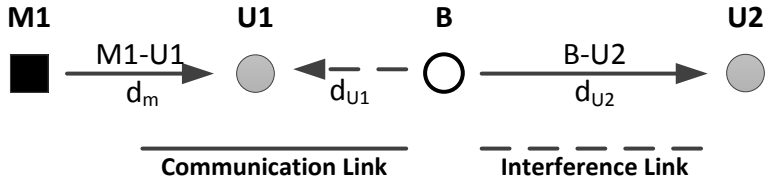

Figure 2-3: Interaction of cellular Infrastructure links and Machine-Type D2D links [PP14].

The low-rate requirement for the MTD-D2D connection allows underlay operation with Successive Interference Cancellation (SIC) during the cellular downlink transmissions. We consider different ways to use SIC and investigate the trade-off between, on one hand, the achieved rate for the downlink cellular users and, on the other hand, the outage probability for the MTC link.

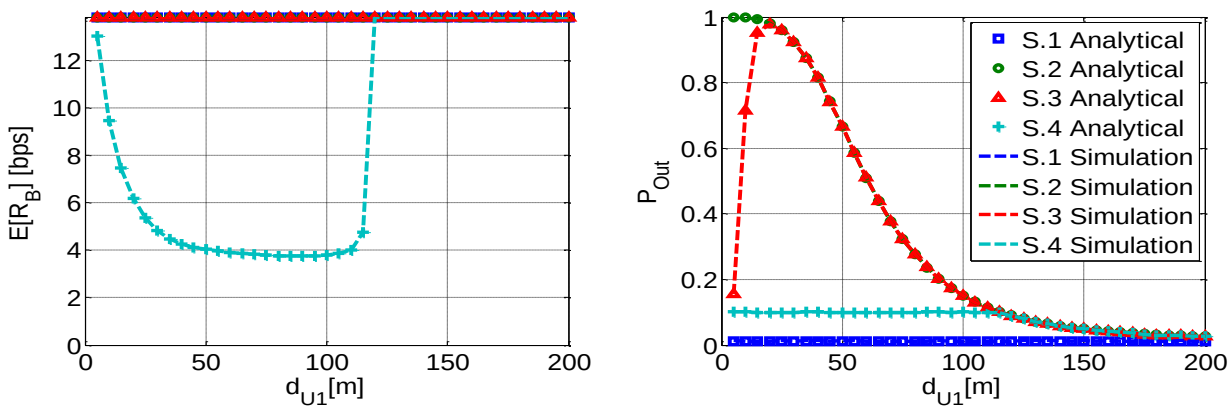

Figure 2-4: Mean Downlink Rate of B-U1, $E[R_B]$, and Outage in MTC-D2D link, P_{Out}, versus distance d_{U1} [PP14].

The model, in [PP14], captures the main performance objectives: outage probability for a given low fixed rate for the Machine-Type communication versus rate maximization for the cellular broadband traffic. System rate maximization is accomplished by the underlay of device-to-device link on the cellular link in the downlink direction.

SIC is an important enabler of underlay D2D communication and it is particularly suitable in conjunction with low-rate MTC signal transmission over the D2D link. In Figure 2-4, is shown the comparison between 4 different resource sharing schemes in the considered setting: (S.1) Perfect SIC; (S.2) No SIC; (S.3) Opportunistic SIC; and finally (S.4) Rate Control and SIC. These results show that indeed low power, fixed rate Machine-Type devices can share the air interface with normal cellular devices, but there can be a rate penalty for the cellular users, as seen in the results of the S.4 scheme. This occurs even when it is assumed that there is no interference from the MTC transmissions to the downlink signals received by the other cellular users and is a result of the rate control for the cellular users in order to meet outage requirements for the MTC users. Further discussion is found in [PP14].

2.3 Radio front end supporting dynamic spectrum usage

For the dynamic spectrum access, conventional zero downconversion architecture is compared against the new High-IF architecture. While the zero downconversion, or homodyne architecture as it is generally called, downconverts the RF into a baseband signal centred around DC, the high-IF system upconverts the same into a higher intermediate frequency thereby providing immunity from the harmonics, image frequencies and the interferes. As mentioned in [MET13-D21] and [MET13-D22], dynamic spectrum access in a cost effective way can be accomplished when the expensive, bulky off-chip components such as SAW filters and duplexers can be eliminated without any RF performance degradation. Any RF performance degradation directly affects the BER. The performance evaluation is performed first by conducting a system study and then proof of concept by a prototype.

System Evaluation of the RF Architecture for Dynamic spectrum Access

An extensive level plan was conducted to compare the RF performances of the two architectures, namely the traditional homodyne receiver and the high-IF architecture. The requirements of a high dynamic range RF front end have been detailed in [HW11]. It is shown that in order to achieve the performance, the wideband filterless RF front end should possess linearity (IIP3) in the order of 26 dBm. Such a high IIP3 is required in order to satisfy the RF performance in the presence of a self-interfering TX Leakage. Level plan was performed for a high dynamic range homodyne transceiver as published in [ASH13]. High performance off-the-shelf components were chosen for the high linearity radio front end. The RF performance of the transceiver is shown below.

Table 2-1 System performance of the homodyne receiver.

Parameters	Achieved in Level Plan
Sensitivity	-103,1 dBm (for 5 MHz)
Noise Figure (NF)	8.8 dB
IIP3	-8.3 dBm
Bandwidth	1.4, 3, 5, 15, 20 MHz
Modulation	QPSK (Pin < -91 dBm), 16 QAM (-91 dBm < Pin < -85 dBm), 64 QAM (Pin > -85 dBm)
Frequency Range	470 MHz – 790 MHz

Even with the high linear components, the wide band homodyne architecture can attain an IIP3 of -8.8 dBm. Further the effect of TX leakage self-interference is also studied in detail. In the absence of SAW filters, it is seen that the self-interference from FDD can result in saturation of its own receiver front end. The requirements of the receiver front end under varying conditions of TX/RX isolation is shown below.

Table 2-2 IIP3 requirements with TX leakage.

Conditions	TX/RX isolation (dB)	TX leakage (dBm)	IIP3 (dBm)
Tx Power = 20 dBm, NF = 8.8 dB, IM3Floor = -99 dBm Blocker = -30 dBm	50	-30	9,5
	40	-20	19,5
	30	-10	29,5
	20	0	39,5
	10	10	49,5

As seen the IIP3 requirements scales inversely with the TX/RX isolation and hence the TX leakage. Since the duplexers and/or SAW filters are intrinsically narrowband, under wideband conditions the isolation has to be provided with separate antennas. Another possible solution is TDD or half-FDD duplexing which avoids the TX leakage at the source.

As opposed to the conventional homodyne architecture, a high-IF architecture is proposed for the wide band radio. In high-IF system, the RF signal is upconverted to a higher intermediate frequency. A narrow band SAW filter (20 MHz) then filters the signal leading to the rejection of all harmonics and interferences leading to better out-of-band IIP3 performance. The RF front end here is wide and the frequency selectivity is provided by the high-IF conversion. The proposed architecture is shown below.

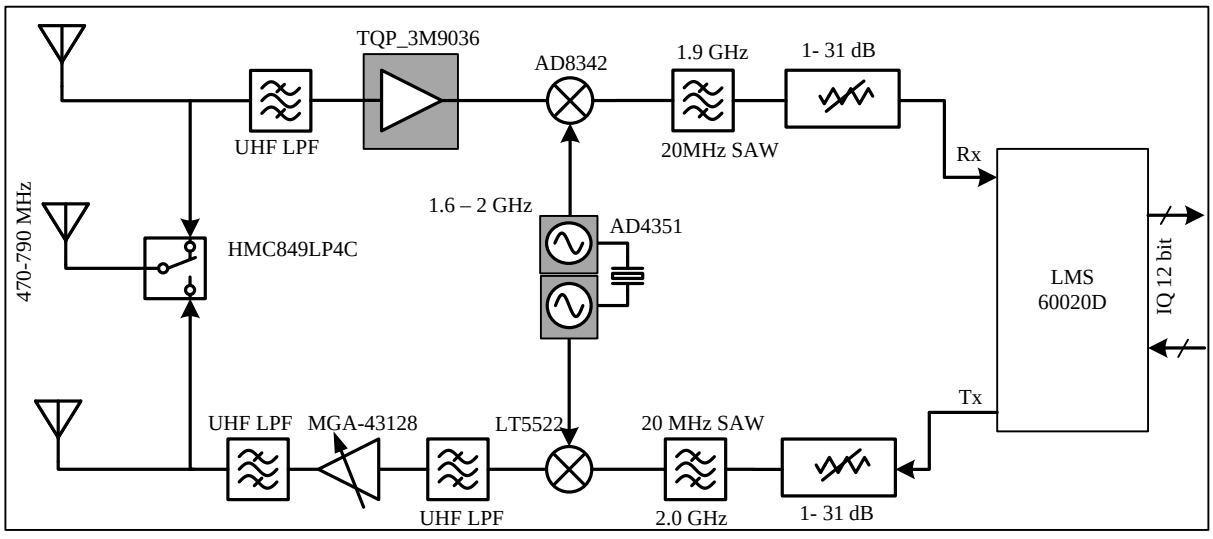

Figure 2-5: Block diagram of High-IF frequency agile RF front end.

Comparison of homodyne and high-IF is shown in the following table. As shown above, the high-IF architecture provides 9 dB improvement on the out-of-band IIP3 and hence an increased dynamic range.

Table 2-3 Comparison of Homodyne and high-IF architecture.

Parameters	Homodyne	High-IF
Sensitivity	-103.6 dBm	-107.3 dBm
NF	8.8 dB	4.5 dB
IIP3(in band)	-8.3 dBm	-7.7 dBm
IIP3 (out-of-band)	-8.3 dBm	0.8 dBm
Dynamic range	95.3 dB	108.1 dB

2.4 Multiple air interface management

This TeCC consists of two topics:

1. Multi-RAT PHY layer design & multi-band processing
2. Software-Defined Air Interface (SoftAI)

Multi-RAT PHY layer design & multi-band processing will be described below. The concept of SoftAI has been sketched in D2.2. It will be further refined when the research in TeCC 8.1 on adaptive FBMC system has matured. Connections exist with other TeCCs affecting TRX configurations, e.g. TeCC 1 (configurations for UDN), TeCC 8 (FBMC configuration modes), and TeCC 11 (different MA modes).

Multi-RAT PHY layer design & multi-band processing

A key 5G technical challenge is to support 1000 times increased capacity while keeping constant energy consumption and infrastructure costs. For that purpose, Flexible Air Interface design, conjunctly exploiting scalable PHY parameters and Multi-Band processing can be beneficial (see section 2.1 and section 5.1) as well as the combination of different air interfaces, where the selection of the air interface is motivated by capacity, QoS and QoE requirements in a proper deployment scenario. Flexible air interface system design is investigated at the PHY layer level where the combination of different RF bands is adjusted with PHY parameters adaptation in order to ensure desired QoS/QoE and to provide scalable radio coverage, compatible with power regulations, propagation constraints and different transmission bandwidths of the FAI system. As an illustration, it may be relevant to double the OFDM sub-carrier spacing to cope with RF phase noise when the RF band is moved from UHF to SHF/EHF bands. Future Wi-Fi hot–spots, able to switch between 5 GHz and 60 GHz, may evolve towards a unified air interface, considering the aggregation of several sub-channels, combined with scalable OFDM parameters' sets, facilitating HW implementation. The IST-FP6 BROADWAY project provides an example of 5 GHz /60 GHz UAI design [BRO02] as well as the multi-RF UWB system "MGWS" recently designed for short range applications [SUM09],[GSG08]. The objective in METIS is to design UAI close to LTE-A and Wi-Fi schemes in order to bring innovative solutions for multi-RAT HETNETs.

"Multiple Interfaces Management" is focused on the combination of and switching between independent air interfaces. It implies to design/define appropriate metrics, function of deployment test case, targeted QoS and radio coverage [UMS12], in order to drive the selection of the most appropriate air interface. The second aspect is to determine the integration methodology of such metrics in multi-RAT architectures.

For that purpose, METIS designed a Green Link Budget (GLB) metric to select the interface and the transmission mode, able to transmit data with a given data rate and QoS, for a

desired radio coverage, while minimizing transmit power required. The appropriate air interface selection process, based on the GLB metric, may exhibit significant gains up to 10 dB. The way to practically evaluate the GLB metric is proposed and integration solutions are currently designed.

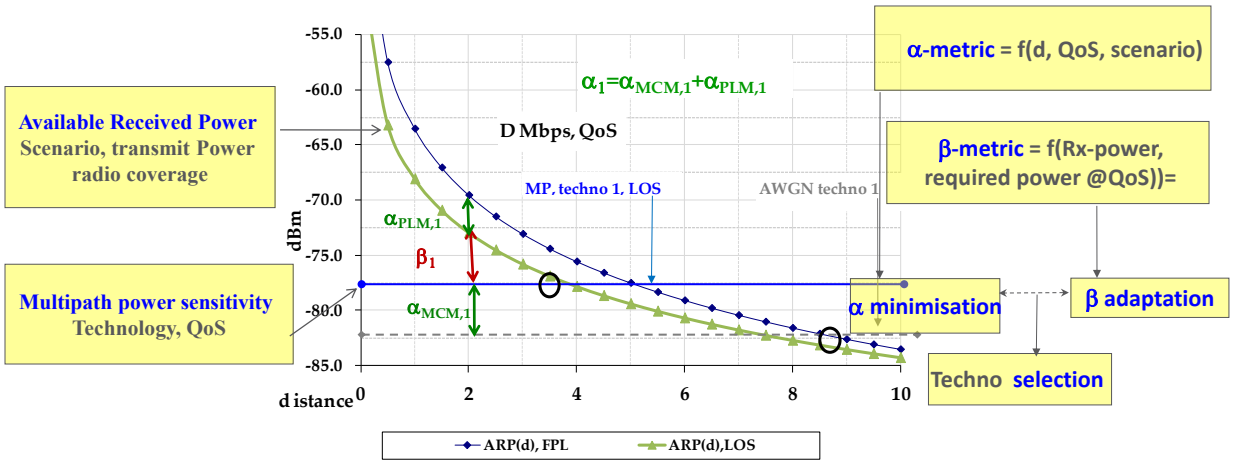

Figure 2-6: The GLB metric description

2.5 Advanced signalling concepts

In [HK12, HK13], a downlink non-orthogonal multiple access is investigated where multiple users are multiplexed in the power-domain, at the transmitter side, and multi-user signal separation is conducted at the receiver side based on successive interference cancellation (SIC).

In [SKB+13, BSK+13], the basic concept and benefits of non-orthogonal multiple access (NOMA) as a candidate for future multiple access schemes are explained and discussed in details. In [SBK+13, BLS+13], initial system-level evaluation results of NOMA were discussed and investigated to demonstrate its potential gains in low and high mobility scenarios assuming with and without SIC error propagation, exhaustive full search on candidate user pairs, and dynamic transmit power allocation such as fractional transmit power allocation (FTPA).

Signalling for non-orthogonal multiple access

Signalling aspects related to multi-user power allocation and MCS selection are also studied for NOMA in order to balance performance gains with signalling overhead. Here, the impact of signalling reduction of full-search power allocation on NOMA performance is investigated.

Full search multi-user power allocation (FSPA)

Exhaustive full search of user pairs and transmit power allocations provide the best performance for NOMA. In the case of full search power allocation, multiple combinations of power allocations are considered for all candidate user sets considered by the scheduler. For FSPA, the number of power sets N to be searched becomes an optimization parameter. With large number of power sets, the performance gains of NOMA increase, while with less number of power sets, we can decrease the amount of downlink signalling. For example, the order of successive interference cancellation (SIC) and information on power assignment do not need to be transmitted in every subframe but rather on a longer time scale.

Main results

Using computer simulations, for a 1x2 SIMO system with BW=10MHz, *K*=10 UEs, maximum multiplexing order *m*=1 or 2 (*m*=1 corresponds to orthogonal multiple access (OMA)), and sub-band user scheduling (with 8 sub-bands), NOMA performance is evaluated assuming no SIC error propagation. As a multi-user power allocation, FSPA is used for the cases of N=50, 5, 3, 2, and 1 power set as follows.

Table 2-4 Power sets

Number of power sets (N)	Candidate power sets: (P1, P2), s.t. P1+P2=P
50	(*n*P, (1-*n*)P), s.t. *n*=0.01:0.01:0.49
5	(0.1P, 0.9P), (0.15P, 0.85P), (0.2P, 0.8P), (0.25P, 0.75P), (0.3P, 0.7P)
3	(0.15P, 0.85P), (0.2P, 0.8P), (0.25P, 0.75P)
2	(0.15P, 0.85P), (0.2P, 0.8P)
1	(0.2P, 0.8P)

According to Figure 2-7a, the cell throughput and cell-edge throughput gains for NOMA over OMA are approximately 33% and 28% for 50 power sets, 30% and 26% for 5 power sets, 28% and 26% for 3 power sets, 27% and 25% for 2 power sets, 26% and 21% for 1 power set, respectively. Thus, even with 1 power set we can maintain 80% of NOMA gains with 50 power sets. The gains in terms of signalling overhead are quite large. Figure 2-7b illustrates the power ratio CDF selected by the scheduler. It is interesting to see that 0.8P (for SIC-order = 1) and 0.2P (for SIC-order =2) are chosen with high probability. This is indeed why we can obtain a large portion of the performance gains of NOMA even with one power set.

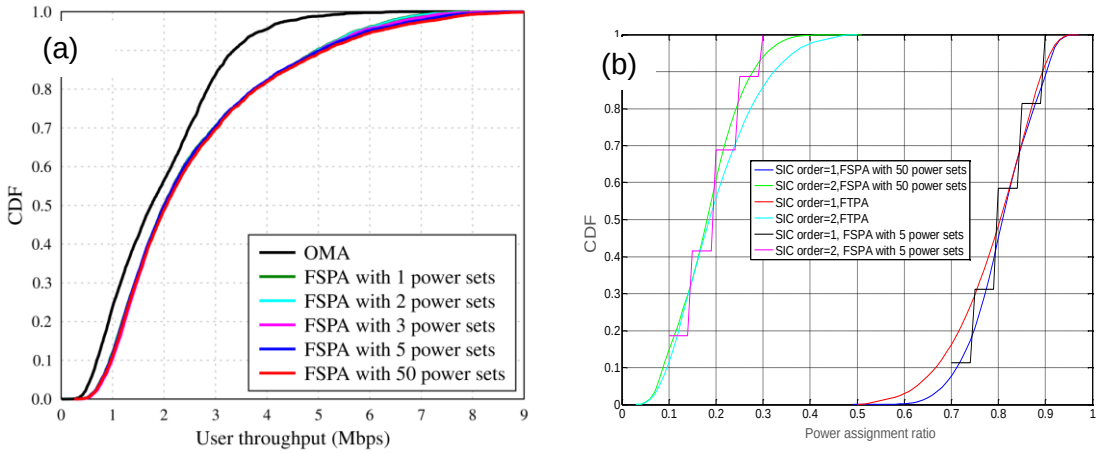

Figure 2-7: (a) CDF of user throughput for OMA (*m* = 1) and NOMA (*m* = 1). (b) CDF of power assignment ratio for SIC-order 1 and 2.

Future Work

In the next steps, we would like to identify the pairs of modulation coding scheme (MCS) and power sets that are selected in the case of NOMA with high probability.

2.6 Air interface for moving networks

This technological component incorporates the requirements of V2X communications into the air interface design. The objective is to improve the robustness of mobile communication links and enable services with strict reliability requirements such as road safety applications. The research embraces novel channel estimation and channel prediction techniques for highly time variant channels, as well as novel metrics for Ultra Realible Communication (URC) based on the prediction of the link reliability.

Framework for URC

As illustrated in Figure 2-8, the proposed system concept for Ultra-Reliable Communications (URC) is based on a “Reliable Transmission Link" (RTL) that is optimized to transmit packets successfully and within a predefined deadline, and an “Availability Estimation and Indication" (AEI) mechanism that is able to reliably predict the availability of the RTL under given conditions. In addition, a novel link control indicator called “Availability Indicator” (AI) signals the outcome of the AEI to the application. In this context, an application requests an RTL by sending an Availability Request (AR) to the AEI. Depending on the implementation details, the AR contains information such as the packet size, the maximum acceptable delay until successful reception or the maximum tolerable error probability. The AEI is designed to indicate to the application the availability of the RTL for the forthcoming transmissions given the AR requirements. For the availability estimation, the AEI needs to monitor the channel conditions, e.g., by evaluating the Signal-to-Noise and Interference Ratio (SINR) and/or the ACK/NACK statistics of the retransmission protocols used at link level. Typically, the AI is a binary value, i.e., either RTL available (AI=1) or unavailable (AI=0). After indicating the RTL availability, the application will be able to use it by transmitting data packets over the RTL (not shown in Figure 2-8). Depending on the implementation, other options might be reasonable as well (e.g., the AI is a soft value that indicates the likelihood that a "reliable transmission link" is available).

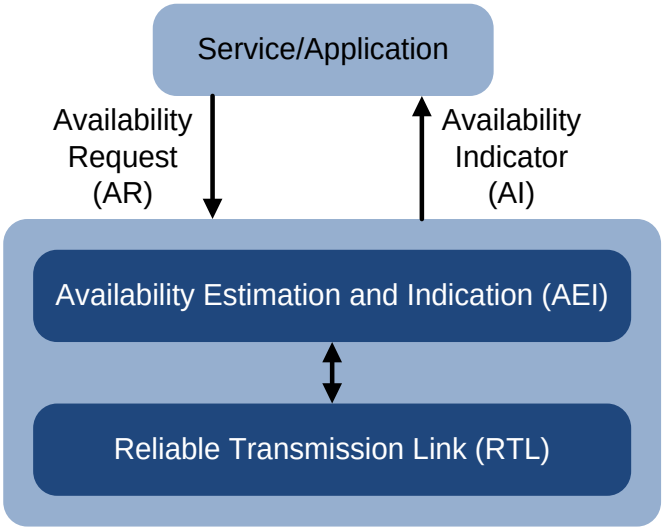

Figure 2-8: Ultra-Reliable Link (URL) concept.

URC Framework for Modelling and Predicting the Reliability of a Link

One of the key enablers for URC is the reliability of transmission success of a given packet [MET13-D11]. This is hard mainly owing to the time-dependent effective link qualities of the communicating devices. However, successful indication of the availability of instantaneous link quality (e.g., by the device) would also allow opportunistic access of ultra-reliable

services/applications when the link conditions are fair enough. A system modelling unit (SMU) is assumed for such an indication which provides the theoretical reliabilities achievable under the constraints of reliability factors (fading, mobility, interference etc). The analysis and prediction at the SMU is based on the reliability analysis methods Reliability Block Diagrams and Markov Chains [Bir10] and the respective Transmission Time to Failure (TTTF) of the individual components.

The KPI's for Reliability Analysis are:

Survival / Reliability Function R(t)

R(t) gives the probability that the transmission does not fail for the interval $[0, t)$. For this reason, it is also referred to as the survivor function since the transmission "survives" for the time t. Mathematically,

$$R(t) = 1 - F(t)$$

Where $F(t)$ is the Cumulative Distribution Function (CDF) of the probability that the TTTF (denoted by T) is greater then $t = 0$ and less then t

$$F(t) = \Pr(T \leq t)\ for\ [0, t)$$

Failure Rate / Hazard Function λ(t)

The conditional probability that the transmission operating failure-free until time t i.e., ($R(T = t{=}1)$ also survives the period Δt.

$$\lambda(t) = \frac{R(t + \Delta t)}{R(t)}$$

Availability (Repairable Systems)

The failure rate is only used for non-repairable systems. For the case of wireless transmission which is a repairable system, Availability (Point Availability) is used which is the *probability of transmission success at a stated instance of time (dependability)*.

Reliability Block Diagrams are used in the analysis by considering individual reliability functions R(t) of pathloss, shadowing and multi-path propagation effects whose assumed life distributions f(t) are given in Table 2-5.

Table 2-5 Statistical distributions of Reliability Factors

EFFECT	DISTRIBUTION	MEAN	VARIANCE
PATHLOSS	Exponential	1	1
SHADOWING	Log-Normal	e^3	$e^6(-1 + e^4)$
MULTIPATH FADING	Rayleigh	$\sqrt{2\pi}$	$4(2 - \frac{\pi}{2})$

The RBD is constructed by assuming transmission as the *series* system where the failure of any of the three components (pathloss, shadowing and multipath fading) would result in the failure of the transmission. Hence the system reliability is calculated as

$$R_{sys} = R_{pathloss} \wedge R_{shadowing} \wedge R_{multipath}$$

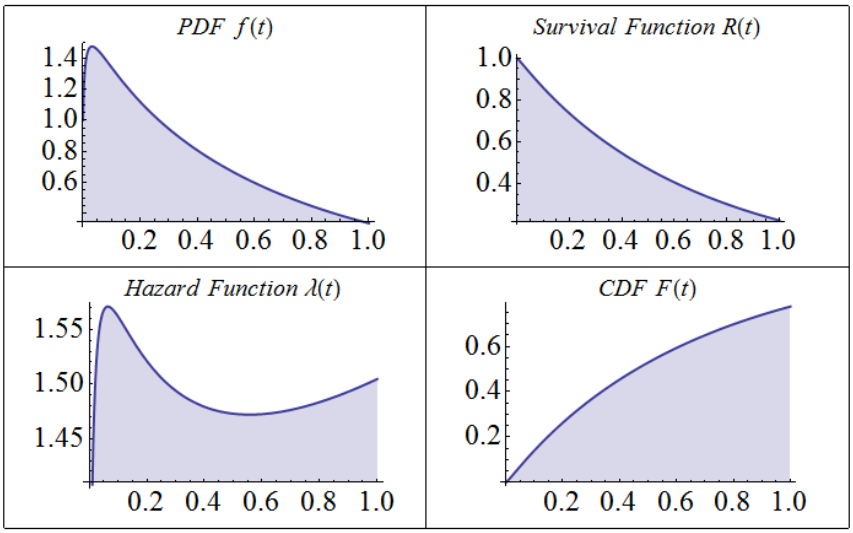

Figure 2-9: System Reliability

Figure 2-9 shows the survival and hazard functions of a single transmission instance. The TTTF can be calculated as the mean of the survival function and in our case is calculated to be 0.65. However, the probability of failure before a random time t can also be calculated and is given in Table 2-6.

Table 2-6 Probability of transmission failure before T

TIME (T)	PROBABILITY OF FAILURE (P<T)	
	Without Retransmissions	With Retransmissions
0.1	0.140881	0.0198475
0.2	0.263554	0.0694608
0.3	0.366532	0.134346
0.4	0.453991	0.206107
0.5	0.528891	0.279726

Retransmissions can be modelled by incremental redundancy. However, the results here assumed that the operating conditions are similar for both the transmission instances which does not hold on reality due to the channel time diversity.

Reliability prediction is done by considering the wireless channel as a repairable system in which case the failure rate translates into Availability and repair rate into Maintainability. The repairable system analysis can be done by more sophisticated reliability analysis techniques using Multi-level Markov Chains with arbitrary failure (λ) and repair (μ) rates. λ is based on the reliability factors and μ is based on the pre-emptive maintenance measures carried on the transmission (Link adaptation via power control, MCS and other Error Correction techniques).

Channel estimation for V2V links

A channel estimation algorithm for vehicle-to-vehicle (V2V) wireless communication has been developed [BSM14]. The vehicular channel is modelled using a geometry-based stochastic channel model with discrete static, discrete mobile, and diffuse scatterers, see Figure 2-10. The model reveals that the channel representation in delay-Doppler domain can be divided into four regions. In each region, the V2V channel can be modelled using a hybrid sparse/diffuse (HSD) model. Prior art on hybrid channel estimation for linear time-invariant channels is extended to the time-varying case. Furthermore, the effects of pulse shape leakage are explicitly determined and compensated. Simulation results shows that exploiting

the V2V channel properties in the delay-Doppler domain, yields significantly improved channel estimates over unstructured approaches (more than 10 dB gain in SNR) [BSM14].

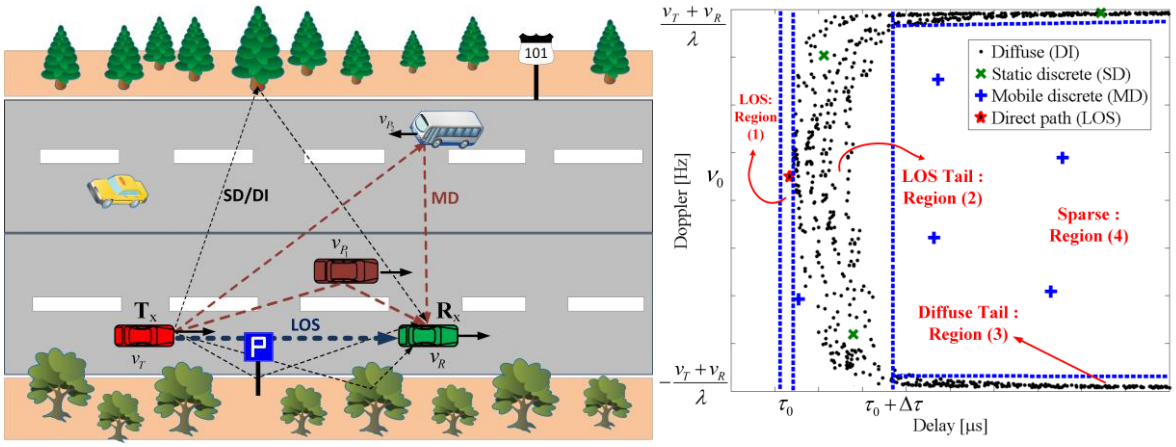

Figure 2-10: A geometrical description of scattering environment and the transmitting and receiving vehicles (left) and the corresponding channel in the delay-Doppler domain (right). Each multipath component gives rise to a sparse component in the delay-Doppler domain.

Channel prediction for the backhaul link of moving cells/networks

Channel state information at transmitters is important for advanced transmission schemes. However, feedback and transmission control delays of multiple milliseconds result in severe outdating of this information at vehicular velocities. Channel prediction based on extrapolation of the short-term fading has proven to be inadequate at vehicular velocities and high carrier frequencies.

We are therefore evaluating a new scheme that was proposed in [SGA+12], which may radically extend the prediction horizon when used on vehicles: Use an additional antenna, a "predictor antenna", placed in front of the transmission antennas in the direction of travel. This approach can provide an order-of-magnitude improvement in channel prediction performance as compared to Kalman or Wiener-extrapolation of previous measurements based on the channel statistics. As recently shown in [PSS13], the resulting increased CSI quality could enable massive MIMO antennas to let narrow beams track fast-moving vehicles even in the presence of multipath propagation which generates very fast fading.

We have investigated how different types of antenna designs on vehicles affect the attainable cross-correlation between the channel measured by the forward predictor antenna and the channel later experienced by the main antenna, when it has moved to the position previously occupied by the predictor antenna (illustrations are given in the annex). The attainable precision in the prediction of complex channel gains is directly related to this cross-correlation [SGA+12].

2.7 Faster than Nyquist (FTN)

The continuous evolution of Internet services and the increasing emergence of new applications require future wireless networks to search for advanced solutions, offering higher data rate with more efficient band usage. FTN, first introduced in 1975 by Mazo, turns out to be a good candidate to satisfy these needs. By transmitting the data with a rhythm faster than the Nyquist condition, FTN can theoretically provide a higher data rate than the Nyquist-based systems, with the drawback of introducing interference into the transmission.

Capacity and spectral efficiency for FTN signalling

Non-orthogonal transmission schemes such as Faster-Than-Nyquist (FTN) signalling have the potential to increase the capacity by using pulses with excess bandwidth which are different from sinc pulses that can't be realized practically [RA09], [ARÖ13]. For example, by using root raised cosine (RRC) pulses for the transmit filters, the capacity increases by increasing the roll-off factor (α) which can be shown by evaluating the FTN capacity equations constrained for independent and identically distributed (i.i.d.) Gaussian alphabet in [ET13]. In order to analyse the FTN spectral efficiency defined as the sum rate in bits/sec/Hz, we will consider a shared resources medium, assuming K-user multi-access channel (MAC); the signals are placed at centre frequencies $kf_{C,int}, k = 0, \pm 1, \dots, \pm(K-1)/2$; Gaussian signalling is used, treating interference as noise, i.e., assuming simple receivers; all users use RRC pulses with absolute bandwidth $A = (1+\alpha)W$ where W is the 3 dB bandwidth, all signals have equal power P and have at most one interferer at each frequency, $A/2 \leq f_{C,int} \leq A$. The analytical details are presented in [EK14].

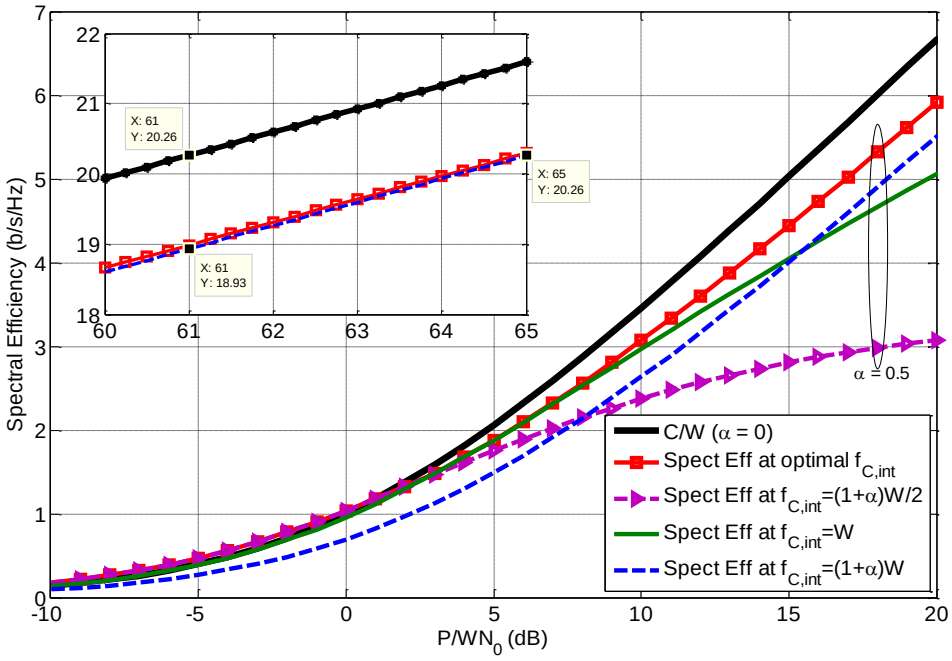

Figure 2-11: Spectral efficiencies for roll-off factor $\alpha = 0.5$ for the system point of view realization.

Two realizations are considered in the evaluation: the system point of view where the power per Hertz is $(\frac{P}{f_{C,int}})$and the per user point of view where the power per Hertz is $(\frac{P}{W})$. For the system point of view realization, the spectral efficiencies using RRC pulses of $\alpha = 0.5$ optimized over $f_{C,int}$, i.e., the smallest possible $f_{C,int}$ that results in the highest possible spectral efficiency value, where $(1+\alpha)W/2 \leq f_{C,int} \leq (1+\alpha)W$ is shown in Figure 2-11 compared to the spectral efficiencies using RRC pulses of $\alpha = 0.5$ which are achieved by different values of $f_{C,int}$ and the spectral efficiency using sinc pulses, each of absolute bandwidth W, without any interference. At low SNR, it is best to choose $f_{C,int}$ as small as possible to get higher spectral efficiency, i.e., potential improvement of spectral efficiency by squeezing more pulses. At high SNR, it is best to avoid interference. For different roll-off factors and the second system realization figures, refer to the annex.

Apart from the theoretical capacity investigations for FTN signalling, we also considered practical systems and studied its gains. FTN is also well suited for applications that need low cost transmitters and flexible rate adaptation. Simulation results showing the flexibility in terms of throughput by just changing the FTN rate and not the modulation scheme or coding rate are available in the annex.

Symbol-by-symbol detection of multi-carrier FTN signalling

In order to exploit the theoretical gain in practical systems, sophisticated receivers have to be used to cope with the intentional ISI. In addition, when FTN signalling is combined with the Multi-Carrier Modulations (MCMs), the interference is introduced in a two-dimension lattice, which calls for a more sophisticated receiver, together with an affordable complexity. Publications related with FTN detection typically make use of sequence detectors for taking into account the ISI introduced at the transmitter (e.g. [PAR08, DRO10, DRO11, KB12, MS10]). The target of this study is to propose and analyse a symbol-by-symbol detection strategy based upon the maximum likelihood (ML) principle. Key advantage is the possibility for achieving a high degree of parallelization. In Figure 2-12 the block diagram of the receiver is depicted.

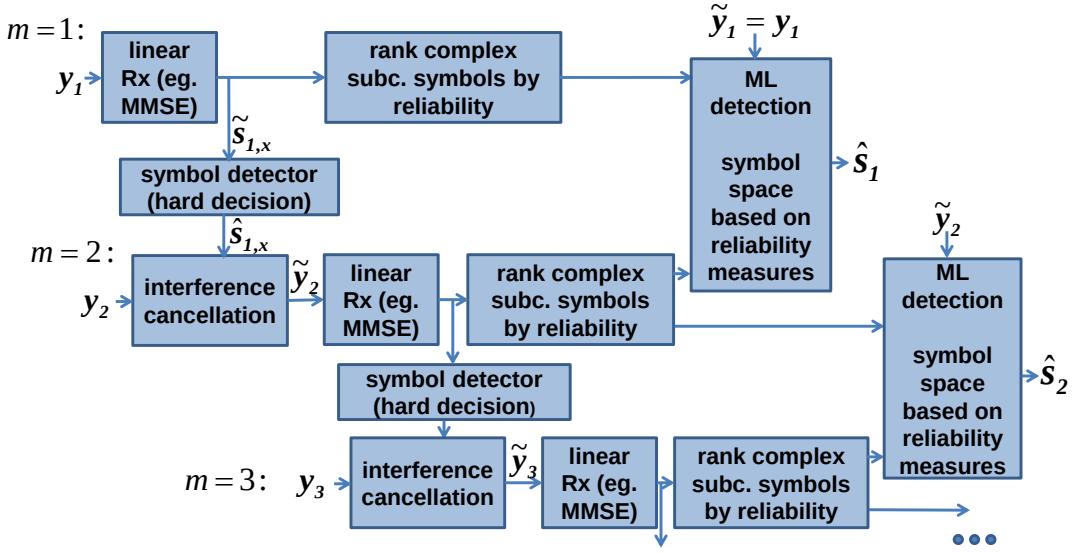

Figure 2-12: ML based detector with linear pre-processing and interference cancellation for search space reduction (*m* is the symbol number within the processed block of symbols).

The proposed scheme is related with concepts available in the area of MIMO detection (e.g. [RGA02]). A full ML detector exhibits exponential complexity in terms of number of subcarriers carrying data and number of multi-carrier symbols being overlapped. To reduce the search space the ML detector has to cover, we make use of reliability ranking and interference cancellation. The received symbol vector y_m is linearly detected (e.g. making use of the MMSE principle). Those estimates are then used to determine reliability measures per complex subcarrier symbol (e.g. based upon the distance to the closest decision threshold). By doing so, the search space of the ML detector may be reduced to only search for the least reliable symbols. Another means to reduce complexity is to apply interference cancellation based upon the outputs of the linear detector. The calculation of the ML metrics may be performed in a parallel manner as each single metric is independent of the others. If interference cancellation is used the single multicarrier symbols are to be detected consecutively. Otherwise, each single symbol may be detected concurrently. For a given setup (OFDM,

K'_{sccr}=24 subcarriers per sub-band, QPSK) the complexity could be reduced from $K_{ML,es} = (K_{MOD})^{K'_{scrr} K_{MCSymb}} = 4^{24\cdot 3} = 2.23e43$ metric calculations in case of exhaustive search to only 64 with applying the proposed scheme with only minor performance degradations (K_{MOD} refers to the modulation order, K'_{MCSymb} to the number of multicarrier symbols overlapping). Overlapping factors up to 1.15 have been investigated. A more detailed description of the detection principle and performance graphs are given in [SW13].

Combining FTN with FBMC

In addition to the application of FTN to OFDM described in the section above, FBMC should also be considered as alternative basic transmission waveform. To this end, this section aims to provide a preliminary analysis for a new transmission mode, which combines FTN with Filter-Bank Multi-Carrier/Offset Quadrature Amplitude Modulation (FBMC/OQAM). The analysed receiver uses the turbo equalizer, named Minimum Mean-Square Error Interference Canceller–Linear Equalizer (MMSE IC-LE), because it gives a good compromise/trade-off between complexity and QoSefficiency.

The FTN-FBMC/OQAM transceiver chain is illustrated in the figure below. On the transmitter side, FTN is combined with FBMC/OQAM modulation scheme, while on the receiver side, MMSE IC-LE scheme is used to iteratively suppress the interference caused by FTN and the channel.

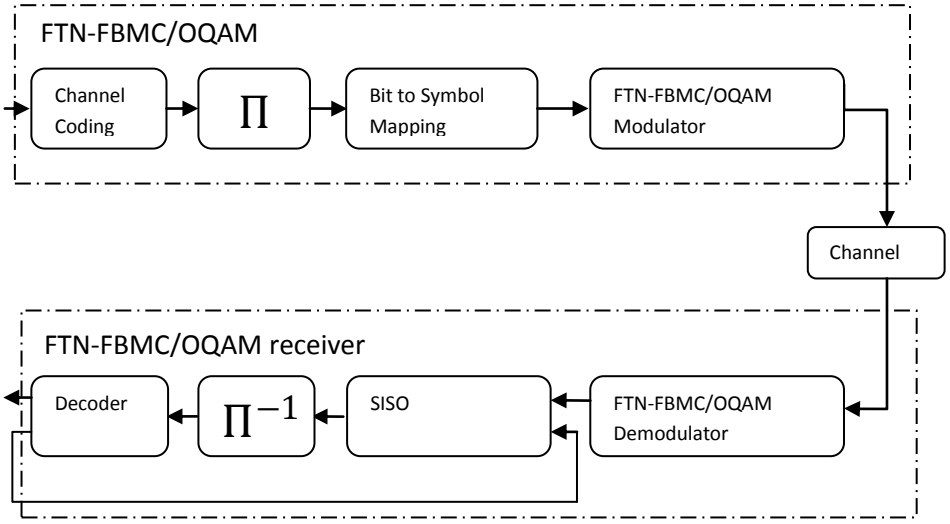

Figure 2-13: FTN-FBMC/OQAM transceiver chain

With this chain, we intend to investigate the FTN limit for different constellation orders as well as different waveforms. The results are reported in the table below in which the number following the acronym indicates the overlapping factor of the prototype filter. For instance, IOTA4 corresponds to the IOTA prototype filter with a length equal to four times the (I)FFT size (64 for this table). The three other prototype filters are designed using either the Extended Gaussian Function (EGF) or the Time Frequency Localization (TFL) criterion as in [SSL02], or the frequency selectivity (FS) criterion, as defined in [PS11] In Table 2.7 the FTN limit is the packing factor for which a BER of 10^{-5} can be reached for the different schemes. E.g. 0.5 means that we are twice faster than Nyquist.More details can be found in annex.

Table 2-7 FTN limit table

Pulse Shapes	QPSK	16QAM	64QAM
SRRC4 (roll-off=0.3)	0.8	>0.9	>0.9
SRRC4 (roll-off=0.3)	0.8	0.9	0.9
FS4	0.7	0.9	0.9
IOTA4	0.6	0.8	>0.9
TFL1	0.5	0.7	>0.9
EGF4 (spreading factor=2)	0.5	0.8	>0.9

Precoding and Frequency Domain Equalization for MFTN

The challenge of the FTN is at the receiver side due to the interference components. The addition of a frequency selective channel will complicate this further. Most methods developed so far [LG03] [RA09] [YC10] consider interference contaminated FTN sequence as some form of a convolutional code and hence utilize Viterbi based algorithms together also with different coding techniques to recover the transmit symbols. In addition, successive interference cancellation techniques are possible. The objective here is to employ precoding methods to compensate for the generated interference due to FTN as one option. In the case of FBMC, similar scenario is seen where there is significant amount of intersymbol and intercarrier interference to be mitigated. Thus as detailed in Section 2.8, one option is to consider the application of precoding and evaluate the performance. Another is to consider frequency domain equalization investigated in [S13] in a more general setting for application in multicarrier FTN (MFTN) case.

2.8 Filtered and filterbank based multi-carrier

This subchapter proposes new multicarrier based schemes and algorithms to address the challenges for future mobile wireless system. Two schemes are covered in this subchapter, i.e. FBMC and UFMC. Both schemes are using digital filtering methods to shape the multicarrier waveform for offering better PHY layer performance. They are distinct from each other in the orthogonality sense and in the transceiver design.

2.8.1 FBMC based waveform & transceiver design

FBMC (Filterbank Multicarrier)-Offset QAM (FBMC/OQAM) transceiver uses a pair of filter-banks (analysis and synthesis filter) to perform pulse shaping for each individual subcarrier. The advantages of FBMC in comparison to CP-OFDM are lower leakage power into the neighbouring frequency (sub)bands and better robustness against Doppler spread and synchronization errors.

Besides the above mentioned advantages, FBMC embeds also features such as degrees of freedom in adopting appropriate waveforms for specific scenarios and applications, and more flexibility for frame structure due to the CP removal.

In this subsection, several approaches are proposed to solve the open issues for FBMC: 1) signal transition time due to filtering (the “tail”) which leads to overhead for short package transmission; 2) to exploit the degrees of freedom gain of FBMC prototype filtering, esp. under different services and channel conditions; 3) MIMO precoding as the OQAM orthogonality is relaxed to real field only.

Weighted Circular Convolution FBMC and Frame Design

OFDM/OQAM incurs an excess overhead caused by transition times at the beginning and the end of a transmission burst. The overhead duration equals length of the prototype filter, which is normally at least 4T for an acceptable ISI/ICI (T denotes symbol duration). In the following, we propose a technique called Weighted Circular Convolution to remove the tails of OFDM/OQAM signal while preserving its real orthogonality. Full description of the proposed technique is referred to [AJM13].

Transmitter: In contrast to conventional OQAM modulation, which linearly convolves with prototype filter on each subcarrier, the new scheme modulates a data block of N OQAM symbols, where the data block is sequentially repeated and appropriately weighted such that the output of the OFDM/OQAM modulator is periodic. Due to its periodicity and special structure, the entire output signal can be reconstructed using only a portion of duration NT/2 of the signal. Therefore, it is sufficient to transmit this portion (which has no tails). This can be implemented by passing the data block through the regular OFDM/OQAM modulator and then applying "Weighted Crop-and-Add".

Receiver: The received signal is first passed through a "Weighted Append" module, which performs the reverse of the transmitter operation. The resulting signal is passed through the regular OFDM/OQAM demodulator to recover the data block.

Time Windowing: The sharp transitions at both ends of the weighted circularly convolved OFDM/OQAM signal result in PSD side-lobes increase. This issue is solved by appending proper time windowing signals to both ends of the tail-removed signal. Simulations show that a total time-windowing overhead of T/4 for the entire signal burst is enough to preserve the PSD performance.

Simulation Results: Here, we provide simulation results for an OFDM/OQAM transmission with N=2 OQAM symbols, 600 subcarriers and the subcarrier spacing of 15 kHz. The prototype filter is a truncated root-raised cosine (RRC) with roll-off factor α=1 and truncation length 4T. For time-windowing, we use raised cosine window with duration $\mathrm{T_w} = \mathrm{T}/4$. In Figure 2-14, we compare PSD of the weighted circularly convolved OFDM/OQAM with time-domain windowing with those of linearly convolved OFDM/OQAM signals with and without truncation. For truncation, a portion of length $\mathrm{NT}/2 + \mathrm{T_w} = \mathrm{T} + \mathrm{T_w}$ from the middle of the time-domain signal is kept. For the sake of comparison, we also applied the $\mathrm{T_w}$ windowing to the truncated signal. Table 2-8 lists EVM (Error Vector Magnitude) of the demodulated OQAM constellation points (soft values).

Frame structure design: based on the proposed Circular Convolution algorithm, a LTE-like frame structure can be designed and the details are given in the appendix.

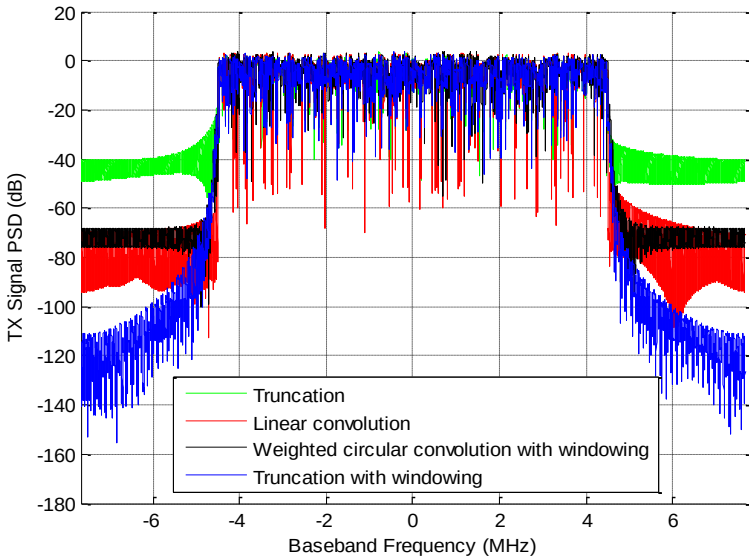

Figure 2-14 Spectrum comparison for burst of N=2 OQAM symbols: Windowing size = T/4.

Table 2-8 EVM comparison of transmission techniques for N=2.

	Linear Convolution	Weighted Circ. Conv. with Time-windowing	Linear Conv. with Truncation	Linear Conv. with Truncation and Time-windowing
$T_w = T/4$	-69.47 dB	-43.83 dB	-20.16 dB	-17.11 dB

Transceiver Processing Techniques for MIMO FBMC Systems

FBMC systems have a significant amount of inter-carrier-interference (ICI) and inter-symbol-interference (ISI), which degrades the system performance when operating under fading channels, although, by design, these effects are negligible in AWGN channels. We consider a multicarrier MIMO-FBMC system with 2M subcarriers, with a single transmitter and a receiver, each equipped with NA antennas. The bit error rate (BER) performance of a (MIMO) FBMC system is analyzed comprehensively and it is shown that the system can achieve low error performance [SRL14] comparable to MIMO-OFDM and as opposed to single tap filtering or zero forcing (ZF). The performance is evaluated for various linear and non-linear transceiver processing techniques, which attempt to mitigate the effect of ICI and ISI in MIMO FBMC systems. The filter used is g[k] and the filter length is L. The system model and further details are given in the annex. We consider a time-invariant Rayleigh fading channel, where the channel impulse response spans Λ sampling intervals. The sampling corresponds to original symbol duration before FBMC mapping. We assume that all antenna paths undergo independent fading. For the receiver processing techniques discussed, we assume the receiver has perfect channel state information (CSI). For the precoding methods discussed, we assume perfect CSI is available at both the transmitter and the receiver. This assumption is to be relaxed later on. The complexity and performance trade-off is considered for these cases. In particular punctured Tomlinson Harashima precoding (THP) technique is proposed which shows feasibility of FBMC with significantly lower BER as shown compared to ZF. The approach is to remove the error floor by precoding, at a slight loss of throughput, by not using one or more antennas for some symbols in some subcarriers. We call this puncturing. We can limit the maximum interference on a symbol to ε with r iterations. Signal amplitude without interference is set to unity. The following Figure 2-15 shows the average BER parameterized by the number of channel taps Λ with first tap variance is unity and the rest is of equal strength giving an overall variance of 1.2.

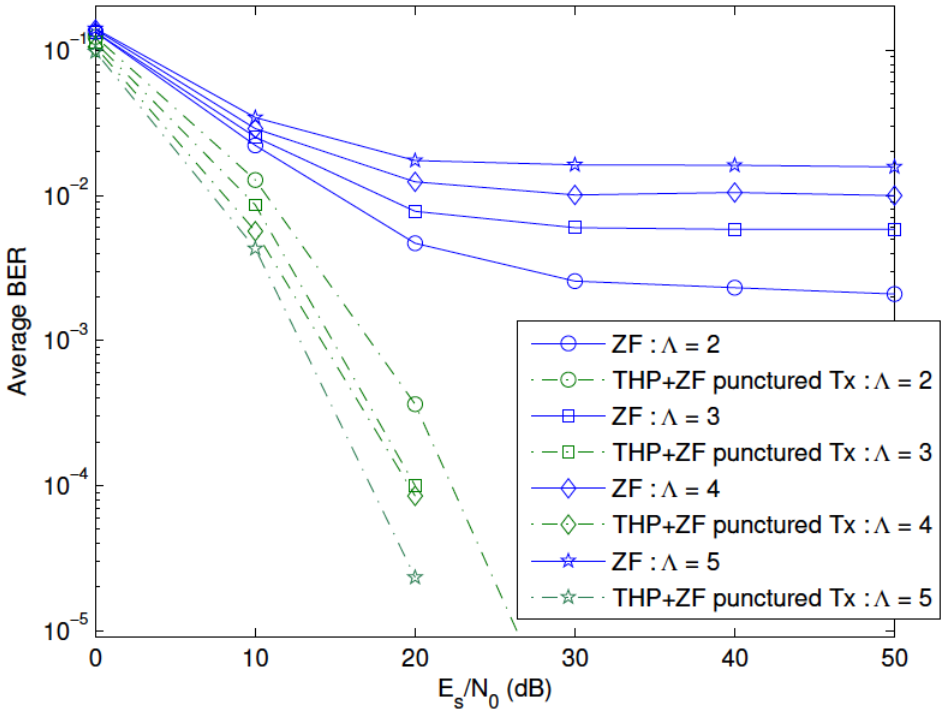

Figure 2-15: Average BER Performance with 2M=16, L=63,r max=3, ε=1.

Windowed Cyclic-Prefixed FBMC/Circular OQAM (WCP-COQAM)

In the literature, many alternative MCM schemes are proposed to replace CP-OFDM. They can be mainly categorized into two groups. One group uses the linear convolution for the filtering and the schemes include FBMC/OQAM [FAB95] and FBMC/FMT [CEO02]. The other group is based on circular convolution such as GFDM [FKB09] and CB-FMT [Ton13]. Nevertheless, all these alternatives have their own drawbacks and advantages. The WCP-COQAM is a combined version of these two groups which intends to minimize the drawbacks and keep maximally the advantages from the predecessors. Note that the concept of WCP-COQAM is partially in line with the Weighted Circular Convolution FBMC.

With respect the schemes of the first group, the problems solved by WCP-COQAM are

- Orthogonality issue in multi-path channel (problems with FBMC/OQAM and FBMC/FMT).
- Complex equalization issue (problems with FBMC/OQAM and FBMC/FMT)
- Complex receiver with Alamouti STBC issue (problem with FBMC/OQAM and FBMC/FMT)
- Subcarrier spacing enlarging issue (problem with FBMC/FMT)
- Burst transmission issue (problem with FBMC/FMT and FBMC/OQAM)

With respect to the second group schemes, the problems solved by WCP-COQAM are

- Orthogonality issue (problem with GFDM)
- Complex receiver with Alamouti STBC issue (problem with GFDM)
- Subcarrier spacing enlarging issue (problem with CB-FMT)

The initial implementation of WCP-COQAM is composed of two steps. 1) COQAM modulation and 2) add CP then windowing process. Details can be found in [LS14]. Besides the

abovementioned advantages, WCP-COQAM can also provide high degree of flexibility for receiver process which can be beneficial to different transmission circumstances.

The Table below provides a summary of the pros and cons of these different MCM scheme.

Table 2-9: Comparison of MCM schemes for various criteria

	CP-OFDM	GFDM	FMT	FBMC/OQAM	WCP-OQAM
PSD	✗	✓	✗	✓	✓
Multipath	✓	✗	✓	✓	✓
RX complexity	✓	✗	✗	✗	✓
STBC	✓	✗	✗	✗	✓
Burst trans.	✓	✓	✗	✗	✓
Flex. TX/RX	✗	✗	✓	✓	✓

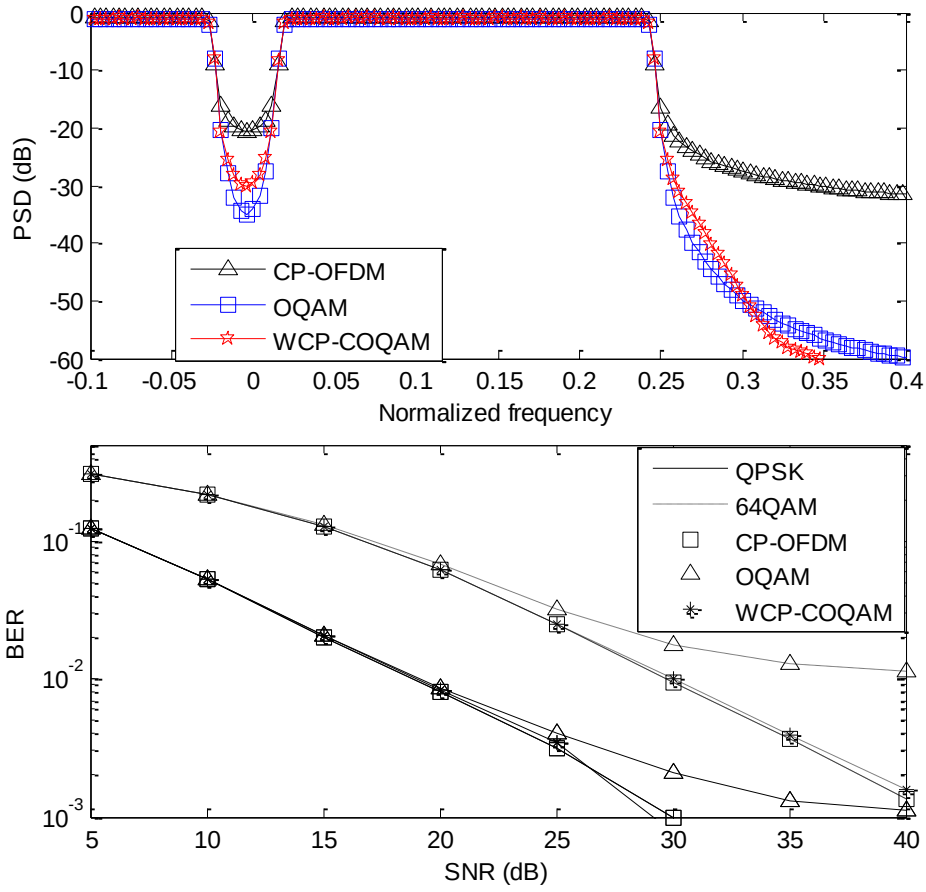

Figure 2-16 PSD and BER comparisons: WCP-COQAM vs. OQAM vs. CP-OFDM

The figure gives our simulation results compared with CP-OFDM and the classical FBMC/OQAM. More extensive comparison with other state of the art schemes will be provided in the future. The detailed simulation parameters can be found in [LS14].

Channel adaptive pulse shaping

It is well known that an adaptation of the pulse shape to the channel's energy spread in time and frequency will improve the transmission performance, since ISI and ICI can be minimized. However, information on quantitative potential performance gains in practical scenarios is not yet found in the literature. The potential of adapting the pulse shape to the channel conditions in an FBMC system is therefore analyzed here. Based on the ambiguity function of the pulse shape and its distortion due to the delay and Doppler spread channel, we evaluate the reconstruction quality of the pulse in terms of an SIR measure. It turns out that considerable SIR gains can be achieved by adapting the pulse shape to the channel, in particular if severe Doppler distortions are present.

For the research results presented here, we have selected the IOTA (Isotropic orthogonal transform algorithm) pulse, which is based on extended Gaussian functions (EGF) and allows adapting the pulse shape to the 2D channel scattering function of the channel by adjusting a parameter α. Based on this example, we show the potential of adapting the pulse in delay and Doppler spread channels by comparing its performance to that achievable with the well-studied PHYDYAS pulse. The parameter α of the IOTA pulse affects the power distribution of the pulse in the time/frequency space, and it can be chosen as follows:

- $\alpha=2$ the power is isotropically spread in the time/frequency grid for OFDM/OQAM, which is spanned by subcarrier spacing F0 and sampling period T/2.
- $\alpha>2$ the pulse is broadened in frequency domain, making it less prone to frequency spreads / shifts, as imposed by Doppler effects
- $\alpha<2$ the pulse is broadened in time domain, making it less prone to time spreads / shifts, as imposed by delay spread channels

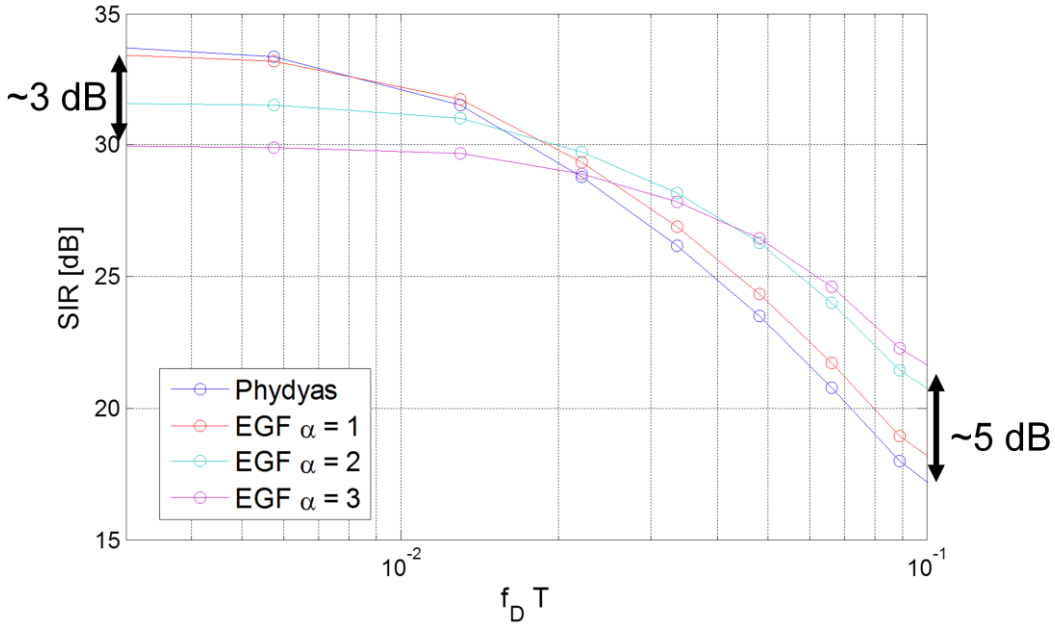

Figure 2-17: Pulse reconstruction performance in doubly dispersive channel

In Figure 2-17, we assume a constant RMS delay spread of 0.01T and a variable Doppler spread. We can observe that at low Doppler, PHYDYAS pulse achieves the best performance, exceeding that of IOTA with α = 3 by 3 dB. For high Doppler, this IOTA pulse excels the performance of PHYDYAS by roughly 5 dB. In line with the theory, when following the transition between these two extremes, we observe that there is an area where IOTA with α = 2 provides the best SIR performance. However, compared to the other 2 IOTA candidates,

this pulse can provide an additional SIR gain of not more than 0.5 dB. It is thus questionable whether the IOTA pulse with $\alpha = 2$ should be considered for pulse adaptation in a practical system. Due to the close behaviour of PHYDYAS and IOTA with $\alpha = 1$, the two IOTA candidates with $\alpha = 1$ and $\alpha = 3$ seem to be the most suitable for practical pulse adaptation. More comprehensive studies of channel adaptive pulse shaping can be found in [FPS14].

2.8.2 Universal Filtered Multicarrier (UFMC)

UFMC (aka UF-OFDM – Universal Filtered OFDM) is a new waveform concept combining the advantages of OFDM and FBMC. The following figure depicts the block diagram of an exemplary UFMC transceiver.

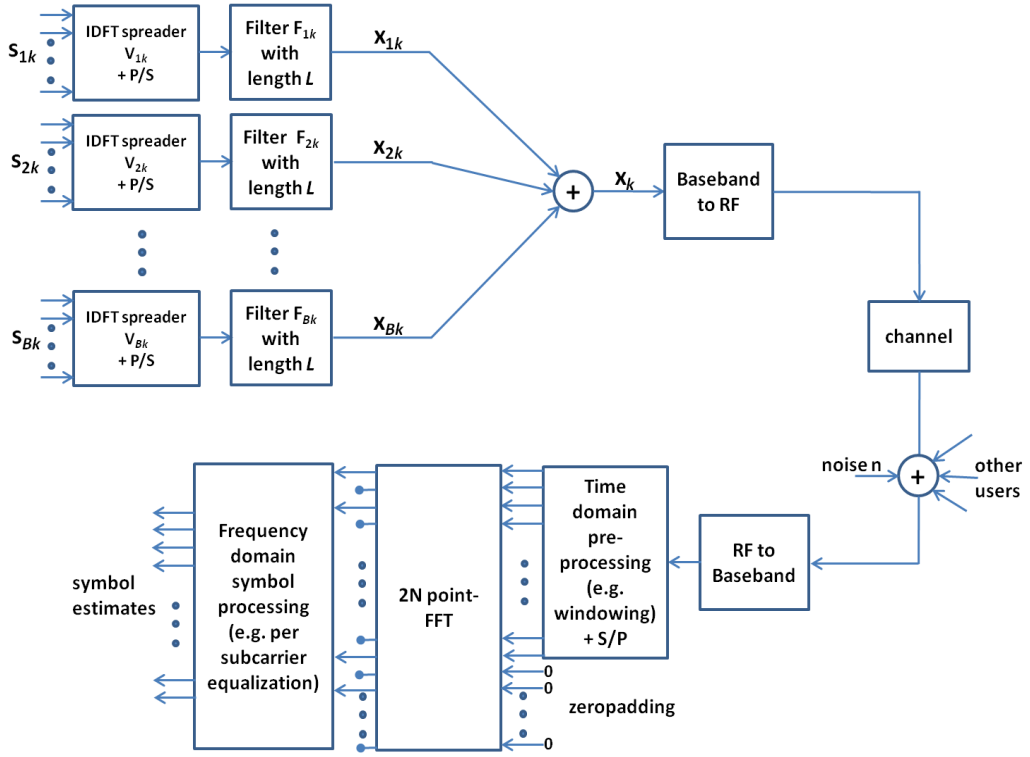

Figure 2-18: Block diagram of the UFMC transceiver (here: Rx based on FFT processing).

The time domain transmit vector x_k for a particular multi-carrier symbol of user k is the superposition of the sub-band-wise filtered components, with filter length L and FFT length N (for simplicity we drop the time index m):

$$\underset{[(N+L-1)\times 1]}{\boldsymbol{x}_k} = \sum_{i=1}^{B} \underset{[(N+L-1)\times N]}{\boldsymbol{F}_{ik}} \underset{[N\times n_i]}{\boldsymbol{V}_{ik}} \underset{[n_i\times 1]}{\boldsymbol{s}_{ik}}$$

For each of the B sub-bands, indexed i, the n_i complex QAM symbols - gathered in s_{ik} - are transformed to time domain by the IDFT-matrix V_{ik}. V_{ik} includes the relevant columns of the inverse Fourier matrix according to the respective sub-band position within the overall available frequency range. F_{ik} is a Toeplitz matrix, composed of the filter impulse response, performing the linear convolution. Varying n_i has impact to the time domain overhead, as the filter length scales accordingly and to the side-band levels at the edge of the sub-bands and thus to the interference level between sub-bands in case of time and frequency offsets. So far we apply n_i=12 leading to reasonable performance measures and being compatible to LTE parameters. After superposition, the sum signal is up-converted and RF processed. The detector receives the noisy superposition of all users' transmissions. After conversion to baseband the received signal vector may optionally be processed in time domain, e.g.

windowing may be applied to suppress multi-user interference, and after FFT conversion in frequency domain (any procedure known for CP-OFDM is applicable here – e.g. related to channel estimation and equalization) to improve the signal quality.

Some of the key advantages of UFMC are:

- Support of relaxed synchronism both with respect to timing and carrier frequency (originating from e.g. applying open-loop synchronization and cheap oscillators) enabling energy and overhead efficient inclusion of MMC traffic without introducing severe interference [5GNOW-D31] (relevant for CoMP joint transmission and joint reception, too [VWS+13]). Main motivation is to enable cost effective sensor devices with very high battery lifetimes.
- Support of short burst transmissions without introducing excessive signal overheads thanks to the good time-localization of UFMC (similar to CP-OFDM) while having much better frequency-localization on sub-band level [SWC14].
    - To enable fast TDD switching for fast and flexible UL/DL switching.
    - To enable low latency transmissions, very short Transmission Time Intervals (TTIs) are to be employed.
    - To enable energy efficient communications by minimizing on times of low-cost devices.
    - To support very small packet transmissions efficiently.
    - To support small signalling messages, downlink (DL) synchronization symbols and uplink (UL) sounding with high efficiency.
- Use of QAM enabling the use of any available technique for CP-OFDM in the same manner (e.g. MIMO techniques, beamforming, complex pilot sequences, DFT spreading to reduce PAPR). With UFMC we are able to make use of the vast amount of available signal processing techniques originally designed for OFDM.
- Suitable for fragmented spectrum, less frequency guards required than with CP-OFDM, more spectrally efficient than CP-OFDM [SWC14].

2.9 Modulation & coding and new channel coding concepts

Two different aspects are considered in this section which is related to the modulation and coding techniques. The first one is oriented towards the reduction of energy consumption, thanks to the implementation of constant amplitude modulations. The second one is focused on the modulation and coding improvement, which is twofold: the first option is to improve the implementation efficiency on the receiver side by optimizing its complexity with respect to the performance; the second option is to re-consider the standard adaptive coding and modulation scheme by answering the question whether lattice codes could be an interesting alternative in 5G communications.

2.9.1 Constrained envelope coded modulation

The envelope property of the modulated signal after D/A conversion is typically characterized by means of the peak-to-average power ratio (PAPR) [FKH08, eq. (15)], [NP00], or the Raw Cubic Metric (RCM) as defined in [FKH08, eq. (16)], which is closely related to the 3GPP Cubic Metric (CM) defined in [3GPP-R4040367]. The rationale behind CM and RCM is the fact that the primary cause of transmit-signal distortion is the third order nonlinearity of the amplifier gain characteristic.

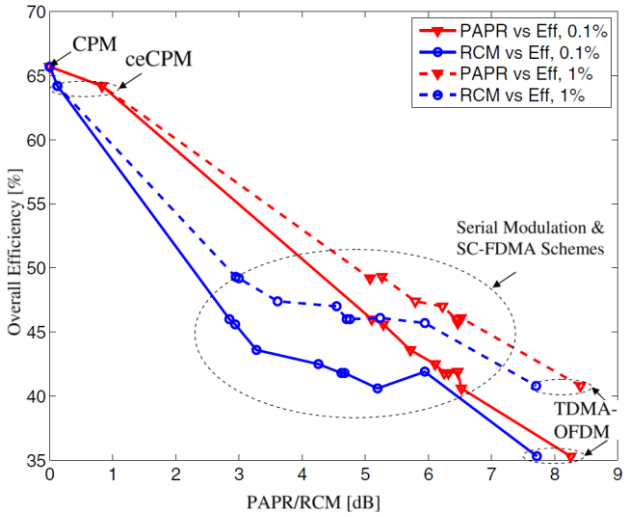

Figure 2-19: Maximum overall HPA efficiency versus mean PAPR and RCM of various modulated signals with 1% and 0.1% clipping level [SE10].

In Figure 2-19, we show how these metrics relate to the overall efficiency of a typical High Power Amplifier (HPA) for a set of signals having different envelope properties [SE10]. Here, the HPA overall efficiency is defined as $\eta_A=P_{out}/(P_{DC}-P_{IN})$, where P_{IN} is the RF power at the input of the HPA; P_{out}: resulting RF output power and P_{DC} is the power at the Direct Current (DC) input of the amplifier. As shown in Figure 2-19, HPAs are most efficient when they are driven into saturation. Therefore, input power back-off reduces the overall efficiency of the HPA and is detrimental to devices with limited energy resources. The key to substantially reduce the envelope variations is to avoid zero-crossings in the modulated pulse shaped baseband signal.

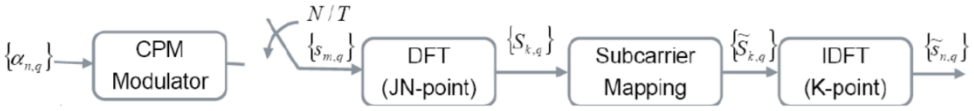

Figure 2-20: CPM-SC-FDMA precoder [WPS11].

For this reason, SC-FDMA employing a sub-sampled Constant Phase Modulation (CPM) encoder as precoder of SC-FDMA with I-FDMA subcarrier mapping, see Figure 2-20, was suggested in [MET13-D22] as an energy-efficient constrained-envelope coded-modulation multiple-access scheme with potential applicability for, in particular, the MMC horizontal topic. The reason is that CPM-SC-FDMA yields very good envelope properties, down to a fraction of a dB (i.e. similar to Constrained Envelope Continuous Phase Modulation (ceCPM) [SS03] in Figure 2-19), while at the same time maintaining the OFDMA structure. This allows for a simple multiple access scheme through frequency division and permits coexistence with adaptive OFDMA and reuse of the OFDMA transceiver structure currently in use in OFDMA-based systems.

The scheme might also be useful for high bandwidth and coverage limited mmW scenarios (UDN, V2V) with high requirements on transceiver energy efficiency and robustness to non-linear HPAs, e.g. due to cost and severe peak power limitations, but with modest requirements on spectral efficiency due to large available bandwidth and dense reuse enabled by short transmission distances.

In the annex (see section 5.9) we summarize the results from [WPS11] showing that CPM-SC-FDMA can outperform convolutionally encoded Quadrature Phase Shift Keying (QPSK) by up to 4 dB in end-to-end power efficiency, takingHPA power backoff into account (disregarding

baseband power consumption). In this comparison, convolutional coding is used as a reference for two reasons:

- The partial 4-ary CPM encoder is already including coding with 4 bits in its state memory, sampled twice per symbol interval. So a fair comparison is to use the best rate 1/2 convolutional code with constraint length 5 together with QPSK for SC-FDMA. These schemes have the same spectral efficiency, and the same transmitter complexity in terms of number of state bits. (The receiver for the CPM-SC-FDMA scheme has in addition some phase states, but might be reduced to only two with negligible loss using trellis folding.)
- The intended application at the time of the article that the results come from where short packets.

2.9.2 Advanced coding and decoding

Adaptive complexity flexible baseband: Application on iterative MIMO receivers

Coded modulation schemes with multiple antennas offer a large number of parameters that need to be defined depending on the target application. Such parameters need to take into account input constraints related to KPIs such as intended throughput, error rate, SNR, latency and resulting complexity. Receiver-side constraints, such as power consumption can also be of interest especially for handheld and MTC devices. A wide range of suboptimal receiver-side algorithms are derived in literature. They enable hardware implementations of complex algorithms. However, published results often evaluate these reduced-complexity variants on a limited set of parameters related to the considered technique and to its system integration environment. A larger scale study of such algorithms dedicated to iterative MIMO receivers is targeted in this work.

Turbo decoding algorithms, reduced complexity MIMO detection, iterative algorithms at the receiver side and their corresponding quantization are investigated. Effect of coding rate, channel type, frame size, number of iterations are also taken into account. For a target performance, the best set of parameters is chosen. The resulting complexity in terms of number of quantized arithmetic operations and number of memory accesses is identified.

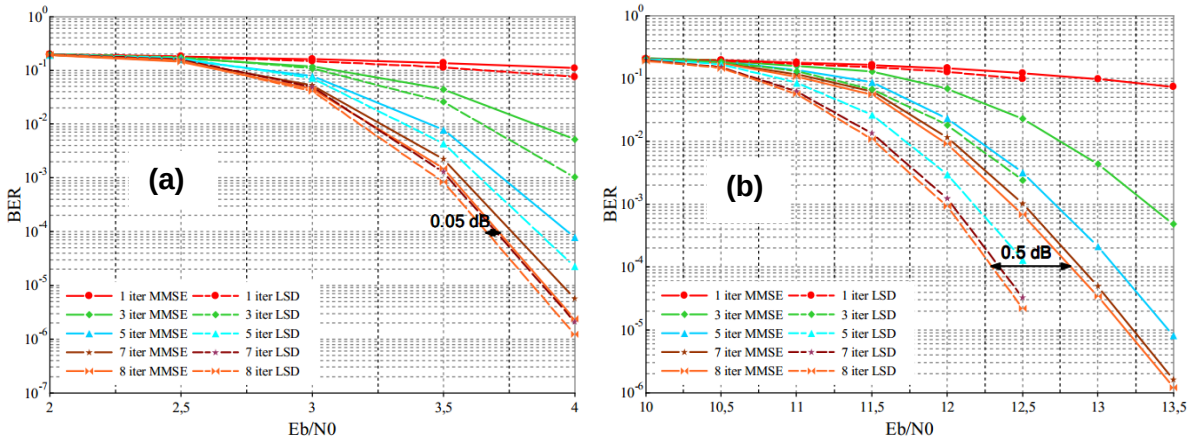

Figure 2-21: BER comparison of MMSE and LSD MIMO detection algorithms. QPSK (a) and 64 QAM (b), code rate R=1/2. 4 transmit and receive antennas, 1920-bit frame size, 8 receiver iterations, Rayleigh fading.

As an example, Figure 2-21 compares Bit Error Rate (BER) simulation results over a Rayleigh fast fading channel for two reduced complexity MIMO algorithms: iterative Minimum Mean Squared Error (MMSE)-based algorithm and iterative soft input soft output List Sphere Decoding (LSD)-based algorithm for QPSK (a) and 64-QAM (b) respectively. LTE turbo code was used for a coding rate of R=1/2 and a frame size of 1920 bits. A MIMO system with four transmit and receive antennas was considered. Extrinsic information was exchanged between the output of the turbo decoder and the MIMO detector; eight iterations were performed.

The gap in performance between compared reduced-complexity algorithms varies with the constellation size to attain/reach 0.5 dB for the 64-QAM case in favour of LSD. Larger differences of several decibels were observed over a block fading channel. In addition, differences vary considerably with frame size. Chosen list sizes of the LSD algorithm for the QPSK and 64-QAM cases of Figure 2-21 are 16 and 256 candidates respectively.

Complexity per detected symbol and iteration of compared algorithms is summarized in Table 2-10. Considering typical fixed-point representation (see annex 5.9), the complexity is normalized and presented in terms of equivalent add 1-bit, memory read 1-bit and memory write 1-bit operations. We use *t* to represent the average number of visited nodes in the LSD algorithm. MMSE algorithm complexity is independent from constellation size. The complexity of LSD varies greatly with *t*. Values of *t* vary with system parameters and the encountered channel model. For a chosen set of coding and modulation scheme, *t* decreases with the SNR.

Table 2-10 Example of complexity comparison of LSD and MMSE algorithms corresponding to simulations shown in Figure 2-21

Constellation	MMSE complexity			LSD complexity		
	Add (1bit)	Read (1bit)	Write (1bit)	Add (1bit)	Read (1bit)	Write (1bit)
QPSK	41577	184	32	943t	12t	56
64-QAM	41577	184	32	2957t	32t	56

As a conclusion, important gains can be achieved by adequate receiver design. Unfortunately, often a compromise has to be made between performance and complexity. It goes farther than the choice of the reduced complexity algorithm to the large number of receiver parameters.

Practical lattice codes

Lattice codes have been proved to achieve the capacity of the AWGN channel, and have been shown to solve various communication theory issues. However, most of the results are theoretical. So we are interested in this technical component to investigate whether lattice codes could be considered as a promising modulation and coding scheme in practice.

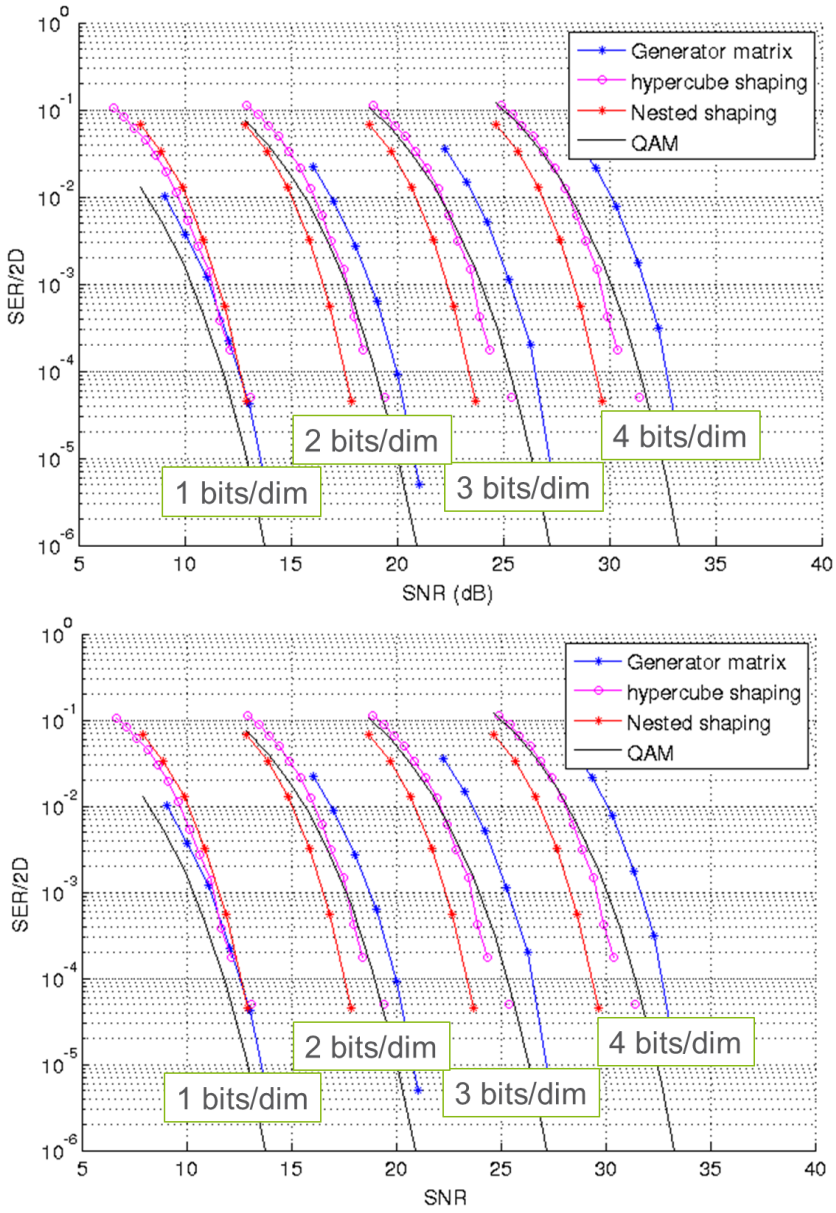

Figure 2-22: Symbol error rate comparison on an AWGN channel between uncoded QAM modulations and lattice code E8 for several spectral efficiencies.

In Figure 2-22, a symbol error rate comparison is performed between a classical QAM modulation and the lattice code E8 [CS98], for several spectral efficiencies. Depending on the encoding techniques, lattice codes are not always performing better than QAM (as when 1 bit/dimension is transmitted). Moreover, the best encoding technique, namely “nested shaping”, performs better than the other ones for spectral efficiencies greater or equal to 2 bits per dimension. The benefit of the lattice code in this context is revealed as the spectral efficiency is increased. The reason is that the higher density of Lattice E8 (compared to QAM) is revealed when the number of points selected for transmission is higher.

2.10 Advanced transceiver design

Two different schemes in the transceiver design are considered in this section. First simultaneous transmission and reception is investigated for short range communication. The main bottleneck is the self-interference caused to the receiver side by the considerably strong transmit signal of the same terminal. More specifically an underlay device to device (D2D) link performance is analysed under different self-interference conditions taking cellular link into account. Next a multi rate equalizer is proposed to mitigate intersymbol interference (ISI) as an alternative to OFDM based multicarrier systems. Traditionally the complexity of equalizers has been the main disadvantage for moving away from single carrier communication for high data rate applications.

2.10.1 Full Duplex TRX

We investigate the feasibility of full duplex (FD) communications, in underlay D2D networks [HRL14]. We study the sum ergodic rate of an underlay D2D network when D2D users operate in FD mode and compare the performance to a HD underlay D2D network with equivalent total energy and radio frequency (RF) hardware complexity. Furthermore, we compare the performance of both HD and FD D2D networks to a conventional cellular network. Next, we analyse the case when transmit power adaptation is used at the D2D nodes to maintain a maximum interference constraint on the cellular network. Our analytical results can be used to identify when FD networks are advantageous to improve the overall system sum-rate.

SYSTEM MODEL

In this section, we present the network models used for our analytical study. We consider a single circular cell with radius Rc with BS located at the centre of the cell. A single cellular user (CU) and a pair of D2D users (D1 and D2) are located inside the cell. The D2D pair is assumed to be operating using the same resources as the uplink of the CU. We assume that the transmitters do not have channel state information (CSI). Two communication modes are considered for the D2D pair.

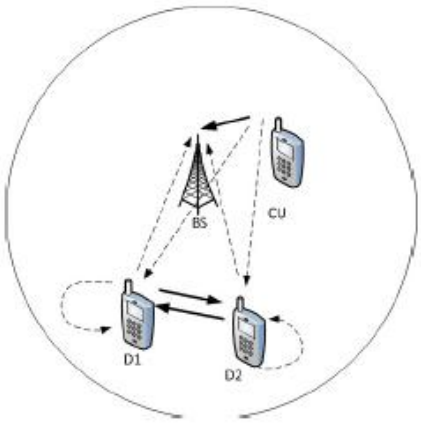

Figure 2-23: Underlay D2D network model, where the solid lines denote the desired signals and the dashed lines denote the interference links.

1) FD Mode: In the FD mode, both D2D users transmit and receive at the same time instant using the same frequency band. We assume a 1X1 FD D2D system where each node requires 1 up-converting RF chain for TX, 1 down-converting RF chain for RX and 1 up-converting RF chain for SI cancellation. A total transmission period of T seconds is considered. The available power at D2D nodes is P_d. Therefore, the total energy consumed by the D2D pair in the FD mode is $2P_dT$.

2) HD Mode: In the HD mode, each D2D user transmits for T_2 time period. In order to make a fair comparison between the FD mode and the HD mode, we assume that both systems have equal RF hardware complexity. Since in the FD mode, a D2D node uses 2 up-converting RF chains and 1 down-converting RF chain, similar to [DMK13], we define an equivalent HD system with two up-converting RF chains for TX and one down-converting RF chain for RX. Therefore, the RF equivalent HD system for 1X1 FD pair is a 2X1 multiple-input single-output (MISO) system. In order to keep the total energy consumption of the two modes equal, each antenna transmits with power P_d with unit energy symbols, such that the total energy consumed is $2P_dT$.

In the first stage of this work, we assume that there is no interference coordination between the cellular network and the D2D pair. The channels between all the entities are assumed to be flat Rayleigh faded with average fading power of unity. We assume a log-distance path loss model with reference distance of 10 m. The performance metric we are interested in is the sum ergodic rate of the network. We derive closed-form expressions for the sum ergodic rate for both FD and HD modes. Furthermore, to understand the feasibility of D2D networks over conventional networks, we compare both FD and HD D2D systems with a two-way relay network (TWRN), where the BS acts as a relay between the two D2D users to facilitate the data exchange in a spectrally efficient manner.

NUMERICAL RESULTS

Here we provide some numerical results to verify the analysis. For our numerical results, we assume a circular cell of radius 250 m. The CU location is uniformly distributed at a distance r_1 from the BS. The position of the D2D pair is fixed at a distance r_2 from the BS. Carrier frequency of 2.4 GHz is used for path loss calculations with path loss exponent of 2. The D2D pair is assumed to be located 10 m apart from each other. The transmit power of the CU is set to 24 dBm.

Noise variance N_0 is assumed to be -116.4 dBm. In all simulation results, 10000 random CU locations were used with 1000000 independent channel realizations. MATLAB software is used to perform the simulations and to compute the theoretical values of sum ergodic rates.

Figure 2-24 shows the sum rate performance comparisons for each mode as a function of the distance of the D2D pair from the BS. Transmit power of the D2D users is set to 20 dBm with no maximum interference constraint. The CU is located near the BS at a distance of 75 m. One can observe that the theoretical results are in excellent agreement with the simulation results. It can be observed that the D2D communication is beneficial when the users are closer to the cell edge. The HD mode outperforms FD mode when the self-interference cancellation is below 75 dB.

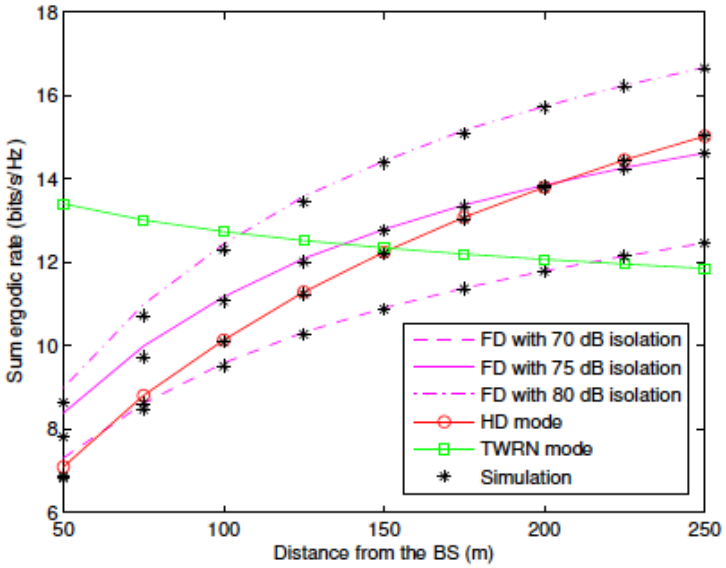

Figure 2-24: The sum ergodic rates of the system as a function of the distance of D2D pair from the BS.

2.10.2 Multi-rate Equalizer for Single-Carrier Communications

Single-carrier (SC) communications enjoy various advantages over multi-carrier (MC) communications such as lower peak-to-average power ratio (PAPR) and better time-frequency localization. These two factors lead to cheaper and more power efficient transceivers. Therefore, SC communications is a viable alternative for D2D, MMC, and V2V communications. However, the advantages of the SC communications come at the cost of inter-symbol interference (ISI) which requires an equalizer at the receiver side. Although trellis based equalization algorithms provide optimal performance, the computational complexity of these equalizers is prohibitively high. Therefore, linear equalizers that have performance far from being optimal, are employed in practice. The suboptimal performances of linear equalizers have to be compensated by using error-correction codes with coding rates much lower than the capacity of the ISI channel. Therefore, the equalizers are the bottleneck in SC communications, which prevents the throughput of the SC systems achieving the one of the MC communications. If better practical equalizers are developed for SC communications, throughput of the SC communications can approach the throughput of the MC systems. [BDFT10]. Throughput of the SC systems can even surpass their MC counterparts if power-amplifier inefficiencies due to MC transmission is taken into account.

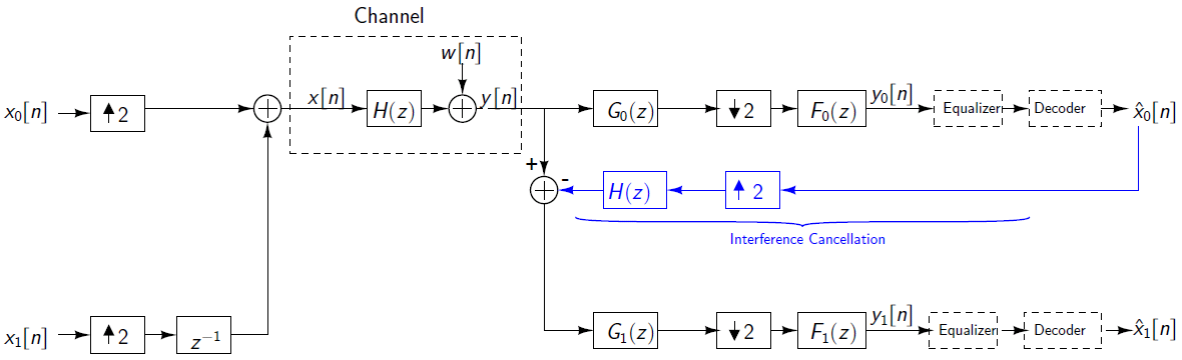

Figure 2-25: Block diagram of decomposition of a channel into two parallel sub-channels.

A multi-rate equalizer is proposed in [BJ13] to handle the ISI problem encountered in SC communications. This equalizer decomposes the original channel into two half-rate channels as shown in Figure 2-25. The first one of these channels is the equivalent channel between $x_0[n]$ and $y_0[n]$ and the second channel is the one between $x_1[n]$ and $y_1[n]$. Notice that no transmit filter bank is employed in this system. Thanks to this fact PAPR is not increased. Furthermore, due to this fact, both channels use the entire bandwidth and the two channels are not necessarily orthogonal.

The transfer functions of the receive filter bank depend on the channel transfer function and the aim of the receive filter bank is not to cancel ISI. The aim of $G_0(z)$ is suppressing the interference due to $x_1[n]$ prior to downsampling. $G_0(z)$ makes the additive noise colored and $F_0(z)$ whitens it after downsampling. The output of this whitening filter, $y_0[n]$, can be regarded as the output of a channel whose input is $x_0[n]$. The equivalent channel between $x_0[n]$ and $y_0[n]$ still suffers from ISI and needs to be further equalized. However, at this point we assume that we have an equalizer and decoder that correctly detects $x_0[n]$. This assumption allows us to perform interference cancellation in the detection of $x_1[n]$. Since $G_1(z)$ receives an interference free signal, its aim is not interference suppression but to make sure that sufficient statistics are preserved in the downsampling operation. The job of $F_1(z)$ is to whiten the noise which is colored by $G_1(z)$. The equivalent channel between $x_1[n]$ and $y_1[n]$ constitutes the second channel that can be synthesized out of the original channel. Notice that this channel also suffers from ISI and needs further equalization.

The half-rate channels synthesized out of the original channel can be further decomposed to 2^M parallel channels of rate 2^{-M} by applying the very same idea recursively. Empirical results shown in the annex demonstrate that all of these parallel channels tend to become memoryless as M increases regardless of the original channel transfer function. Hence, the channel equalization goal is achieved. The only requirement for achieving this goal is that the transmitted signal must be generated by multiplexing independently encoded signals. This equalizer does not put any stress on channel coding. Any good code that is designed for flat channels can be employed.

Theoretical achievable rates with this equalizer are numerically evaluated. The results indicate that even for channels with severe ISI, the MRE can get close to the independent identically distributed (i.i.d.) rate of the channel by employing channel codes designed for flat channels. In this respect, MRE clearly outperforms linear equalizers and it even outperforms the genie aided decision feedback equalizer.

Every filter and downsampler occurring in the block diagram shown in Figure 2-25 can be trivially implemented in frequency domain. Therefore, MRE has a complexity in the order of linear equalizers that is $N \log N$ where N is the FFT size. The complexity increases only linearly with M which is quite manageable. Furthermore, all of the filters occurring in MRE have causal and stable nature. Therefore, they can be implemented in frequency domain evenif a cyclic prefix is not transmitted via overlap-add and overlap-save methods.

2.11 Multiple Access

The scenarios in METIS envision ultra-dense networks handling large number of simultaneous transmissions in a small geographical area thereby posing new challenges for the multiple access (MA) where large number of users connect to the cloud, D2D and massive set of machine to machine (M2M) communications takes place. Massive sets of MTC devices force great demands for current multiple access schemes that need to be evolved to permit the deployment of MMC. Non-orthogonal design of multiple access can potentially increase system capacity and spectrum efficiency while exploiting the expected future evolution in the receiver processing capability. Relaxed synchronization requirements between users/services

as well as a flexible system design are also desirable in order to adapt the amount of overheads and signalling. Considering the already congested frequency spectrum, a reliable communication is possible by using the underutilized white spaces. This needs a frequency agile front end and MA using such architecture as well as an opportunistic MA for a cognitive architecture.

2.11.1 Non- and quasi-orthogonal multiple access allowing spectrum overload

Non-Orthogonal Multiple Access (NOMA)

Technology description and enablers

As a downlink multiple access, non-orthogonal multiple access (NOMA) is proposed where multiple users are multiplexed in the power-domain on the base station side and multi-user signal separation at the UE side is conducted based on successive interference cancellation (SIC). In addition to the signalling aspects related to NOMA are investigated in Section 2.5, multi-user transmit power allocation, MCS selection and candidate user set selection are key component technologies. At the transmitter side, based on the channel gain (SNR) feedback information from users, multi-user power allocation and MCS selection are conducted, and the user set that maximizes multi-user proportional fairness is scheduled. Dynamic switching between NOMA and OMA is introduced such that NOMA is applied only when it provides gains over OMA.

System and signal models

There are K users per cell and the total transmit bandwidth is divided into different subbands. The transmit signal at every subcarrier of a subband is a simple summation of the coded modulation symbol of all users from a scheduled user set, so that their signals are superposed in the power domain. The received signal at a UE in a subband is represented by the sum of the contribution of the superposed signals, which is impaired by the channel and a contribution given by noise plus inter-cell interference. In NOMA, users with high channel gain and low channel gain are paired. At the UE with high channel gain, SIC receiver is applied in order to first cancel interference from the UE with low channel gain (high transmit power allocation). The UE with low channel gain simply treats interference from the signal of the UE with high channel gain (low transmit power allocation) as noise.

Objective

The objectives are to assess the system-level gains of NOMA over orthogonal multiple access (OMA) (e.g., OFDMA) and to provide a design of its radio interface.

Main results

Using computer simulations, for a 1x2 SIMO system with BW=10 MHz, K=10 UEs, maximum multiplexing order m=1 or 2 or 3 (m=1 corresponds to OMA), and wideband user scheduling, NOMA performance is evaluated. As a multi-user power allocation, FTPA (fractional transmit power allocation) is used. According to Figure 2-26 (a), the performance gains in the overall cell throughput and cell-edge user throughput for NOMA over OMA for m = 2 (m = 3) are approximately 27% (28%) and 34% (39%), respectively. In addition, the performance of NOMA was also evaluated for different average cell-edge user throughputs as shown in Figure 2-26 (b). NOMA provides much higher gains in terms of cell throughput with higher target average cell-edge user throughput.

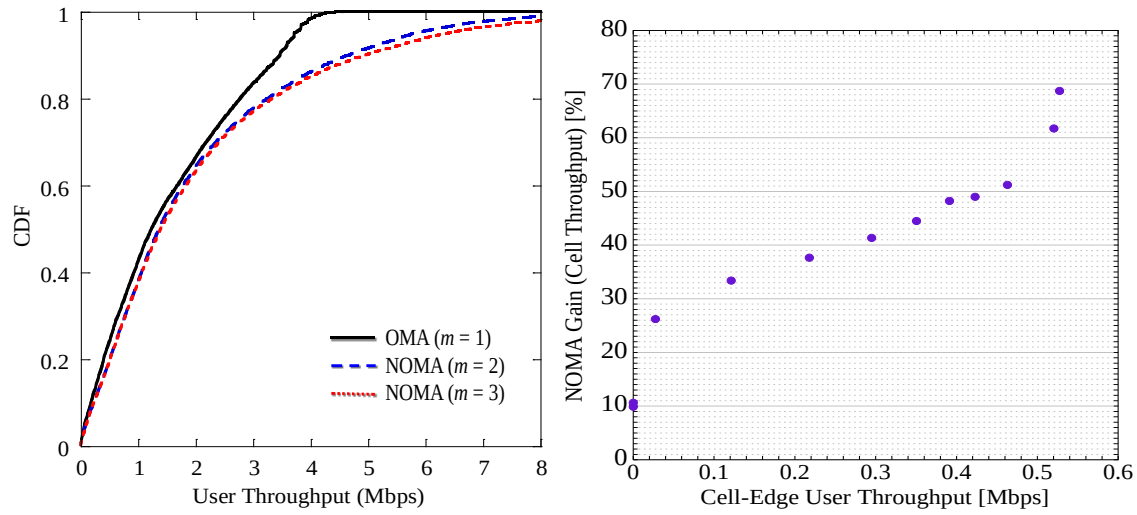

Figure 2-26: left: CDF of user throughput for OMA (*m* = 1) and NOMA (*m* = 2 or 3). right: NOMA (*m* = 2) gains in terms of cell throughput vs. cell-edge user throughput.

UL SCMA Random Access

Sparse code multiple access (SCMA) is a new frequency domain non-orthogonal waveform which offers better spectrum efficiency due to shaping gain of multi-dimensional constellations and allows overloaded non-orthogonal multiple access due to superposition of sparse codewords. As illustrated in Figure 2-27, over each SCMA layer, the SCMA modulator directly maps a block of coded bits to a complex multi-dimensional codeword selected from a layer specific SCMA codebook. Different codewords can be assigned to a user or different users. One application scenario of SCMA is grant-free UL random access where each SCMA layer represents a user. Since the number of multiplexed users can be more than the spreading factor, SCMA based non-orthogonal multiple access scheme can support more connected devices within each scheduling interval. A blind multi-user reception technique is applied to detect users' activities and extract the original data streams from the received signal. Sparsity of SCMA codewords helps to reduce the complexity of the joint detection. This technique is applicable to both mobility and stationary scenarios with timing synchronization maintained.

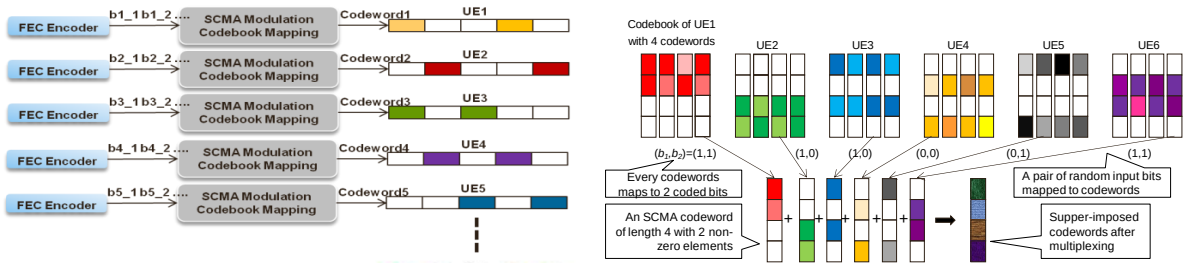

Figure 2-27. SCMA modulation and multiple access using non-orthogonal multiplexing of codewords in the frequency domain. Sparsity facilitates efficient joint detection.

System level evaluations are performed to compare SCMA based and OFDMA based UL random access schemes in terms of supported system loading considering QoE requirements such as maximum latency and average packet drop rate of the overall system. The details of the simulation assumptions and methodology are described in the annex. In SCMA case, users share the same time/frequency resources while they are separated in the code domain. Users randomly pick a codebook set, and transmit one layer of SCMA signal to the target cell. The instantaneous loading of the system depends on the number of active users in each particular transmission time period. An advanced multiuser detector blindly detects the active

users and their corresponding data streams even if users randomly select the same codebook sets. Therefore, the SCMA system is able to tolerate more collisions between users and meanwhile maintain the good quality of detection with affordable complexity due to sparsity of the colliding codewords. For example with 6 QPSK users collision, the detetion complexity of SCMA can be 150 times less than multi-user detection of multi-carrier CDMA. In the OFDMA random access scenario, a user randomly picks an RB among the available RBs for transmission. A collision happens if two or more users select the same RB for a particular transmission time. A sophisticated MLD receiver is used to separate users even if they collide, but the performance capability of the receiver is limited. In OFDMA, the complexity of multi-user MLD detection exponentially grows with the number of colliding users. In addition, some techniques can be applied to further reduce the complexity while maintaining the performance gain and other advantages of SCMA. As shown in Table 2-11, SCMA is able to support around 3 times more loading compared to OFDMA. The gain is higher with a tighter delay requirement.

Table 2-11 Supported loading for UL contention-based SCMA and OFDMA

	Avg system drop rate: ~1%	
	Latency <= 5 ms	Latency <= 10 ms
OFDMA (pkts/TTI)	2.222	2.985
SCMA (pkts/TTI)	8	9.09
SCMA capacity over OFDMA (times)	3.6	3.0

2.11.2 FBMC based multiple access and Cognitive Radio

Multiple Access using Cognitive Radio

From the study carried out from RT3, a high-IF architecture is found to be an ideal candidate for high-dynamic range front end of cognitive radio where frequency selectivity and high dynamic range is ensured under wideband conditions. A prototype of cognitive radio was designed for WLAN applications [SSA+13]. The designed TV white space converter converts the 2.4 GHz WLAN signal into white spaces between 470 MHz to 790 MHz. The complete block diagram is shown below:

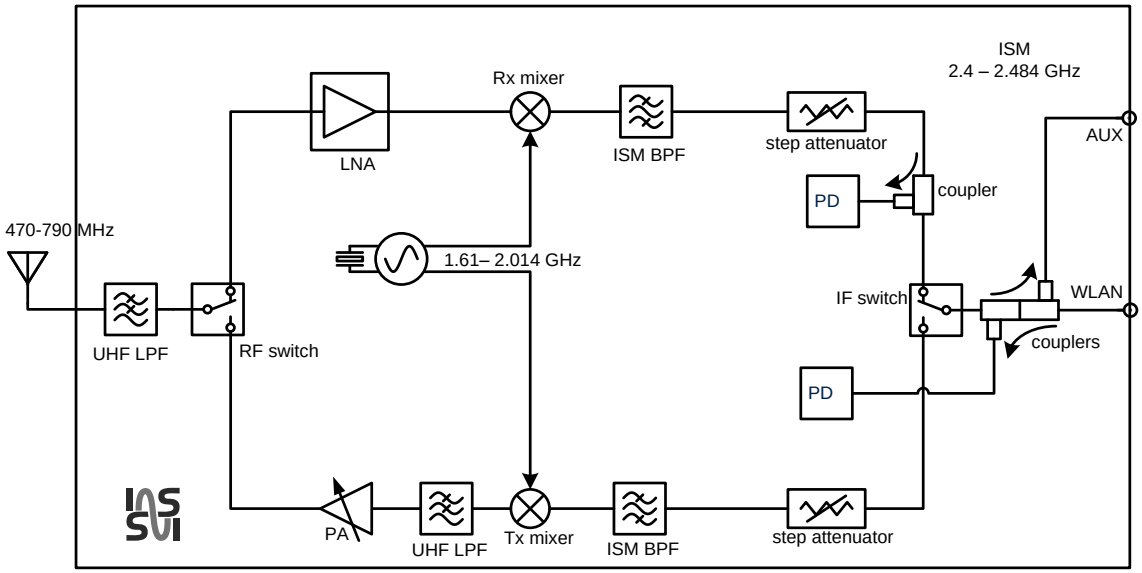

Figure 2-28: Block diagram of the Cognitive Radio front end for WLAN.

Detailed system design can be found in [SSA+13]. The system performance of the above prototype is shown in table below. The prototype is under characterization for RF and packet level performance.

Table 2-12 System performance of 802.11 Cognitive radio.

Parameters	WLAN 802.11b/g	System Performance
Sensitivity	-80 dBm to -66 dBm	-91 dBm
Noise Figure	11 dB to 19 dB	4 dB
Tx power	20 dBm	23 dBm

Precoding and Receiver Processing for Multiple Access MIMO FBMC Systems

The downlink multiple access is considered with different processing techniques to alleviate interference. A multicarrier MIMO-FBMC system with 2M subcarriers is studied (the details of the FBMC system are given in annex 5.8). A single transmitter and 2M receivers in the downlink, each equipped with N_A antennas are considered. The subcarrier filter used is g[k] and the filter length is L. A time-invariant Rayleigh fading channel is assumed, where the channel delay spread spans Λ sampling intervals and where all antenna paths undergo independent fading. For the precoding methods in the downlink, perfect CSI is considered to be available at both the transmitter and the receiving users.

The BER performance is given below considering zero forcing and Tomlinson Harashima Precoding (THP) to cancel the intersymbol and intercarrier interference, employing 16 carriers for a two tap channel. The variance of the first tap is unity and other one equal to 0.2. The number of antennas, N_A is 2 and the filter length, L, is 63. The precoding technique has reduced the error floor in the MIMO FBMC system. However, this does not offer significant performance improvement over zero forcing (ZF). This is because the precoding technique cannot completely remove the interference.

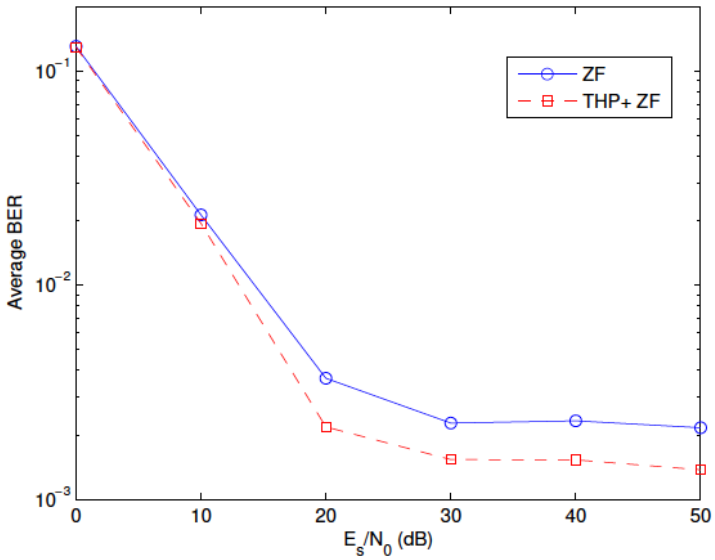

Figure 2-29: Average BER with THP and ZF

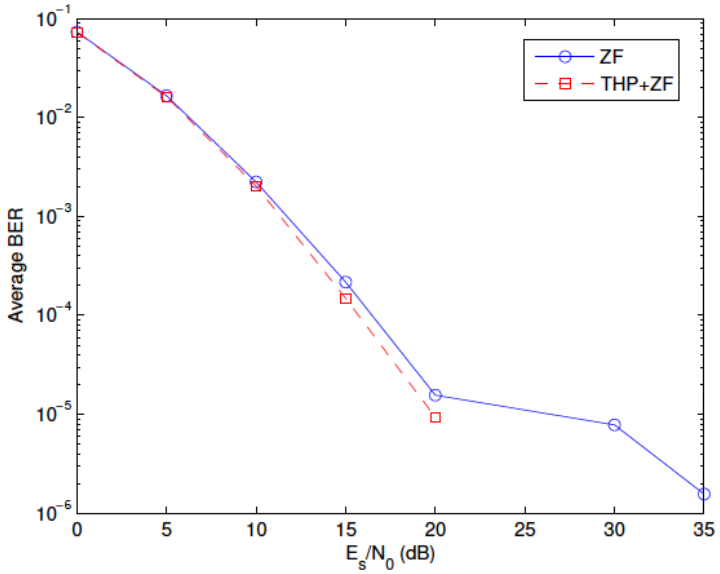

Figure 2-30: Average BER with THP precoding and power normalization

The average BER with the channel allocation with and without THP precoding is given in the previous figure for the same parameters as before. Comparing the results without the use of channel allocation algorithm, it is observed that the channel allocation algorithm lowers the error floor below 10^{-5} without the use of any precoding. The precoding appears to help lower the error rate even further.

2.12 Medium Access Control

The design of Medium Access Control (MAC) protocols that consider the novel requirements and constraints of future applications is an important part of the overall system design of a communication system for beyond 2020. Of the many use cases imaginable for future systems, only a subset will be addressed here explicitly. On the one hand, Massive Machine Communication (MMC) provides a lot of challenges in MAC design to allow the access of huge numbers of devices, which show different traffic behaviours from the usually assumed

human users (2.12.1). On the other hand, Ultra Dense Networks (UDN) also challenge classical MAC paradigms and require careful design especially when mmW (Millimetre Waves) applications are targeted (2.12.3). As synchronized time bases are at the heart of most time division MAC procedures, this topic is of high importance especially in the envisioned highly connected networks of the future (2.12.2).

2.12.1 Contention based massive access

This TeCC consists of three topics:

1. Coded Random Access
2. Coded Access Reservation
3. Advanced physical layer processing for enhanced MAC: Joint detection of node activity and data

The topic contention based massive access consists of two paradigms: random access vs. access reservation. For both, results are presented to provide a first insight which may be the best solution for MMC. Furthermore, results for advanced PHY processing for a joint detection of node activity and data are presented. This technique is very well suited for combination with (coded) random access to lower signalling overhead and increase efficiency.

Coded Random Access:

Analogies between successive interference cancellation (SIC) in slotted ALOHA (SA) framework and iterative belief-propagation erasure-decoding have been established recently, paving the way to enhance SA through application of theory and tools of erasure-correcting codes [Liv11][ZZS13+]. A notable variant of the SIC-enabled SA, called frameless ALOHA, was proposed in [SP13a]. The defining features of frameless ALOHA are: (1) users contend on a slot basis, using predefined slot access probabilities, (2) the length of the contention period (in number of slots), is not fixed a priori, but determined on-the-fly such that the expected throughput is maximized. In [SP13a] it was shown that, a simple criterion for contention termination, based on the monitoring of the fraction of resolved users F_R and instantaneous throughput T_I, coupled with an optimized slot access probability p_a, yields expected throughput T that is the highest in the reported literature for low to moderate number of contending users, i.e., when the number of users N is in the range 50 – 1000. Representative results can be found in 5.12.1.

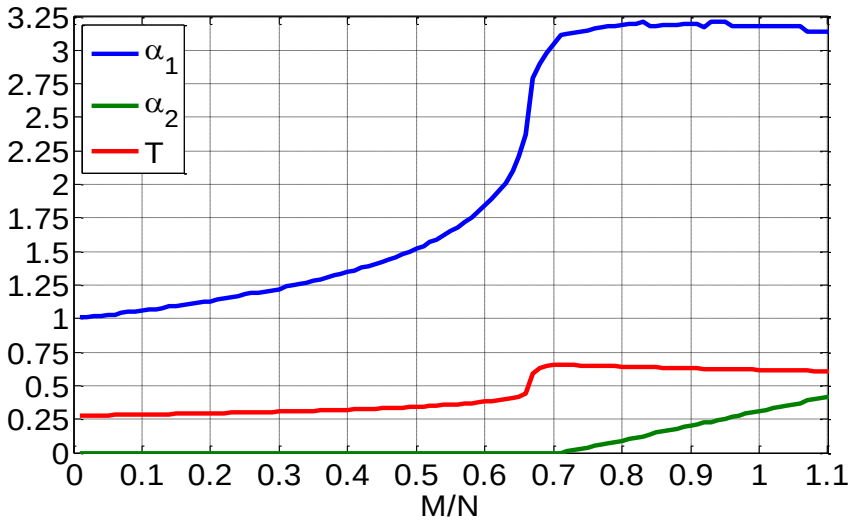

Figure 2-31: Optimal α_1, α_2, and maximal T as functions of the ratio of the number of slots M and number of users N.

A usual assumption in SIC-enabled SA is that the users perform perfect power control, such that their powers and the related packet loss probabilities at the receiving end are equal. However, this may not hold in M2M scenarios with simple terminals. Asymptotic analysis, when the above assumption does not hold was performed in [SP13b], deriving the probability of recovering user transmissions and expected throughput. Figure 2-31 presents the application of the analysis for the frameless ALOHA, in scenario with two user classes, equal fractions of users belonging to each class, and packet-loss probabilities $e_1 = 0.25$ and $e_2 = 0.5$. The aim is to obtain the optimal slot access probabilities for each class $p_1 = \alpha_1/0.5N$ and $p_2 = \alpha_2/0.5N$, such that the expected throughput T is maximised, where α_i is a suitably chosen constant that determines the slot access probability of the ith user class. An important observation can be inferred from Figure 2-31 - if the throughput maximization is the criterion for designing user access strategy, then users with worse channel should not contend, i.e., $\alpha_2 = 0$ for the overall maximum T.

Coded Access Reservation:

In this research track we consider a new class of access reservation protocols, denoted as coded reservation, where the contention phase is redefined through the introduction of coded reservation tokens, which allows the expansion of the contention space to the code domain. These coded reservation tokens are obtained by combining multiple contention frames in a virtual contention frame, and then allowing these users to select one orthogonal resource per contention frame [PTS+12, TPS+13b]. Through this procedure, the users create a coded reservation token, where the length corresponds to the number of frames within the contention frame and the set of possible codewords is denoted as codebook.

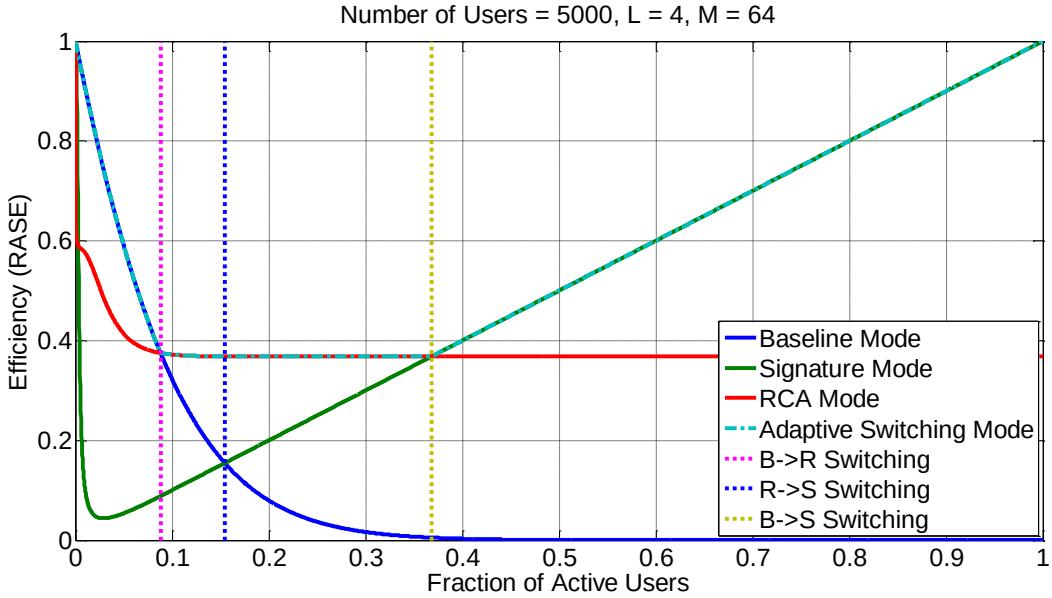

Figure 2-32: Example of different modes available with Adaptive Coded Reservation and respective switching points.

The channel that enables the Coded Access Reservation is the Multiple Access OR Channel, where the concept of superimposed codes is applicable. In particular, when the coded reservation tokens have always a single reservation token active in each contention sub-frame, then the generated codes follow the Kautz-Singleton code construction [KS64]. The Coded Access Reservation methodology enables three access modes:

- (i) access with random generated orthogonal codewords, denoted as Baseline Mode, which represents the one present in current cellular systems such as LTE [TPS+13a];
- (ii) access with random generated codewords, denoted as Random Coded Access Mode [PTS+12, TPS+13b];
- (iii) access with signatures [Gyo03], where each user has been assigned a unique access codeword, denoted as Signature Mode.

Preliminary results, such as the ones depicted in Figure 2-32: Example of different modes available with Adaptive Coded Reservation and respective switching points.Figure 2-32, show that the best suited access mode is dependent on the observed user access load (i.e. the amount of users attempting access to the system). Namely, for low, medium and high loads the suitable modes are respectively the baseline, RCA and signature modes.

The current research is focused on defining the load operating ranges and code length for a given population size, so/in order to formalize an Adaptive Switching Mode as the one depicted in Figure 2-32. The analytical tools used to analyze the performance of this scheme are based on the random codes theory.

Advanced physical layer processing for enhanced MAC:

Joint detection of node activity and data

Massive Machine Communication requires signalling-efficient MAC and PHY technologies, which are able to cope with the huge number of future MTDs in a resource efficient manner. The joint activity and data detection performed by Compressed Sensing based Multi-User Detection (CS-MUD) algorithms has been shown to approach the performance of linear estimation with known sensor activity, by exploiting the channel coding and sporadic nature of MMC traffic in an iterative feedback scheme, thus eliminating the need for signalling of sensor node activity [SBD13a]. With this approach, sensors can transmit when they need to, and the aggregation point achieves the required performance by advanced physical layer processing. Furthermore, asynchronous systems can easily be included into the processing at merely the cost of additional algorithmic complexity, while not degrading the overall performance [SBD13b]. However, some knowledge about the maximum delay is required, which can be achieved by either system design or appropriate estimation techniques. Finally, very simple channel estimation can be achieved by the addition of pilots to very short additional frames, in the order of ¼th of the resources required for transmitting the data [SBD13c]. Depending on system requirements, various trade-offs between performance and channel estimation overhead can be chosen for a given SNR working point.

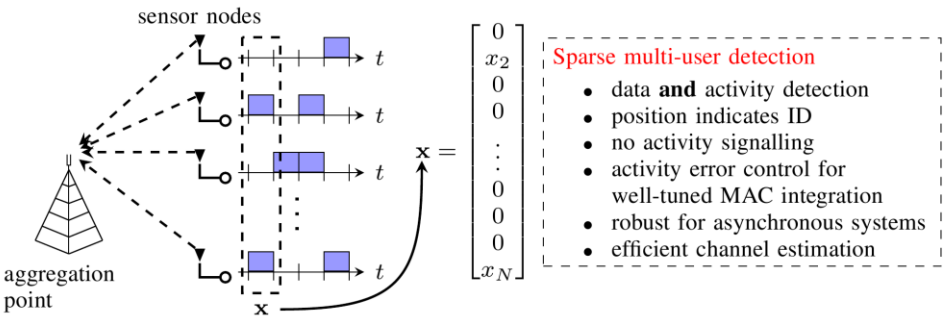

Figure 2-33: MMC System with sporadic traffic

Dealing with joint activity and data detection involves also, besides data errors, activity errors. These error events can be subdivided into false alarm and missed detection errors. It can be assumed that missed detection errors severely affect the system performance as they result in

a loss of data. Therefore, [MBD13] shows how these activity error rates can be controlled at the physical layer. In particular the authors introduce a so called Bayes-Risk detector that allows controlling of false alarm and missed detection errors. This technique allows to predefine certain false alarm error rates that must not be exceeded by the physical layer. For more details and performance evaluation, see annex 5.12.1.

2.12.2 Distributed network synchronization

TDMA requires, by definition, network synchronization. For networks without a central controller or with only limited contact with a central controller, the nodes need to agree on a common clock in a distributed fashion. This is a more challenging problem and is needed in METIS to manage D2D links when the D2D nodes have limited or no contact with the fixed infrastructure.

Based on a practical random broadcast mechanism of message transmission, which is specified in [IEEE-802.11], a novel distributed consensus clock synchronization algorithm is proposed. It is fully distributed in the sense that all the nodes independently execute the same algorithm without the need of a network hierarchy, and it is thus robust to node failures and changing topologies. The key feature of the proposed scheme is that it distinguishes between two different updates—partial update and complete update—for different situations. In partial update, only logical clock offset is changed; while in complete update, both logical clock offset and logical clock frequency are adjusted. In this way, the proposed synchronization scheme can both avoid the problem of frequency over-adjustment and improve the speed of synchronization error decrease. In the absence of transmission delays, the convergence of the proposed synchronization scheme can be theoretically proved. Moreover, by utilizing a threshold for clock update, the proposed scheme reveals robustness even when transmission delays are present. For more details and performance evaluation, see annex 5.12.2.

2.12.3 MAC for UDN and mmW

A layered resource management is proposed for the UDN scenario from spectrum availability to the physical layer as shown in Figure 2-34. The different protocol layers operate at different time scales. Spectrum controller [MET317-D51] is slowest and determines spectrum resources a UDN may use. The UDN Resource Coordination functionality determines communication routes for wireless self-backhaul and performs a partial resource assignment. The MAC determines the actually used resources on which the PHY operates.

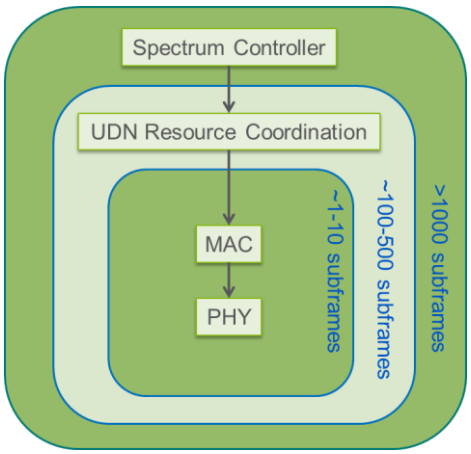

Figure 2-34: Layered resource management in a scheduling unit (called subframe assuming 12.5µs here)

Two key technology components in UDN suggest different MAC approaches. Wireless self-backhauling leads to some kind of mesh structure speaking in favour of distributed MAC.

High-gain beamforming to compensate for higher path-loss at higher frequencies speaks in favour of centralised MAC solution since distributed MAC proposals often suffer from hidden node problems. A template-frame based MAC with flooding is proposed in link level assignment. An additional option/feature is proposed to use a less detailed template-frame with contention based access inside the cluster. The latter utilizes a separate narrow band control channel for gaining access to the media and a separate contention free data channel to mitigate the high probability of collisions for standard contention based schemes at high loads.

The UDN Resource Coordination functionality provides a template frame that is to be used on a long timescale (about 100-500 x12.5µs) to coordinate the transmissions in the UDN. The template frame provides information on allocated, shared and prohibited resources for each link (for each direction from the viewpoint of a node). For the allocated resources the template frame also provides information on which communication route is allocated to the resource.

When the MAC layer in a node intends to access a shared resource it has to announce the intent to the other nodes that share the resource. This announcement is done via flooding using the regular high capacity data channels to the other nodes in the UDN. This procedure delays the access to the shared resources but it allows the network to ensure that no transmission degrades system performance. The proposed flooding scheme prioritizes nodes close to an aggregation node with a wired backhaul; thereby the probability of generating bottlenecks (that would limit the capacity to an entire part of the UDN) is kept low.

In the contention-based option, the UDN Resource Coordination functionality provides the template frame to a cluster of nodes allowing contention based access inside the cluster.

For more details and performance evaluation, see annex 5.12.3.

2.13 Hybrid Automatic Repeat Request (HARQ)

This section addresses different flavours of reliability-based HARQ [TVP+03] [MET13-D22] that is known to have potential for throughput improvements over conventional HARQ on the order of 25% [CWP03] to 35% [WWD+14]. Throughput performance is assessed for a first HARQ scheme, denoted as Incremental Redundancy with Backtrack Retransmission [Pop14], dealing with the fact that the actual channel quality is never known at the time of transmission and introducing a new way to use channel quality feedback with vector quantization. A second HARQ scheme uses a 2bit ACK/NACK for the reliability feedback [WWD+14], and the performance of asymmetric QPSK modulation for conveying the 2bit ACK/NACK is assessed.

Incremental Redundancy with Backtrack Retransmission

If the Channel State Information at the Transmitter (CSIT) is known before the transmission has started, then the transmitter can optimize the transmission parameters, such as the rate and the power. We consider a single antenna system and use the term CSIT to denote the SNR or SINR at the receiver, where the latter reflects the receiving conditions under interference. We consider scenarios in which CSIT becomes available to the transmitter only after the transmission is over. We introduce the concept of *backtrack retransmission (BRQ)* [Pop14], which can be seen as a new type of HARQ, capable to use the delayed CSIT in a way that approaches the average rate achieved with prior CSIT and fixed power. BRQ adapts the data rate using a fixed rate−R codebook and fixed packet length, changing only the amount of parity bits based on the delayed CSIT. By selecting asymptotically high rate R and with full posterior CSIT, the average rate becomes equal to the one with prior CSIT. The transmitter uses the information from the posterior CSIT in order to calculate how many IR bits are needed by the receiver to decode the previous packet, which is buffered at the receiver,

adds new data bits to those and sends a new packet. Eventually, when a packet is successfully decoded, the receiver uses the IR bits of the decoded packets to decode the previous packet, and continues backtracking and using the IR bits to decode all the buffered packets. However, this happens at the expense of increased delay. If a finite number F of feedback bits are available, BRQ leads to a novel transmission scheme: instead of sending feedback after each packet, which is the usual way in HARQ, the feedback bits from multiple slots are assembled and, using vector quantization, provide information relevant to a number of packets transmitted in the past.

BRQ has been evaluated by assuming Rayleigh block fading. Figure 2-35 depicts the average rate as a function of the mean SNR Γ. For each Γ, the average rate is normalized by the optimal average rate that can be achieved if CSIT is known a priori and water filling is applied. Two schemes with posterior CSIT are evaluated, full CSIT and quantized CSIT with F = 1 bit per SNR, respectively. For each scheme, two different rates are chosen, $R = \log_2(1 + 2\Gamma)$ and $R = \log_2(1 + 3\Gamma)$, respectively. As a reference, we have plotted the average rate when full CSIT is known a priori, but without water filling. When R is sufficiently high and full CSIT, the knowledge of posterior CSIT is equally useful as the prior CSIT for average SNRs Γ = 10 dB and higher. With $R = \log_2(1 + 3\Gamma)$ and full CSIT, BRQ tightly approaches the average rate obtainable by water filling for Γ equal to 20 dB or higher.

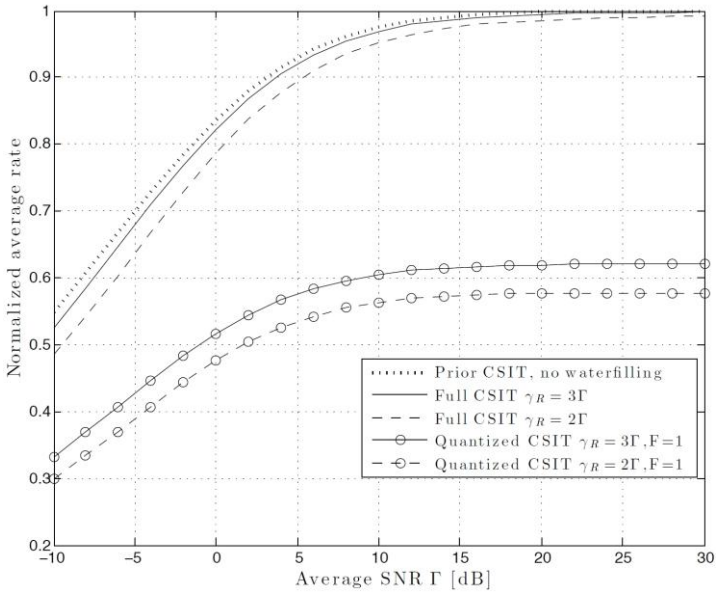

Figure 2-35: Normalized average throughput versus average SNR.

Multi-Level ACK/NACK Transmission Scheme for Reliability-Based HARQ

As shown in [WWD+14], the reliability feedback for reliability-based HARQ can efficiently be implemented by means of a 2bit ACK/NACK message with three NACK levels $\mathrm{NACK_i}, \mathrm{i} \in \{1, 2, 3\}$, de facto without impacting the data throughput while accepting a $\mathrm{NACK_i} \rightarrow \mathrm{NACK_j}$ error rate below 3-5%.

Figure 2-36 (a) shows an asymmetric QPSK (A-QPSK) modulation scheme with parameter α, and Figure 2-36 (b) shows the transmit power saving of A-QPSK over QPSK, when conveying the 2bit ACK/NACK over AWGN channel. It can be seen that A-QPSK achieves power savings over QPSK of up to ~1.38dB for conveying the ACK/NACK. This power saving is achieved by relaxing the $\mathrm{NACK_i} \rightarrow \mathrm{NACK_j}$ error rate to below 3%, while the $\mathrm{NACK} \rightarrow \mathrm{ACK}$ error

rate is below 0.1% [NKM+07]. The result is obtained numerically from approximations of the ACK/NACK error rates by assuming equal a priori probabilities of the $\mathrm{NACK_i}$.

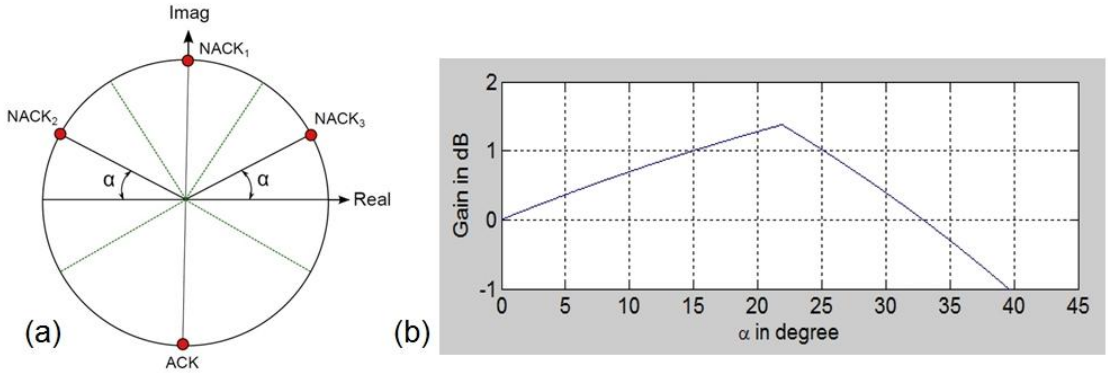

Figure 2-36: A-QPSK modulation constellation (a) and power saving over QPSK (b).

In further work, also the performance of A-QPSK modulation for conveying the 2bit ACK/NACK on LTE Physical Uplink Control Channel (PUCCH) will be assessed.

2.14 Radio link enablers for Radio Resource Management (RRM)

In order to support a smart radio resource management (RRM) algorithm for Device-to-Device (D2D) communications, channel state information (CSI) of overall cellular and D2D links are preferable if they are available at base station (BS) side. With an awareness of these channel state information, BS can allocate radio resource in a smart and global optimal manner. Therefore, an efficient signalling scheme should be designed to provide this information. In this subsection, we propose two signalling schemes for the case where D2D pairs try to reuse cellular uplink spectrum.

Signalling scheme with full channel state information

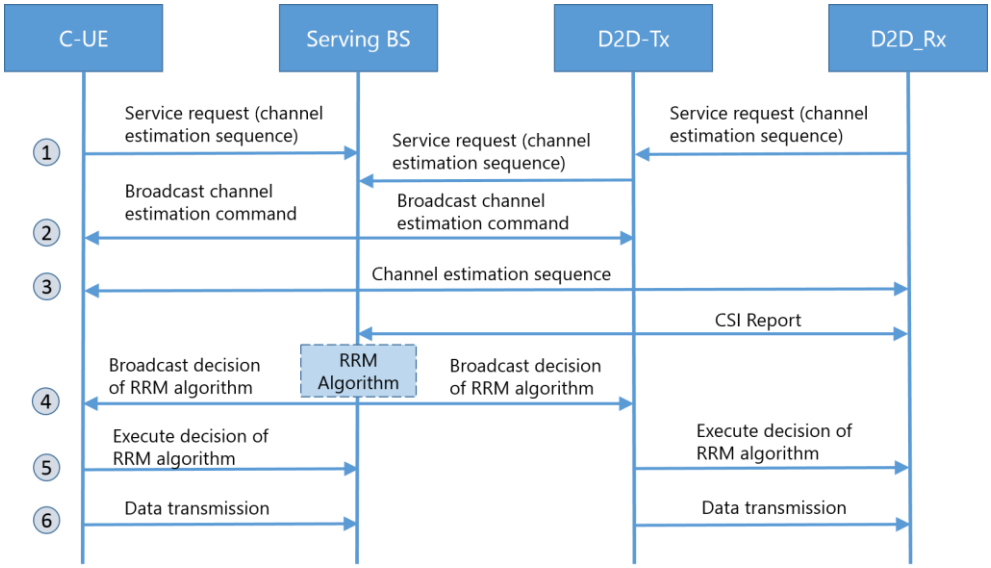

Figure 2-37: Signalling scheme for D2D communications with full CSI

As shown in Figure 2-37, we only demonstrate one cellular user and one D2D pair here. However, there will be more cellular users and D2D pairs inside one cell but we cannot show

all of them in this figure. In the first step, cellular users send service request message to BS. This message can include the channel estimation sequence and therefore BS can detect the channel gains of cellular links. Meanwhile, D2D receivers (Rx's) can also require data streams from D2D transmitters (Tx's) by sending service request messages and D2D Tx's can detect the channel gains of D2D links. By attaching information of detected channel gains and their own channel estimation sequences, D2D Tx's forward the requests to BS and BS can extract the channel gains of both D2D links and the links between D2D Tx's and BS. In the second step, BS broadcasts the channel estimation command to all cellular users and D2D Rx's. Then the cellular users will broadcast their channel estimation sequences to all D2D Rx's. As the fourth step, one D2D Rx detects the channel gains from all cellular users to itself and report these information to BS. Now BS is totally aware of all channel information, including channel gains for both the two desired links and the two interference links. Therefore a network controlled RRM can be performed in BS and then the decision will be broadcasted to cellular users and D2D Tx's. The decision shows which cellular user and which D2D link will share the same resource block. After receiving this decision message, all links execute the decision and start their data transmission.

As we can see from above steps, in order to obtain all channel information, a heavy signalling overhead is required. In the case of *N* cellular users and *M* D2D links, the first step provides $(N + 2 \times M)$ channel gain information and the forth step provides $(M \times N)$ information. The advantage of this signalling scheme is that it enables a global optimized RRM algorithm and introduces an optimal performance. However, since some of the D2D communications scenarios require a low latency and this scheme obviously introduces a large latency to set up D2D communications, it is worth to trade some performance gain by using a simpler signalling scheme.

Signalling scheme with partial channel state information

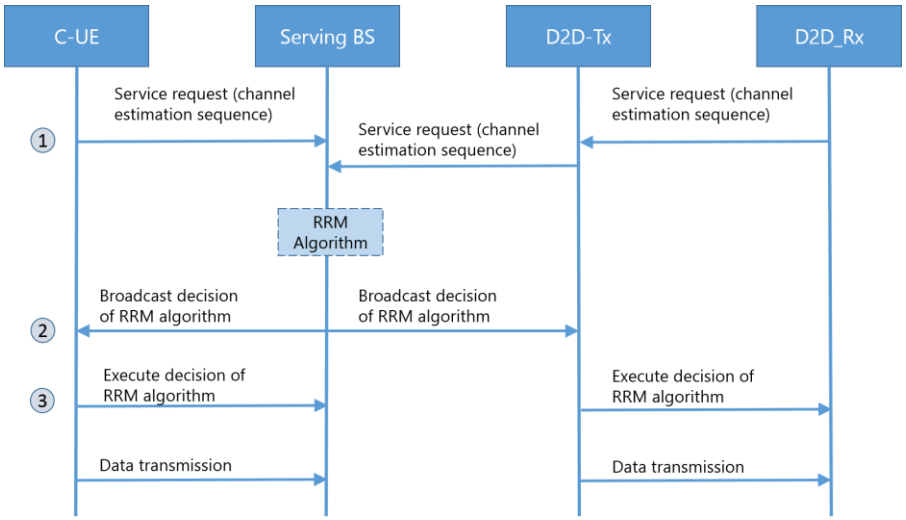

Figure 2-38: Signalling scheme for D2D communications with partial CSI

As shown in Figure 2-38, in this proposed signalling scheme, BS will only gather$(N + 2 \times M)$ channel information. And the channel gain information of interference links from cellular users to D2D Rx's are not used. Thus, the RRM algorithm either simply neglects the interference level for D2D links or uses an offset value to represent the interference level. In this scheme, a fast response time can be provided by network and therefore is applicable in some latency critical scenarios.

3 Conclusion and future work

This document is dedicated to provide the intermediate research results generated so far by the METIS radio link research. These are covering the relevant research areas required for developing a self-contained overall air interface design for 5G. Focus areas are:

1. Flexible air interface
2. Waveforms, coding & modulation and transceiver design
3. Multiple access, MAC and RRM

The first focus area elaborates on concepts for fundamental use cases of the 5G system, such as dense deployments, massive machine communications, dynamic spectrum usage and moving networks. Those concepts cover dedicated frame structures, numerology designs and the applicability of D2D in a cellular setting. Additionally, required management concepts for orchestrating multiple air interfaces are provided. Advanced signalling concepts for novel multiple access schemes and new waveforms complement the research.

The second focus area gives insights into novel concepts as well as enhancements of existing concepts related to signal design. The results given here are pinpointing schemes outperforming the state of the art (e.g. LTE) and thus proposing a redesign for 5G with respect to signal generation. Concepts are presented exceeding the state of the art in terms of throughput (FTN) for modest channel conditions and in terms of flexibility and adaptability (FBMC and UFMC), enabling the system to be more reactive and efficient. Besides enhanced modulation schemes targeting the use of low-cost power amplifiers, advanced coding schemes are presented (among them lattice coding). Advanced transceiver designs are described, evaluating the feasibility of full duplex transmissions on the one hand and multi-rate equalizers for single-carrier communication on the other, the latter providing a low-cost solution to achieve improved equalization performance based on linear receivers.

Finally, the third focus area elaborates on alternative multiple access schemes, where the orthogonality constraint is relaxed to allow for a smooth overload of the spectrum. NOMA makes use of the power domain to separate the users at the receiver, while SCMA exploits sparse codes for that purpose. Another proposal combines FBMC with downlink precoding. With cellular communications, the transmission medium is typically shared. Hence, smart medium access control (MAC) is crucial for achieving high efficiency of the scarce spectrum resources. Therefore, MAC concepts for massive machine, ultra dense and mmW scenarios are devised and analysed. HARQ is and will be an important functionality in wireless communications. Here, existing solutions are enhanced by applying reliability based measures. Finally, RRM signalling schemes for embedding D2D into a cellular network are given, enabling the network to successfully make use of spatial reuse of resources and thus increasing the global throughput.

The main body of this document has given a condensed view of the results elaborated so far. Further details can be found later in this document in the annex as well as in related publications, which have been cited in the main text.

Working towards the next deliverable D2.4, radio link research will continue on the performance evaluation of the single TeCs, refining the proposed concepts and evaluating more clearly the different proposals in the light of an overall system concept. The most promising schemes will - in conjunction with existing radio access technologies and with schemes from other METIS work packages - be chosen as the METIS recommendation for the 5G air interface, suited to address the broad range of requirements the future communication landscape is requesting.

4 References

[3GPP-R4040367] The 3rd Generation Partnership Project (3GPP), TDoc R4-040367, TSG RAN WG4 31, “Comparison of PAR and cubic metric for power derating, Tech. Doc.,” 2004.

[5GNOW-D31] Kasparick M.; Wunder G.; Chen Y. et al., "5G waveform candidate selection," 5GNOW deliverable D3.1, 2013.

[AJM13] Abdoli, M.J.; Jia, M.; Ma, J., "Weighted circularly convolved filtering in OFDM/OQAM," *Personal Indoor and Mobile Radio Communications (PIMRC), 2013 IEEE 24th International Symposium on*, pp. 657-661, 8-11 Sept. 2013.

[ARÖ13] Anderson, J.; Rusek, F.; Öwall, V., “Faster-than-Nyquist Signaling”, *IEEE Trans. Info. Theory*, vol. 101, no. 8, p. 1817-1830, Mar. 2013.

[ASH13] Ashok, A.; Subbiah, I.; Heinen, S., "System design for an experimental cognitive transceiver," *Ph.D. Research in Microelectronics and Electronics (PRIME), 2013 9th Conference on*, pp.229-232, 24-27 June 2013.

[BC11] Borkar, S.; Chien, A., “The Future of Microprocessors,”*Communications of ACM*, vol. 54, no. 5, 2011.

[BDFT10] Benvenuoto N., Dinis R., Falconer D., and Tomasin S., “Single Carrier Modulation with Nonlinear Frequency Domain Equalization: An Idea Whose Time Has Come - Again”, Proceedings of the IEEE, Vol. 98, No. 1, January, 2010

[Bid03] Bidan, R.L., “Turbo-equalization for bandwidth-efficient digital communications over frequency-selective channels”, PhD thesis, INSA de Rennes, Rennes, France, 2003.

[Bir10] Birolini, A., “Reliability engineering”, vol. 5, Berlin, Springer Verlag, 2010.

[BHW98] Benedetto, J.J.; Heil C.; Walnut, D.F., “Gabor systems and the Balian-Low theorem”, *in Gabor analysis and algorithms*, pp. 85-122, 1998.

[BJ13] Bayramoglu, M.F.; Juntti, M., "A multirate equalizer for inter-symbol interference channels based on successive interference cancellation," *Personal Indoor and Mobile Radio Communications (PIMRC), 2013 IEEE 24th International Symposium on*, pp.1472-1477, 8-11 Sept. 2013.

[BLS+13] Benjebbour, A.; Li, A.; Saito, Y.; Kishiyama, Y.,“System-level performance of downlink NOMA for future LTE enhancements,” IEEE Globecom, Dec. 2013.

[BRO02] BROADWAY, IST-2001-32686 project, WP3-D7-Release 1, "Algorithm Enhancement Definition", Nov. 2002.

[BSD13] Bockelmann, C.; Schepker, H.F.; Dekorsy A., “Compressive Sensing based Multi-User Detection for Machine-to-Machine Communication,” *Transactions on Emerging Telecommunications Technologies: Special Issue on Machine-to-Machine: An emerging communication paradigm,* 2013.

[BSK+13] Benjebbour, A.; Saito, Y; Kishiyama, Y; Li, A; Harada, A.; Nakamura, T., "Concept and Practical Considerations of Non-orthogonal Multiple Access (NOMA) for Future Radio Access," IEEE ISPACS, Nov. 2013.

[BSU14] Beygi, S.; Ström, E.G.; Mitra, U, “Geometry-based stochastic modeling and estimation of vehicle to vehicle channels.” *IEEE International Conference on*

Acoustics, Speech, and Signal Processing. May 2014. To appear.

[BTS+13] Berardinelli G.; Tavares F.M.L.; Sørensen, T.B. et al., "Zero-tail DFT-spread-OFDM signals," *Globecom Workshops (GC Wkshps), 2013 IEEE*, 9-13 Dec. 2013.

[CS98] J. H. Conway and N. J. A. Sloane, “Sphere Packings, Lattices and Groups” Springer-Verlag, NY, 1988.

[CWP03] Jung-Fu Cheng; Wang, Y.-P.E.; Parkvall, S., "Adaptive incremental redundancy [WCDMA systems]," *Vehicular Technology Conference, 2003. VTC 2003-Fall. 2003 IEEE 58th*, vol.2, pp.737-741 Vol.2, 6-9 Oct. 2003.

[DCB00] Damen, O.; Chkeif, A.; Belfiore, J.C.,“Lattice code decoder for space-time codes”, IEEE Communications Letters, 4(5): pp 161-163, 2000.

[DJB+95] Douillard, C.; Jezequel, M.; Berrou, C. et al., “Iterative correction of intersymbol interference: Turbo-equalization. European Transactions on Telecommunications”, 6(5): pp 507-511, 1995.

[DMK13] Bharadia, D., McMilin, E., and Katti, S., “Full duplex radios,” SIGCOMM Comput. Commun. Rev., vol. 43, no. 4, pp. 375–386, Aug. 2013.

[DRO10] Dasalukunte, D.; Rusek, F.; Öwall, V., "An Iterative Decoder for Multicarrier Faster-Than-Nyquist Signaling Systems," *Communications (ICC), 2010 IEEE International Conference on*, pp.1-5, 23-27 May 2010.

[DRO11] Dasalukunte, D.; Rusek, F.; Öwall, V., "Multicarrier Faster-Than-Nyquist Transceivers: Hardware Architecture and Performance Analysis," *Circuits and Systems I: Regular Papers, IEEE Transactions on*, vol. 58, no. 4, pp. 827-838, April 2011.

[E12] Everett, E., Full-Duplex Infrastructure Nodes: Achieving Long Range with Half-duplex Mobiles. Masters Thesis, Rice University., 2012, available: http://hdl.handle.net/1911/64704

[EK14] El Hefnawy, M.; Kramer, G., "Impact of Spectrum Sharing on the Efficiency of Faster-than-Nyquist Signaling," *Wireless Communications and Networking Conference (WCNC), 2014 IEEE*, April 2014.

[ET13] El Hefnawy, M.; Taoka, H., "Overview of Faster-Than-Nyquist for Future Mobile Communication Systems," *Vehicular Technology Conference (VTC Spring), 2013 IEEE 77th* , pp.1-5, 2-5 June 2013.

[FAB95] Le Floch, B.; Alard M.; Berrou, C., “Coded orthogonal frequency division multiplexing*”, proceeding of the IEEE*, vol. 83, pp. 982-996, June, 1995.

[FKB09] Fettweis, G.; Krondorf, M.; Bittner, S., "GFDM - Generalized Frequency Division Multiplexing," *Vehicular Technology Conference, 2009. VTC Spring 2009. IEEE 69th*, pp.1-4, 26-29 April 2009.

[FKH08] T. Frank, A. Klein, and T. Haustein, “A survey on the envelope fluctuations of DFT precoded OFDMA,” in Proc. International Conference on Communications ICC, Beijing, China, May 2008.

[FPS14] M. Fuhrwerk, J. Peissig, M. Schellmann, “Channel adaptive pulse shaping for OQAM-OFDM systems”, submitted to EUSIPCO 2014

[Gam10] Gamba, M.T.,“Algorithms and architectures for the detection of MIMO signals”, PhD thesis, Politecnico de Turino, 2010.

[GSG08] E. Grass, I. Siaud et al. "Asymmetric Dual-Band UWB / 60 GHz Demonstrator," in Proc. of IEEE Personal Indoor Mobile Radio Communications, PIMRC'2008.

[Gyo03] Gyori, S., "Signature coding over multiple access OR channel," *Information Theory Workshop, 2003, Proceedings IEEE*, pp.115-118, 31 March-4 April 2003.

[HAD12] Haddad, S., "Iterative receivers: scheduling, convergence speed and complexity", PhD thesis, Electronics Dept., Telecom Bretagne, 2012.

[HK12] Higuchi, K.; and Kishiyama, Y., "Non-orthogonal access with successive interference cancellation for future radio access," APWCS 2012, Aug. 2012.

[HK13] Higuchi, K.; Kishiyama, Y., "Non-orthogonal access with random beamforming and intra-beam SIC for cellular MIMO downlink," IEEE VTC Fall 2013, Sept. 2013.

[HoT03] Hochwald, B.M.; Ten Brink, S.,"Achieving near-capacity on a multiple-antenna channel", IEEE Transactions on Communications, 51(3): pp 389-399, 2003.

[HRL14] Hemachandra, K., Rajatheva, N., Latva-aho, M., "Sum rate analysis for full duplex underlay device to device networks," WCNC 2014, April 2014.

[HW11] Heinen, S.; Wunderlich, R., "High dynamic range RF frontends from multiband multistandard to Cognitive Radio," *Semiconductor Conference Dresden (SCD), 2011*, pp.1-8, 27-28 Sept. 2011.

[IEEE-802.11] IEEE Std 802.11. Wireless LAN Medium Access Control (MAC) and Physical Layer (PHY) specification, 1999 edition.

[Jaf11] Jafri, A.R.,"Architectures multi-ASIP pour turbo récepteur flexible", PhD thesis, Electronics Dept., Telecom Bretagne, 2011.

[JBG+14] N. Jamaly, R. Apelfröjd, A. Belen Martinez, M. Grieger, T. Svensson, M. Sternad and G. Fettweis, "Analysis and Measurement of Multiple Antenna Systems for Fading Channel Prediction in Moving Relays", European Conference on Antennas and Propagation, EuCAP 2014, April 6-11 2014, Hauge, The Netherlands.

[JiJ05] Jianhua, L.; Jian L., "Turbo processing for an OFDM-based MIMO system", IEEE Transactions on Wireless Communications, 4(5): pp 1988-1993, 2005.

[JoW02] De Jong, Y.L.C.; Willink, T.J.,"Iterative tree search detection for MIMO wireless systems", In Proc. of the 56th IEEE Vehicular Technology Conference (VTC-Fall), volume 2, pp 1041-1045, 2002.

[KB12] Kim, Y.J.D.; Bajcsy, J., "Iterative receiver for faster-than-Nyquist broadcasting," *Electronics Letters* , vol. 48, no. 24, pp.1561-1562, November 22nd 2012.

[KMM03] Kavcic, A.; Xiao Ma; Mitzenmacher, M., "Binary intersymbol interference channels: Gallager codes, density evolution, and code performance bounds," *Information Theory, IEEE Transactions on*, vol.49, no.7, pp.1636-1652, July 2003

[KS64] Kautz, W.; Singleton, R., "Nonrandom binary superimposed codes," *Information Theory, IEEE Transactions on*, vol.10, no.4, pp.363-377, Oct 1964.

[LG03] Liveris, A., D., and Georghiades, C., N.,; 'Exploiting faster-than-Nyquist signaling', IEEE Trans. Comm., vol. 51, no. 9, pp. 1502-1511, 2003.

[Liv11] Liva, G., "Graph-Based Analysis and Optimization of Contention Resolution Diversity Slotted ALOHA," *Communications, IEEE Transactions on*, vol.59, no.2, pp.477-487, February 2011.

[LLL05] C. Laot, R. Le Bidan, and D. Leroux, "Low Complexity MMSE Turbo Equalization: A Possible Solution for EDGE" IEEE Transactions on Wireless Communications, 4(3):pp 965-974, May 2005.

[LLS08] Lin, H., Lele, C., and Siohan, P., "Equalization with interference cancellation for hermitian symmetric ofdm/oqam systems," in IEEE International Symposium on Power Line Communications and Its Applications, 2008. ISPLC 2008., 2008, pp. 363–368.

[LPB+13] Laehetkangas, E.; Pajukoski, K.; Berardinelli, G. et al, "On the Selection of Guard Period and Cyclic Prefix for Beyond 4G TDD Radio Access Network," *Wireless Conference (EW), Proceedings of the 2013 19th European*, pp.1-5, 16-18 April 2013.

[LPT+13] Lahetkangas, E.; Pajukoski, K.; Tiirola, E. et al., "On the TDD subframe structure for beyond 4G radio access network," *Future Network and Mobile Summit (FutureNetworkSummit), 2013*, pp.1-10, 3-5 July 2013.

[LPV+14] Lahetkangas, E.; Pajukoski, K.; Vihriälä J. et al., "Achieving low latency and energy consumption by 5G TDD mode optimization", accepted in ICC 2014, workshop on 5G technologies.

[LS14] Lin H.; Siohan P., "An advanced Multi-Carrier Modulation for Future Radio Systems", to appear in ICASSP'14.

[Mas05] Le Masson, J., "Systèmes de transmission avec prcodage linaire et traitement itératif", PhD thesis, Electronics Dept., Telecom Bretagne, 2005.

[MBD13] Monsees, F.; Bockelmann, C.; Dekorsy, A., "Joint activity and data detection for machine to machine communication via Bayes Risk optimization," *Signal Processing Advances in Wireless Communications (SPAWC), 2013 IEEE 14th Workshop on*, pp. 435-439, 16-19 June 2013.

[MBH13] Matz, G.; Bolcskei, H.; Hlawatsch, F., "Time-Frequency Foundations of Communications: Concepts and Tools," *Signal Processing Magazine, IEEE*, vol. 30, no. 6, pp. 87-96, Nov. 2013.

[MBW13] Monsees, F.; Bockelmann, C.; Wubben, D.; Dekorsy, A., "Compressed Sensing Bayes Risk Minimization for Under-Determined Systems via Sphere Detection," *Vehicular Technology Conference (VTC Spring), 2013 IEEE 77th*, pp.1-5, 2-5 June 2013.

[MET13-D11] ICT-317669-METIS/D1.1: Scenarios, requirements and KPIs for 5G mobile and wireless system.

[MET13-D21] ICT-317669-METIS/D2.1: Requirements analysis and design approaches for 5G air interface.

[MET13-D22] ICT-317669-METIS/D2.2: Novel radio link concepts and state of the art analysis.

[MET13-D5.1] ICT-317669-METIS/D5.1: Intermediate description of the spectrum needs and usage principles.

[MKL+12] Michailow, N.; Krone, S.; Lentmaier, M., "Bit Error Rate Performance of Generalized Frequency Division Multiplexing," *Vehicular Technology Conference (VTC Fall), 2012 IEEE*, pp.1-5, 3-6 Sept. 2012.

[MMM+12a] Michelusi, N.; Mitra, U.;Molisch, A., "UWB sparse/diffuse channels, part I: Channel models and Bayesian estimators," IEEE Trans. Signal Process., vol. 60, no. 10, pp. 5307-5319, 2012.

[MMM+12b] Michelusi, N.; Mitra, U.; Molisch, A., "UWB sparse/diffuse channels, part II: Estimator analysis and practical channels," IEEE Trans. Signal Process., vol. 60, no. 10, pp. 5320-5333, 2012.

[MS10] McGuire, M.; Sima, M., "Discrete Time Faster-Than-Nyquist Signalling," *Global Telecommunications Conference (GLOBECOM 2010), 2010 IEEE*, pp. 1-5, 6-10 Dec. 2010.

[NKM+07] NTT DoCoMo, KDDI, Mitsubishi Electric, NEC, Panasonic, Sharp," Repetition of ACK/NACK in E-UTRA Uplink," 3GPP R1-070101, 2007.

[NP00] R. van Nee and R. Prasad, OFDM for Wireless Multimedia Communications, 1st ed. Artech House, 2000.

[PAR08] Prlja, A.; Anderson, J.B.; Rusek, F., "Receivers for Faster-than-Nyquist signaling with and without turbo equalization," *Information Theory, 2008 IEEE International Symposium on*, pp. 464-468, 6-11 July 2008.

[Pop14] Popovski, P., " Delayed Channel State Information: Incremental Redundancy with Backtrack Retransmission," accepted at IEEE ICC 2014, available at http://arxiv.org/abs/1401.6846.

[PP14] Pratas, N.K., Popovski, P., "Underlay of Low-Rate Machine-Type D2D Links on Downlink Cellular Links", accepted on M2M-IoT workshop in ICC 2014.

[PS11] D. Pinchon and P. Siohan, ''Oversampled paraunitary DFT filter banks: A general construction algorithm and some specific solutions'', *IEEE trans. on Signal Processing*, Vol. 59, N° 7, pp. 3058-3070, July 2011.

[PSS13] D.-T. Phan-Huy, M. Sternad and T. Svensson, "Adaptive Large MISO Downlink with Predictor Antenna Array for Very Fast Moving Vehicles", 2013 International Conference on Connected Vehicles (ICCVE'2013), Las Vegas, December 2013.

[PTM10] Pande, H.K.; Thapliyal, S.; Mangal, L. C., "A new clock synchronization algorithm for multi-hop wireless ad hoc networks," *Wireless Communication and Sensor Networks (WCSN), 2010 Sixth International Conference on*, pp.1-5, 15-19 Dec. 2010.

[PTS+12] N. K. Pratas, H. Thomsen, C. Stefanovic, and P. Popovski, "Code-expanded random access for machine-type communications," in Globecom Workshops (GC Wkshps), 2012 IEEE, pp. 1681–1686, 2012.

[RA09] Rusek, F.; Anderson, J., "Constrained Capacities for Faster-than-Nyquist Signaling", *IEEE trans. Info. Theory,* vol. 55, no. 2, pp. 764-775, Feb. 2009.

[RA09b] Rusek, F.; and Anberson, J,; 'Multistream faster than Nyquist signaling', IEEE Trans. Comm., vol. 57, no. 5, pp 1329-1340, May 2009.

[RGA02] Reid, A.B.; Grant, A.J.; Alexander, P.D., "List detection for multi-access channels," *Global Telecommunications Conference, 2002. GLOBECOM '02. IEEE*, vol. 2, pp. 1083-1087, 17-21 Nov. 2002.

[S13] Sugiura, S.; 'Frequency-Domain Equalization of Faster-than-Nyquist Signaling', IEEE Wireless Communication Letters, 2013, Vol. 2, Issue 5, pp. 555-558.

[SBD13a] Schepker, H.F.; Bockelmann, C.; Dekorsy, A., "Improving Greedy Compressive Sensing Based Multi-User Detection with Iterative Feedback," *Vehicular Technology Conference (VTC Fall), 2013 IEEE 78th*, pp.1-5, 2-5 Sept. 2013.

[SBD13b] Schepker, H.F.; Bockelmann, C.; Dekorsy, A., "Coping with CDMA Asynchronicity in Compressive Sensing Multi-User Detection," *Vehicular Technology Conference (VTC Spring), 2013 IEEE 77th*, pp.1-5, 2-5 June 2013.

[SBD13c] Schepker, H.F.; Bockelmann, C.; Dekorsy, A.,"Exploiting Sparsity in Channel and Data Estimation for Sporadic Multi-User Communication," *Wireless Communication Systems (ISWCS 2013), Proceedings of the Tenth International Symposium on*, pp.1-5, 27-30 Aug. 2013.

[SBK+13] Saito, Y.; Benjebbour, A.; Kishiyama, Y.; and Nakamura, T.,"System-level performance evaluation of downlink non-orthogonal multiple access (NOMA)," IEEE PIMRC 2013, Sept. 2013.

[SD11] Schepker, H.F.; Dekorsy, A.,"Sparse Multi-User Detection for CDMA transmission using greedy algorithms," *Wireless Communication Systems (ISWCS), 2011 8th International Symposium on*, pp.291-295, 6-9 Nov. 2011.

[SE10] T. Svensson, T. Eriksson, "On Power Amplifier Efficiency with Modulated Signals," Vehicular Technology Conference (VTC 2010-Spring), 2010 IEEE 71st , vol., no., pp.1,5, 16- 19 May 2010.

[SF11] Schenato, L.; Fiorentin, F., "Average timesynch: A consensus-based protocol for clock synchronization in wireless sensor networks," Automatica, vol. 47, no. 9, pp. 1878–1886, September 2011.

[SGA+12] M. Sternad, M. Grieger, R. Apelfröjd, T. Svensson, D. Aronsson and A. Belén Martinez, Using "Predictor Antennas for Long-Range Prediction of Fast Fading for Moving Relays", IEEE Wireless Communications and Networking Conference (WCNC'2012), 4G Mobile Radio Access Networks Workshop , Paris, April 2012.

[SGS+13] Sun, W.; Gholami, M.R.; Strom, E.G. et al., "Distributed clock synchronization with application of D2D communication without infrastructure," in *Proceedings of IEEE Global Communications Conf. (GLOBECOM) Workshop*, December 2013.

[SKB+13] Saito, Y.; Kishiyama, Y.; Benjebbour, A.; Nakamura, T.; Li, A.; and Higuchi, K.,"Non-orthogonal multiple access (NOMA) for future radio access," IEEE VTC spring 2013, June 2013.

[SP13a] Stefanovic, C.; Popovski, P., "ALOHA Random Access that Operates as a Rateless Code," *Communications, IEEE Transactions on*, vol.61, no.11, pp.4653-4662, November 2013.

[SP13b] Stefanovic, C.; Popovski, P.,"Coded slotted ALOHA with varying packet loss rate across users," *Global Conference on Signal and Information Processing (GlobalSIP), 2013 IEEE*, pp.787-790, 3-5 Dec. 2013.

[SRL14] Soysa, M, Rajatheva, N., Latva-aho, M., "Linear and Non-linear Transceiver

Processing for MIMO-FBMC Systems", ICC 2014, 10-14 June, Sydney.

[SS03] T. Svensson, A. Svensson, "Constrained Envelope Continuous Phase Modulation," Vehicular Technology Conference, 2003. VTC 2003-Spring. The 57th IEEE Semi-annual , vol.4, no., pp.2623-2627 vol.4, 22-25 April 2003.

[SSA+13] Subbiah, I.; Schrey, M.; Ashok, A. et al., "Design of a TV white space converter prototype towards cognitive radio for WLAN routers," *Cognitive Radio Oriented Wireless Networks (CROWNCOM), 2013 8th International Conference on*, pp.208-213, 8-10 July 2013.

[SSL02] P. Siohan, C. Siclet and N. Lacaille, "Analysis and design of OFDM/OQAM systems based on filterbank theory'', *IEEE Transactions on Signal Processing*, pp. 1170-1183, Vol. 50, N° 5, May 2002.

[SUM09] Siaud & A.M. Ulmer-Moll, "Advanced Multi-Band UWB-OFDM air interfaces for WPAN MGWS," Wireless World Research Forum, WWRF#23, Peking, Oct. 2009

[SW13] Schaich, F.; Wild, T., "A Reduced Complexity Receiver for Multi-Carrier Faster-Than-Nyquist Signaling," *Proceedings of 9th International Workshop on Broadband Wireless Access, IEEE Globecom'13,* Atlanta, GA, USA, December 2013.

[SW14] Schaich, F.; Wild T., "Waveform contenders for 5G - OFDM vs. FBMC vs. UFMC", *Proceedings of 6th International Symposium on Communications, Control, and Signal Processing (ISCCSP 2014),* Athens, Greece, May 2014.

[SWC14] Schaich, F.; Wild, T.; Chen, Y., "Waveform contenders for 5G – suitability for short packet and low latency transmissions", *Vehicular Technology Conference (VTC Spring), 2014 IEEE 79th*, May 2014.

[TLS+12] Tirronen, T.; Larmo, A.; Sachs, J. et al., "Reducing energy consumption of LTE devices for machine-to-machine communication," *Globecom Workshops (GC Wkshps), 2012 IEEE*, pp.1650-1656, 3-7 Dec. 2012.

[Ton13] Tonello, A.M., "A novel multi-carrier scheme: Cyclic block filtered multitone modulation," *Communications (ICC), 2013 IEEE International Conference on*, pp.5263-5267, 9-13 June 2013.

[TPS+13a] Thomsen, H.; Pratas, N.K.; Stefanovic C., "Analysis of the LTE access reservation protocol for real-time traffic," IEEE Communication Letters, 2013.

[TPS+13b] Thomsen, H.; Pratas, N.K.; Stefanovic C., "Code-expanded radio access protocol for machine-to-machine communications", in Transactions on Emerging Telecommunications Technologies, 2013

[TR36.814] 3GPP Working Group, "Future advancements for E-UTRA physical layer aspects", TR 36.814, March 2012.

[TRL+13] Tiirola, E.; Raaf, B.; Lahetkangas, E. et al, "On the design of discovery patterns for half-duplex TDD nodes operating in frame-based systems," *Future Network and Mobile Summit (FutureNetworkSummit), 2013*, pp.1-9, 3-5 July 2013.

[TSK02] Tuchler, M.; Singer, A.C.; Koetter, R.,"Minimum mean squared error equal-ization using a priori information", IEEE Transactions on Signal Processing, 50(3), pp 673-683, March 2002.

[TVP+03] Tripathi, V.; Visotsky, E.; Peterson, R.; Honig, M., "Reliability-based type II hybrid ARQ schemes," *Communications, 2003. ICC '03, IEEE International Conference on*, vol.4, pp.2899-2903 vol.4, 11-15 May 2003.

[UMS12] A.M. Ulmer-Moll, I. Siaud, “A green link budget CQI metric for multi-RAT HET-NETS”, software demo, International conference TIA’2012, Green Touch, Dallas meeting, June 2012.

[VWS+13] Vakilian, V.; Wild, T.; Schaich, F. et al., “Universal Filtered Multi-Carrier Technique for Wireless Systems Beyond LTE”, *Proceedings of 9th International Workshop on Broadband Wireless Access, IEEE Globecom'13,* Atlanta, GA, USA, December 2013.

[WBS+02] Witzke, M.; Baro, S.; Schreckenbach, F. et al., “Iterative Detection of MIMO Signals with Linear Detectors”. In Proc. of the Asilomar Conference on Signals, Systems and Computers, volume 1, pp 289-293, Nov. 2002.

[WPS11] M. Wylie-Green, E. Perrins, T. Svensson, “Introduction to CPM-SC-FDMA - A Novel Multiple-Access Power-Efficient Transmission Scheme.” IEEE Transactions on Communications, (7) pp. 1904-1915, 2011.

[WWD+14] Woltering, M.; Wuebben, D.; Dekorsy, A. et al, “Link Level Performance Assessment of Reliability-Based HARQ Schemes in LTE,” *VTC 2014-Spring*, *IEEE,* May 2014.

[YC10] Yoo, Y., G.,; and Cho, J., H.; ‘Asymptotic optimality of binary faster than Nyquist signaling’, IEEE Comm. Letters, vol. 14, no. 9, pp 788-790, Sep. 2010

[YSZ+04] Yongmei, D.; Sumei, S.; Zhongding L.,“A list sphere decoder based turbo receiver for groupwise space time trellis coded (GSTTC) systems”, In Proc. of the IEEE 59th Vehicular Technology Conference (VTC-Spring), volume 2, pp 804-808, 2004.

[ZZS+13] Zanella, A.; Zorzi, M.; dos Santos, A.F. et al, "M2M massive wireless access: challenges, research issues, and ways forward", *IEEE Global Communications Conference Globecom 2013*, Atlanta, USA, Dec. 2013.

5 ANNEX 1: Performance results

This section goes beyond the key outcomes elaborated so far within the METIS radio link research described in section 2. Detailed performance evaluations are given in the following sections. The general section structure follows the structure of section 2.

5.1 Unified air interface design for dense deployments

Harmonized OFDM:

Like described in chapter 2.1, “harmonized OFDM” refers to the approach of scaling the frequency and time domain numerology, such as used bandwidth, SC spacing and CP length, as a function of carrier frequency, while utilizing the same base clock and baseband design for different parts of spectrum. The idea is illustrated on high level in Figure 5-1. More detailed investigation of the exact values and allocation of the step positions are left for further study. The exact values and allocation of the steps need to be further aligned with available bandwidth on different frequency ranges together with the considerations concerning e.g. phase noise behaviour. For example, a set of OFDM parameters on mmW frequency bands proposed and used in the UDN study together with related environmental assumptions are: BW 100-2000 MHz; indoor and outdoor RMS delay spreads below 100 ns; inter-node distance indoor <20m (typ. 10m), outdoor <50m; and subcarrier spacing 360 kHz (alt. 720 kHz).

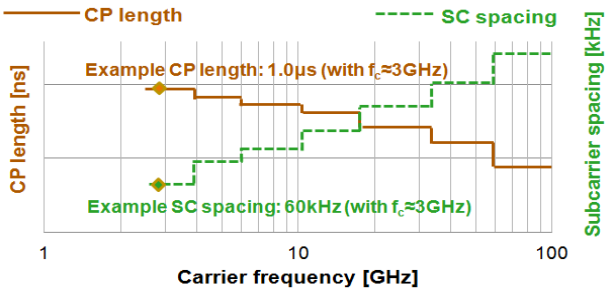

Figure 5-1: Harmonized OFDM concept

UDN optimized frame structure:

The proposed UDN optimized frame structure was illustrated in Figure 2-1.

In order to enable robust and fast control plane, control signalling is embedded to each frame and time separated from the data plane. Control symbols are located before data symbols in order to allow fast and cost efficient pipeline processing in the receiver. It is possible to use different SC spacing, coding and modulation schemes for control and data planes. Control part of the frame provides possibility to include both RX and TX resources for control, allowing the devices in the network to both receive and send control signals, such as scheduling requests (SRs) and scheduling grants (SGs), in every frame. TX and RX control parts are proposed to be symmetrical in order to enable link independent multiple access.

In addition to scheduling related control information, control plane may also contain reference signals (RS), used for cell detection and selection, frequency domain scheduling, precoder selection and channel estimation. In order to allow fully flexible allocation of different control and data part patterns for consecutive frames, TX and RX control parts need to be separated from each other and from the data symbols with a GP, leading to total number of 3 GPs per frame. In frequency direction, the spectrum can be divided to separate allocable frequency resources.

Rest of the frame after the control part is dedicated for data plane. In order to achieve low complexity, data part in one frame contains only transmitting or receiving possibility for data symbols. DMRS symbols, used to estimate the channel and its covariance matrix, are located e.g. in the first OFDMA symbol in the dynamic data part and can be precoded with same vector/matrix with data.

The possibility to allocate data part of a frame either for transmitting or receiving enables fully flexible UL/DL ratio switching for data transmission. In other words, the proposed physical frame structure does not create any such UL/DL ratio restrictions for either UL or DL data transmissions that exist for example in current LTE-A (where UL/DL ratio is always restricted by certain configuration and cannot be modified in fully flexible manner). The decreased frame overheads, such as reduced GP & CP and the increased frequency efficiency due to large bandwidth, together with flexibility in UL/DL ratio improve the maximum link spectral efficiency (LSE) achievable with the proposed UDN optimized frame structure compared to existing systems, such as LTE-A. The proposed frame structure enables also a large amount of other benefits and enablers, like described in Section 2.1.

Relevance of UDN optimized air interface to MMC scenario:

MMC scope focuses to the connectivity for a massive amount of simple and cheap devices transmitting low amounts of non-delay sensitive data and requiring a very long battery life. According to WP5, the most suitable frequency range for MMC communications is estimated to be on relatively low spectrum area, such as below ~1 GHz for deep indoor coverage and below ~3 GHz for gateway-infrastructure links (in comparison to e.g. UDN scenario where spectrum above ~30GHz is assumed to be utilized). Required bandwidth for MMC communications is estimated from several hundred kHz to a few MHz, in comparison to e.g. UDN scenario where devices support larger bandwidths, such as 200 MHz – 2 GHz with relatively large minimum bandwidth granularity unit, e.g. chunks of 10 – 100 MHz.

Since the UDN optimized air interface enables aspects important also for MMC scenarios, such as extremely low power consumption and efficient discovery of a massive amount of devices together with consideration of low cost, it would be beneficial to utilize the UDN framework also for MMC. In order to minimize the power consumption and the cost of machine type devices (MTDs), the bandwidth capability of MTD needs to cut down. This can be realized with a division to sub-channels and by utilizing sub-channel specific IFFT, further leading to lower sampling rate and FFT size compared to UE's having higher bandwidth capability. The principle is illustrated in Figure 5-2. Co-existence and orthogonality between a MTD (utilizing ~1MHz spectrum that can be considered feasible for simple MTD devices) and a high end devices (with higher bandwidth capability) in the same UDN framework can be obtained by applying the same subcarrier spacing. The frame numerology (such as guard times) and structure can in this respect therefore also be similar for these two application types. The receiver that needs to be able to receive from both the high end UDN device and from the MTD device, such as a receiver located in eNB/AP, can be realized with one big IFFT with properly matched subcarriers. An example numerology (feasible for carrier frequencies around 10GHz) is given in Table 5-1. Further, in order to maximize the power efficiency, it may be beneficial to utilize single carrier DFT preceding the conventional OFDMA processing, resulting to lower peak-to-average power ratio (PAPR) in the machine type devices.

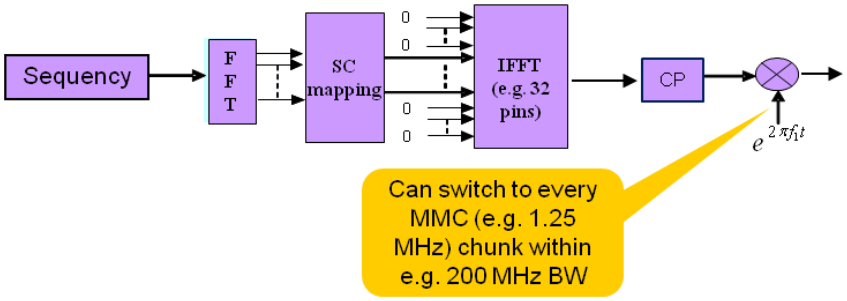

Figure 5-2: Sub-channel specific IFFT.

Table 5-1 Example numerology comparison between a typical UDN and a machine type device.

	High end device (BW = 200MHz)	Machine type device (BW = 1.25MHz)
Spectrum usage eff	0.96	0.96
Clock Rate [Mchip/s]	**245,76**	**1,92**
Subcarrier spacing [kHz]	**60**	**60**
Ts [us]	16.67	16.67
n FFT	**4096**	**32**
# eff sub-carriers	3200	20
# zero sub-carriers	896	12
Frame length [ms]	0.25	0.25
# GP	3	3
# symbols per frame	14	14
CP [us]	1	1
GP [us]	0.89	0.89

Flexible TTI for efficient energy saving and extreme high-speed transfer:

Performance evaluation

Simulation setups:

- Fix+: An “improved” fix TTI approach
  - An IP packet is always sent in one block, i.e., TTI (the “+”)
  - UEs check DL in subframe basis, for DL assignments and UL grants
  - UEs can in UL promptly send IP control or small data packets in each subframe
    - Semi-persistent transmission by using some reserved UL ASU:s
- Flex: A simple version
  - A TTI can always hold an IP packet
  - UEs check DL in frame basis, and active in UL frame-basis when having UL data
    - Pre-scheduled ASU:s for multiple IP packets in the buffer for both DL and UL
- Flex+
  - Multiple IP packets of a UE can be grouped into one MAC block

› Queue the blocks (UEs) with the oldest IP packet first in the line

Table 5-2 Simulation parameters

Simulation type	**Monte Carlo simulation in static radio channel and dynamic traffic environment**
Frame structure	TDD
Bandwidth	2 GHz (shared by all APs)
Radio spectral efficiency SISO assumed	up to 3 information bit/s/Hz
ASU in bandwidth	100 MHz
ASU in time	12.5 us
Subframe	12.5 us
Frame	125 us
Deployment	office hall with 7 UEs and 2 APs, equally distributed along circles
Traffic	mix of file synchronization (50%), streaming (25%) and video conferencing (25%) including IP control packets

Performance analysis - Relative active time of UEs

Different TTI structures give significant impacts on the UE receiving time indicating possible utilization of DRX. Relative to Fix+, Flex can save 71% and Flex+ 78%.

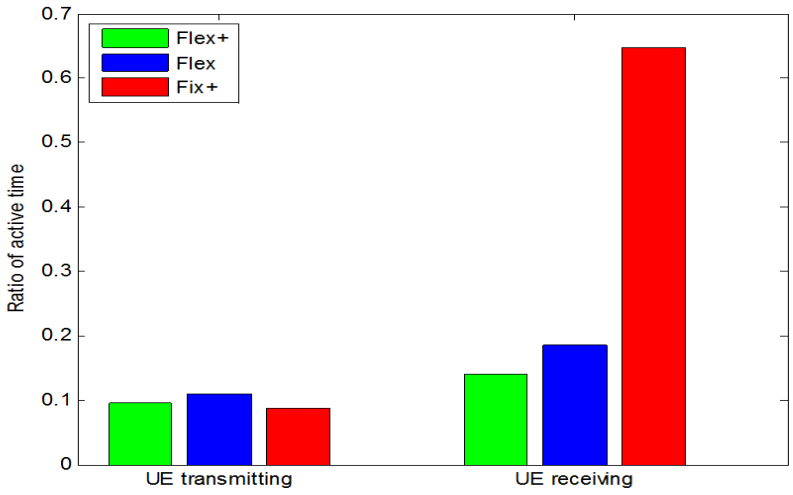

Figure 5-3: Relative active time of UEs

Performance analysis - Relative active time of Aps

Flex+ scheme can save 49% of transmission time which can be utilized for micro-sleep in the AP.

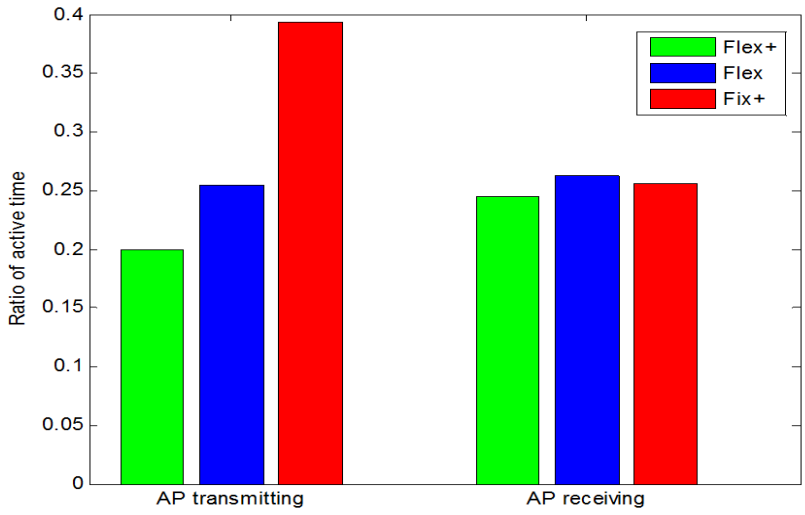

Figure 5-4: Relative active time of Aps

Average utilization of spectrum blocks or ASUs

Flex+ TTI needs 20 % less resources in downlink and 25 % less resources in uplink by grouping several IP packets into one scheduled block of data.

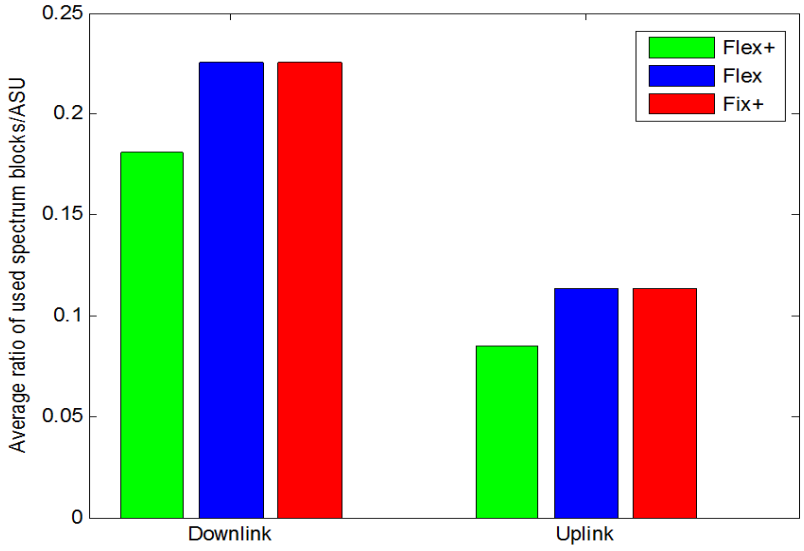

Figure 5-5: Average utilization of spectrum blocks

5.2 Optimized signalling for low-cost MMC devices

MMC-Type D2D Links:

Further discussion on the obtained results as well as detailed analysis of the considered scenarios is found in [PP+14].

5.3 Air interface supporting new and dynamic spectrum usage

The performance of the conventional homodyne for a wideband RF front end [ASH13] proved that with the even with the linear blocks, the self interference from its own TX is a critical issue. This self interference present when TX is operating simultaneously with RX under an FDD operation intermodulate with other in band signals resulting in masking its own RX signal resulting in signal to noise ratio degradation. The performance of such a TRX is evaluated in under standard LTE conditions. The performance table in section 2.3 shows that high degree of isolation is required under wideband conditions for dynamic spectrum RF front end without which an FDD operation is not possible. To some extent some of the problems can be addressed with a high IF architecture. By upconverting the RF signal rather than downconverting, the effect of harmonics and image can be suppressed and with the resulting high out of band linearity TX leakage effect can also be reduced [SSA+13].

5.4 Multiple interface management

Multi-RAT PHY layer design & multi-band processing has been described together with some initial evaluation results in the main part of the document, and the concept of SoftAI has been sketched in D2.2. Work in both these research activities is currently in progress; however, there are no further results available to be highlighted or referenced.

5.5 Advanced signaling concepts

For non-orthogonal multiple access (NOMA), some initial results have been presented in the main part of the document. Current work focuses on identifying the pairs of modulation coding scheme (MCS) and power sets that are selected in the case of NOMA with high probability.

5.6 Air interface of moving networks

Channel estimation for V2V links

The scatters will cause multipath propagation by interaction with the transmitted signal. If we consider only single interactions with the scatters, then each scatterer will give rise to exactly one multipath component with a certain delay and Doppler shift. The delay and Doppler shift of each multipath component are easily calculated from the positions and velocity vectors of the transmitter, receiver, and scatterer. We classify scatterers as static discrete (SD), moving discrete (MD) or diffuse (DI). The SD scatters are relative large reflectors, e.g., road signs while MD scatters are moving vehicles. The DI scatterer are smaller scatterers placed at the side of the road, see Figure 2-10.

Even though the channel is sparse in the delay-Doppler domain, the sparsity is not directly observable due to leakage. The leakage is due to finite bandwidth and finite time-duration of the transmitted signal. If not properly compensated for, the leakage will degrade the performance of an algorithm that assumes perfect sparsity. Moreover, the diffuse components will make the channel partially non-sparse. In the following, we will present results for a standard least-squares channel estimator, which does not exploit the hybrid sparse/diffuse (HSD) structure of the channel, and a number of novel estimators that are based on an HSD algorithm called g-Thres [MMMZ12a, MMMZ12b].

The simulated scenario is an 18 m wide highway with 10 m wide strips on each side containing 1000 diffuse scatterers in a length of 400 m. The transmitter and receiver are traveling with 100 and 105 km/h. respectively, in the same direction together with 5 other vehicles (MD scatterers). The geometry also includes 10 SD scatterers. The carrier frequency is 5.9 GHz and the transmitted signal has bandwidth 20 MHz and duration 1.6 ms. The gThres algorithm comes in three main variations: “sparse only”, which ignores the diffuse component, “HSD”, which takes into account both sparse and diffuse components, and “Regional HSD”, which use also the u-shape structure of the delay-Doppler domain representation of the

channel, see Figure 2-10. Furthermore, the leakage is optionally compensated. The mean-squared error (MSE) for the estimators are plotted versus signal-to-noise ratio in Figure 5-6. Further details on the novel estimators and simulation parameters are found in [BSM14].

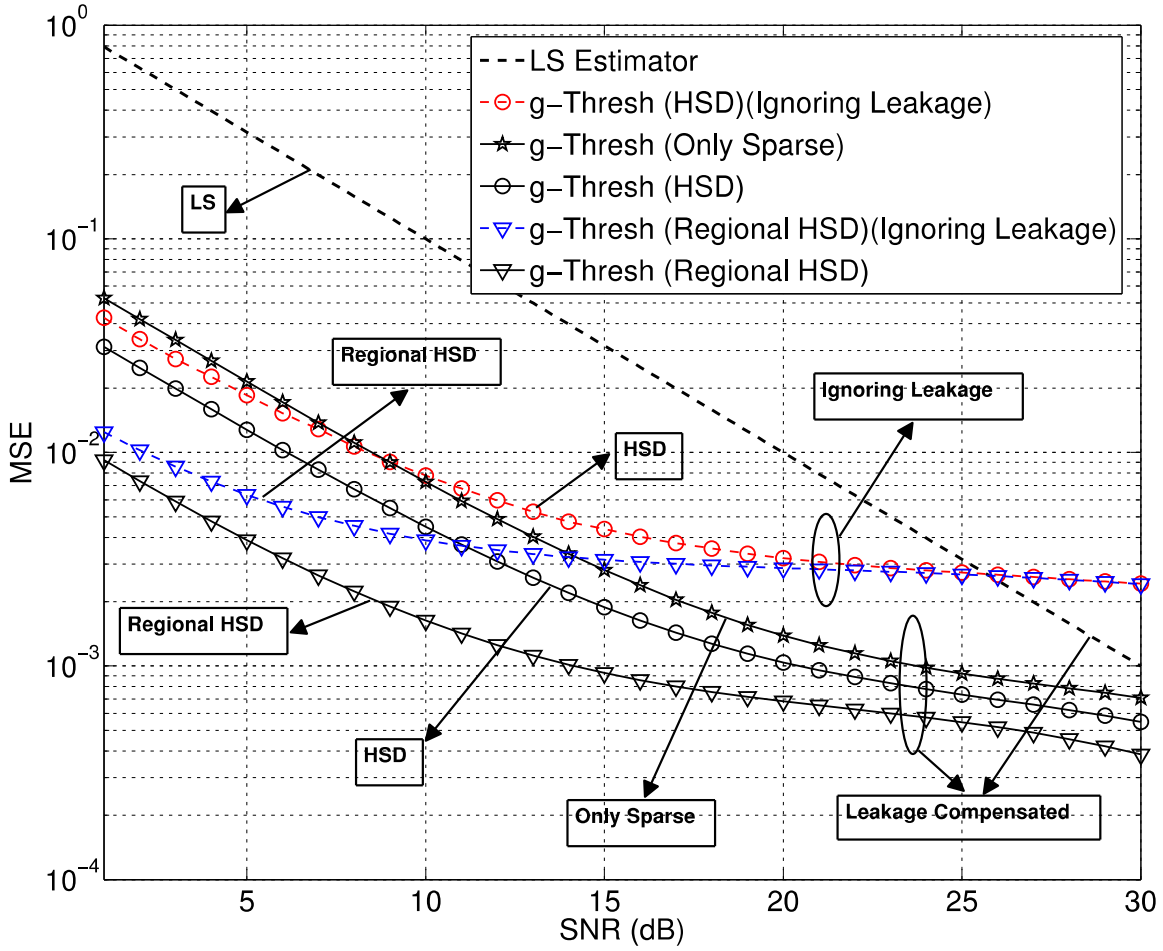

Figure 5-6: Mean-squared estimation error versus signal to noise ratio for the considered channel estimators

Channel prediction for the backhaul link of moving cells/networks

The use of monopole antennas placed on flat and uncluttered vehicles roofs has so far provided the highest correlations, resulting in average cross-correlations of 0.97-0.98 for antenna separations of 0.5-3 wavelengths. See the Figure 5-7 below, which is based on measured data obtained in cooperation with TU Dresden, using a 20 MHz OFDM signal working at 2.68 GHz, at 50 km/h vehicle velocity.

The useful antenna correlation is however reduced due to mutual electromagnetic couplings with very closely spaced antennas, around 0.25 wavelengths apart. In [JBG+14], a simple and efficient scheme has been found that counteracts this effect. It is based on using an open-circuit antenna decoupling method. The effect on the average antenna correlation of using such a pre-compensator is shown in Figure 5-7.

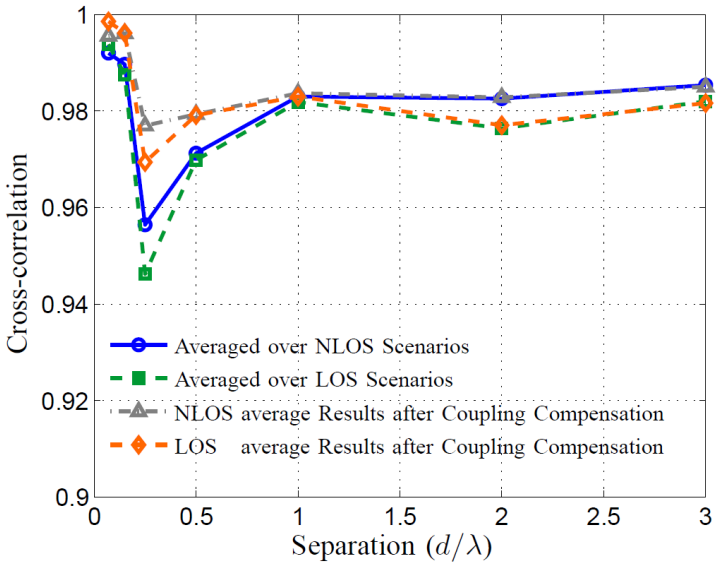

Figure 5-7: Mean measured cross-correlations between the received signals in line-of-sight (LOS) and non-line-of-sight (NLOS) scenarios, as a function of the spacing between the forward predictor antenna and a rearward main antenna on the roof of a vehicle moving at 50 km/h. Results are shown without and with the use of a pre-compensator of the mutual electromagnetic coupling between the antennas.

5.7 Faster than Nyquist (FTN)

Capacity and spectral efficiency for FTN signaling:

For a system point of view realization, the spectral efficiencies using RRC pulses of $\alpha = 0.2$ are shown in Figure 5-8. The reference curve is the black one which shows the spectral efficiency of sinc pulses, each of bandwidth W with no interference. The red curve shows the spectral efficiency of the optimized values of $f_{C,int}$ for different SNR values. The blue curve shows the spectral efficiency using RRC pulses in case of no interference. The other two curves shows the spectral efficiencies using RRC pulses with different values of $f_{C,int}$. Also as mentioned in Section 0, at low SNR, It is best also to choose $f_{C,int}$ as small as possible to achieve higher spectral efficiency and the reason is the increase of the power per Hertz as $f_{C,int}$ decreases for large K. At high SNR, interference should be avoided.

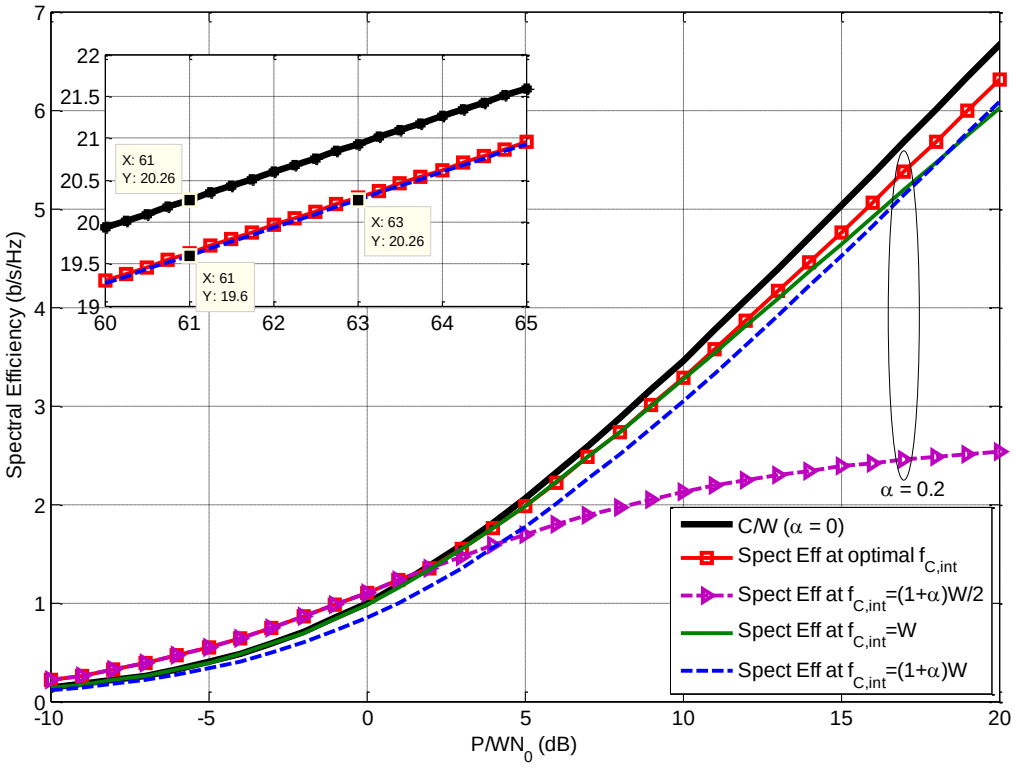

Figure 5-8: Spectral efficiencies for roll-off factor $\alpha = 0.2$ for the system point of view realization.

For the per user point of view realization, the spectral efficiencies curves using RRC pulses of $\alpha = 0.5$ and 0.2 are shown in Figure 5-9 and Figure 5-10 respectively. We conclude from the curves that as the interference increases, the spectral efficiencies decrease.

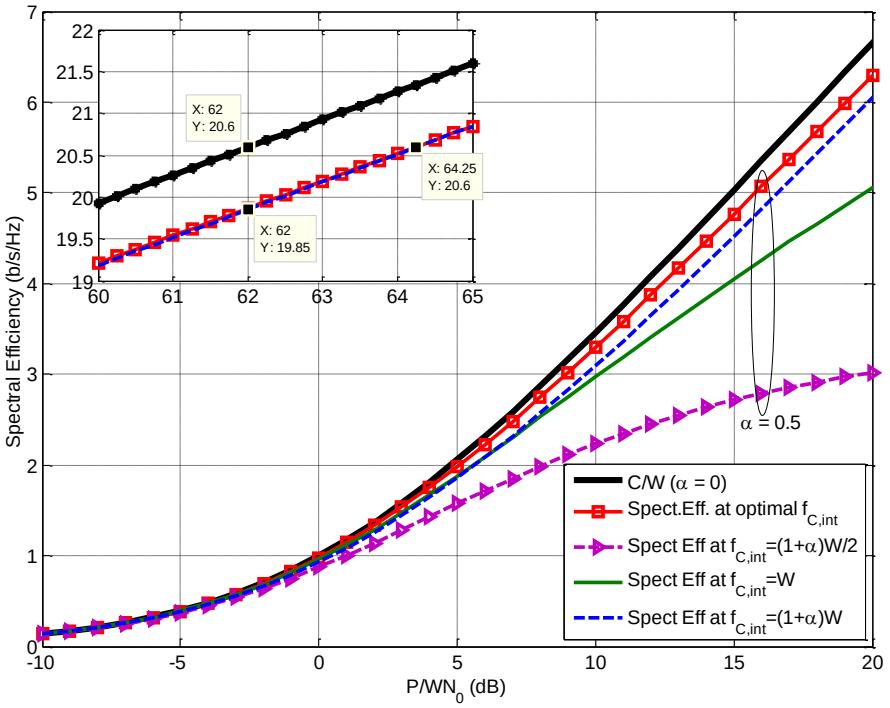

Figure 5-9: Spectral efficiencies for roll-off factor $\alpha = 0.5$ for the per user point of view realization.

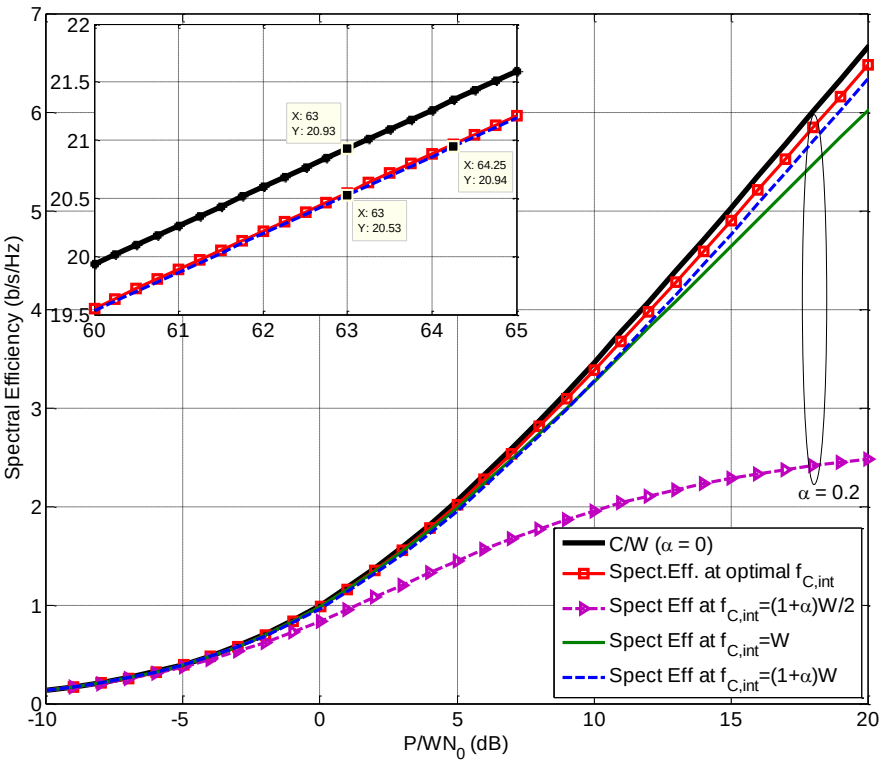

Figure 5-10: Spectral efficiencies for roll-off factor $\alpha = 0.2$ for the per user point of view realization.

After showing the theoretical capacity analysis of FTN signaling, we investigate FTN in a practical system where a single user is considered without having interference from different systems or users. As mentioned in Section 0, FTN signaling achieves flexible throughput levels by using different FTN rates. We simulated a BPSK system with (7,5) convolutional code of rate ½ and soft output BCJR equalization. The transmit and receive filters are RRC pulses of roll-off factor 0.5. The number of information bits per frame is 1000 and the number of sent frames is 1000. Figure 5-11 shows the resulting normalized throughput curves, with respect to the number of information bits per frame, using different FTN rates. We observe that at high E_b/N_0, the throughput is doubled using 50% FTN signaling, i.e., doubling the Nyquist rate, without using a higher order modulation scheme or different code rate.

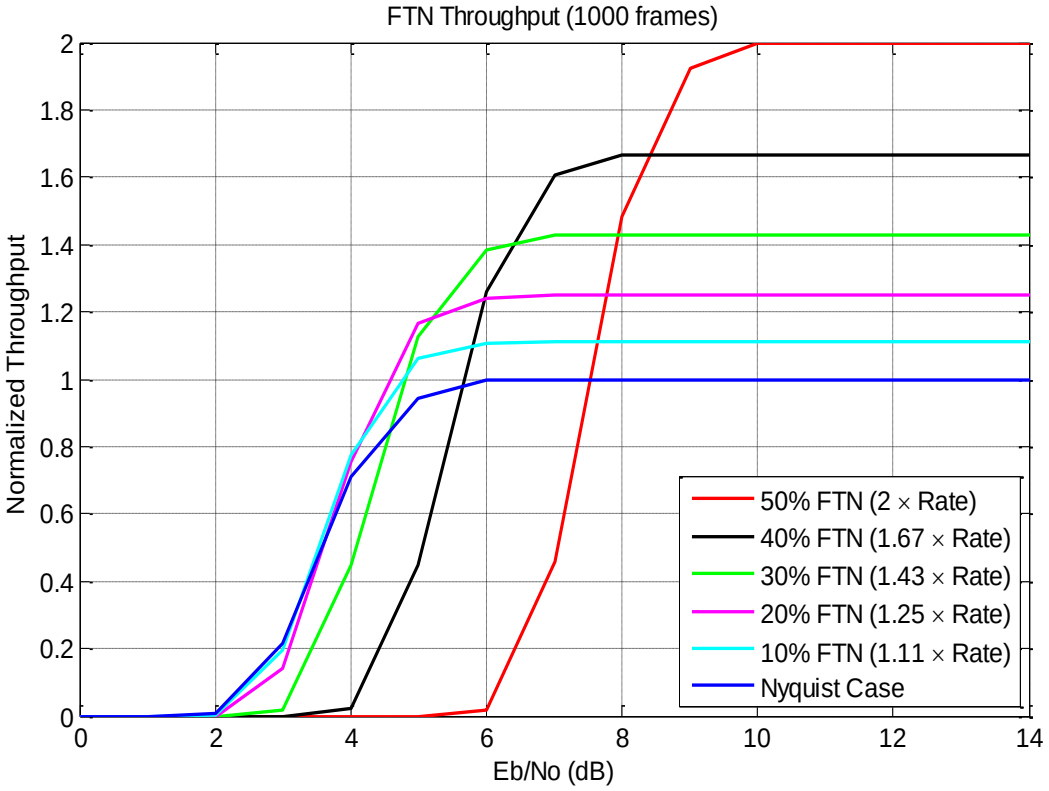

Figure 5-11: Normalized throughput curves for different FTN rates.

Using FTN on the top of OFDM/OQAM

The use of FTN in OFDM/OQAM falls into the MFTN. Furthermore, FTN might be considered as an option in complement with the classical OFDM/OQAM scheme, which can be switched on and off based on channel conditions. In our system, the pulses are only packed closer in time axis, while the frequency packing factor can be considered to be 1. Note that, even in this scenario, ICI still exists in the transmitted signal, as illustrated in Figure 5-12. Here, the FTN data on different subcarriers and time instants are represented by triangles, while the classical OFDM/OQAM signal presented in circles is kept as a reference.

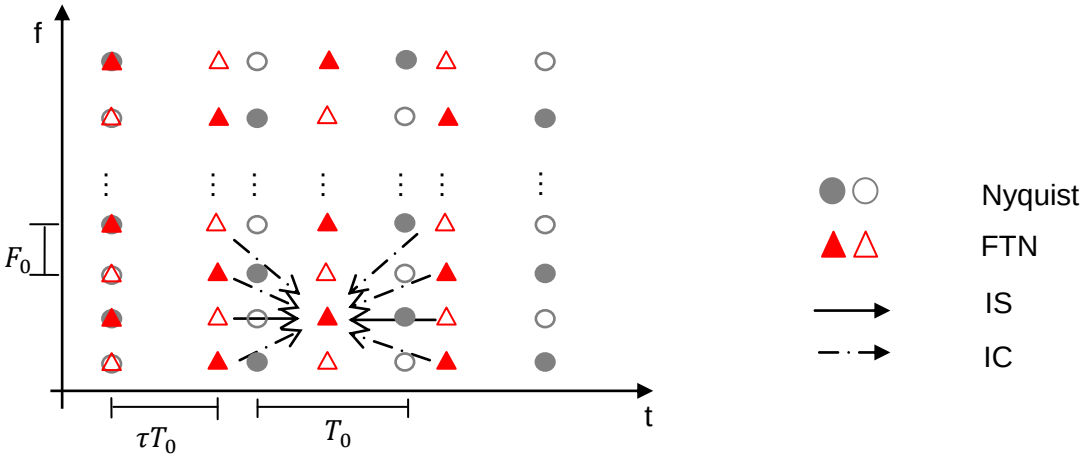

Figure 5-12: FTN in OFDM/OQAM

The prototype functions $p'_{m,n}(t)$ when FTN is in use can be represented as

$$p'_{m,n}(t) = e^{i(m+n)\frac{\pi}{2}} e^{i2\pi m F_0 t} x(t - n\tau T_0)$$

where τ is the packing factor on time axis and $0 < \tau \leq 1$. Note that $\{p'_{m,n}(t)\}$ is no longer a Hilbert basis.

The OFDM/OQAM/FTN transmission chain is illustrated in Figure 5-13. At the side of the transmitter, FTN is combined with OFDM/OQAM modulation scheme, while at the receiver side, MMSE IC-LE scheme is used to iteratively suppress the interference brought in by FTN and the channel.

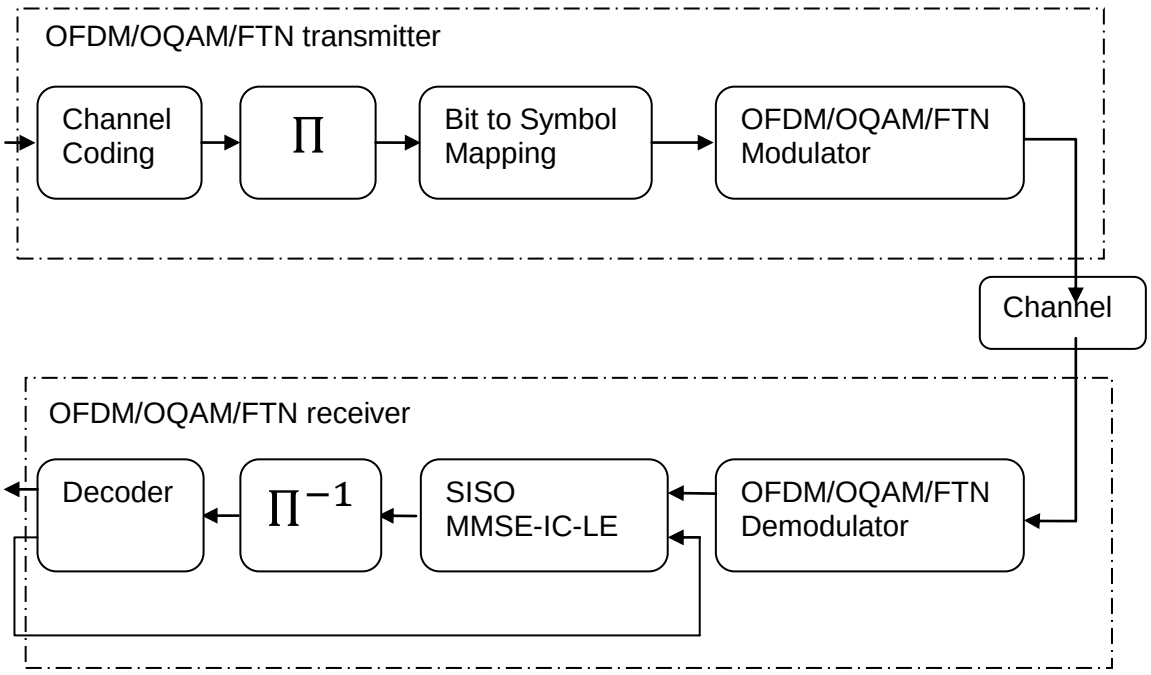

Figure 5-13: OFDM/OQAM/FTN Chain

Interferences are cancelled in a 2 stage process, ICI cancelling and ISI cancelling. Figure 5-14 describes the inner structure of SISO MMSE IC-LE where ICI and ISI are predicted using the feedback from the decoder and then cancelled respectively.

In Figure 5-15, consider the red triangle as the element to equalize. The ICI to it is then predicted by the ICI predictor using the blue triangles which represent the estimated data on side subcarriers. The ISI are predicted using the estimated data on the same subcarrier at different time instants, represented here by orange triangles.

An equivalent channel taking into account the ISI introduced by FTN should be estimated while calculating the coefficients of filter **f** and **g.** This is out of the scope of this report and will not be detailed here.

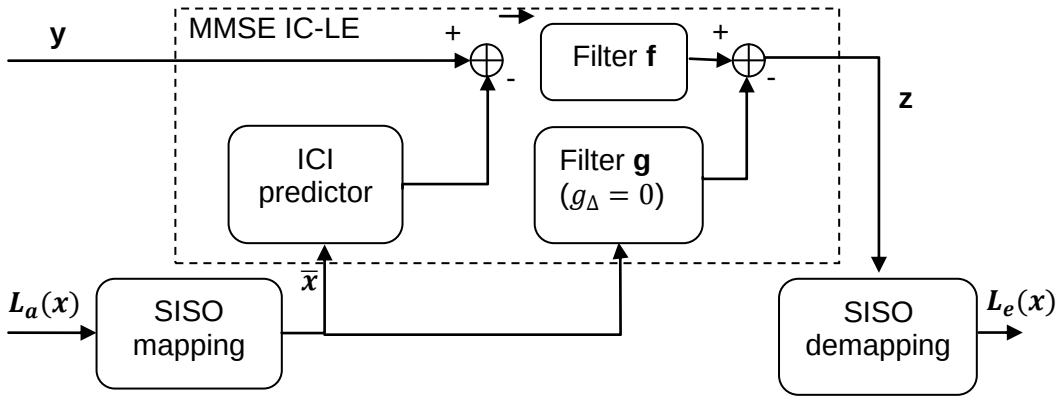

Figure 5-14: Structure of SISO MMSE IC-LE used in OFDM/OQAM/FTN chain

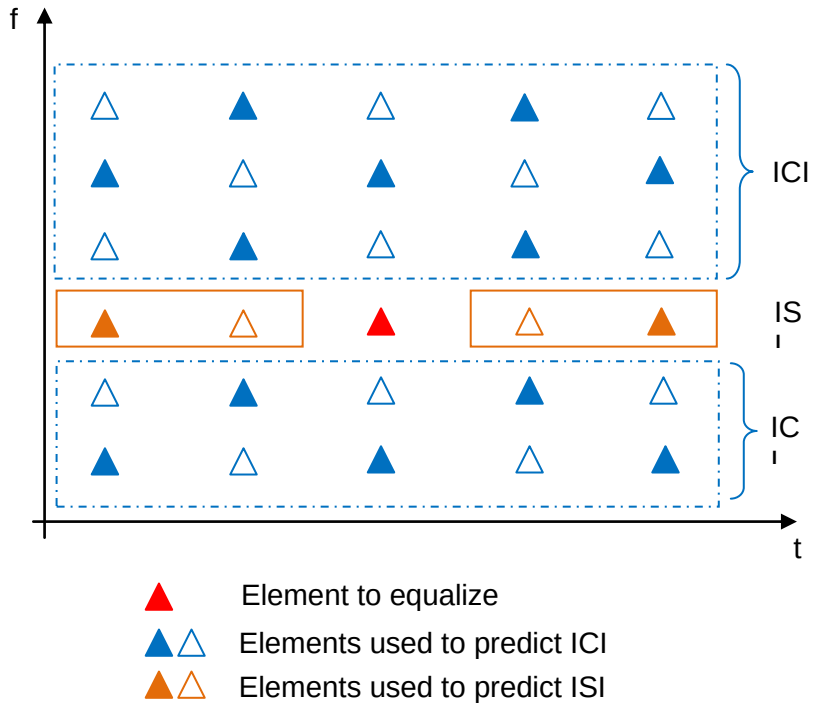

Figure 5-15: ICI and ISI prediction and cancelling

Note that the interference can be suppressed in another way if we inverse the time and frequency axis which is represented in Figure 5-16. This method shows a better waterfall for

certain prototype functions according to our simulation, but will not be detailed in this report. The results illustrated in 2.7 are obtained using the interference cancelling scheme in Figure 5-14.

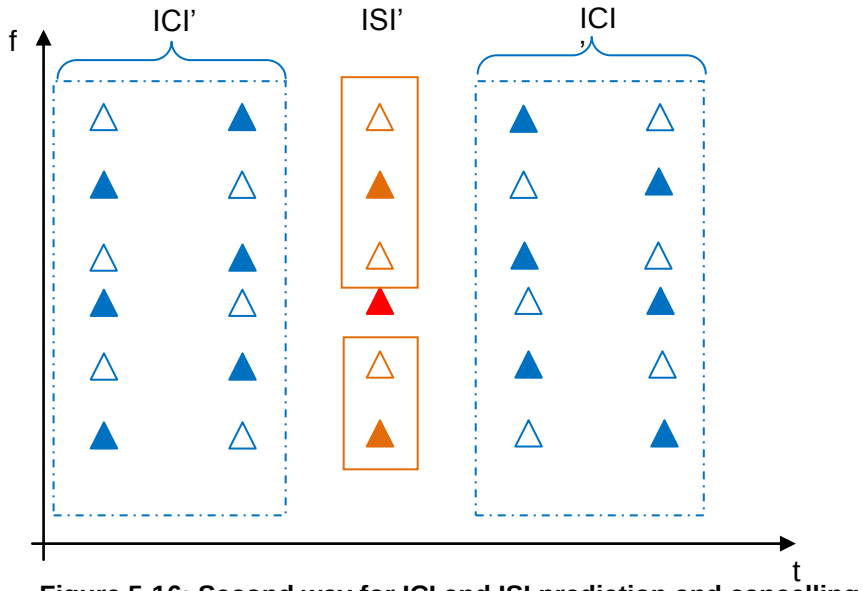

Figure 5-16: Second way for ICI and ISI prediction and cancelling

5.8 Filtered and filterbank based multi-carrier

5.8.1 FBMC based waveform and transceiver design

Weighted Circular Convolution FBMC and Frame Design

By using the proposed Circular Convolution algorithm, the LTE-like frame with common control channel can be designed as follows (see Figure 5-17 for detail):

- The control and data symbols are independently modulated and transmitted using tail-removed FBMC
- Time windows are appended to both ends of the CCCH signal and also the data signal
- The right time window of the previous TTI and the left time window of the current TTI overlap in W_1
- The right time window of the CCCH signal and left time window of the data signal overlap in W_2
- W_1 also includes the channel's delay spread in addition to the right window of the CCCH signal
- TTI alignment with OFDMA: $W1+W2+(M+N)\times T_{FBMC}/2=T_{OFDM-TTI}$
- Example (Symbol-level alignment):

$$M=27,\ N=2,\ W_1=W_2=16.7\ \mu s,\ T_{FBMC}=T_{OFDM}$$

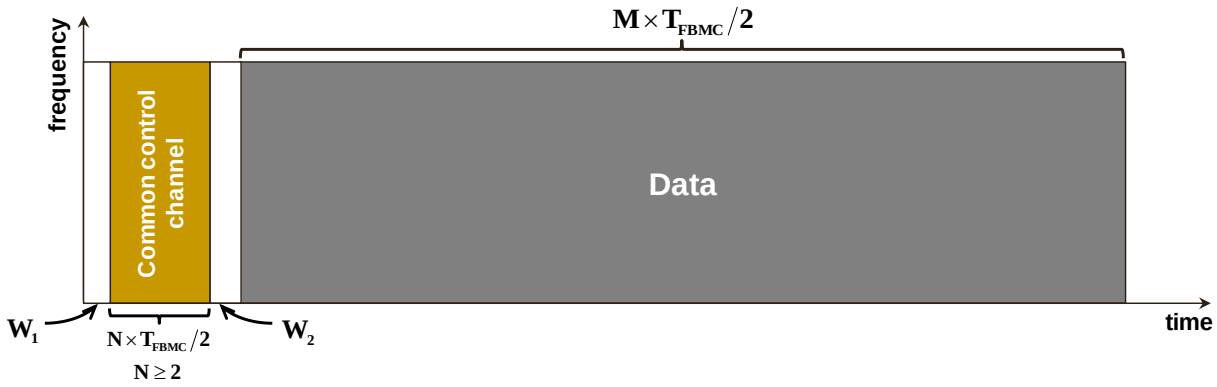

Figure 5-17 WCCF with Time Windowing for common control channel

Time Windowing Overhead Removal in TDD Mode

- As see in Figure 5-17, the guard time between downlink and uplink transmissions in TDD mode is exploited to reduce/remove the windowing overhead

  - t_1 : UE stops listening to DL signal
  - t_2 : UE starts UL transmission (transmission of the UL time window)
  - t_3 : BS stops DL transmission (transmission of the DL time window)
  - t_4 : BS starts listening to UL signal
  - $t_2 - t_1$: DL-to-UL switching time in UE (≈ 20 μs)
  - $t_4 - t_3$: Propagation time between the neighboring base stations to avoid inter-cell interference for the UE-to-BS transmission

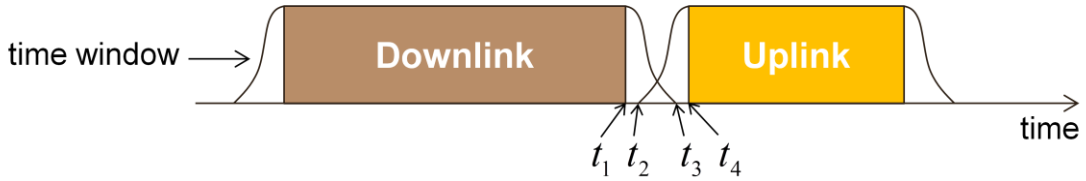

Figure 5-18 Time windowing overhead removal in TDD mode

Transceiver Processing Techniques for MIMO FBMC Systems

In this work we evaluate the performance of linear receiver processing and precoding techniques in MIMO FBMC systems. We further evaluate the performance of the EIC method proposed in [LLS08], for MIMO FBMC systems. We investigate the performance of an iterative EIC technique, and the performance of EIC in conjunction with error correction coding and lower the error floor significantly. We further propose a new iterative precoding technique to minimize the ICI and ISI, resulting in a much better performance.

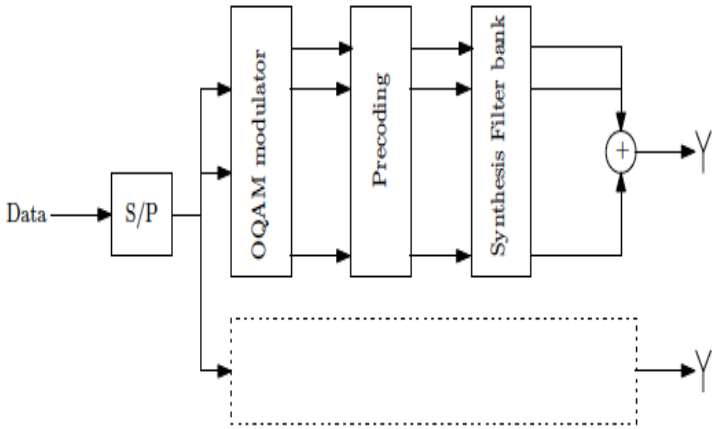

Figure 5-19: Transmitter system model

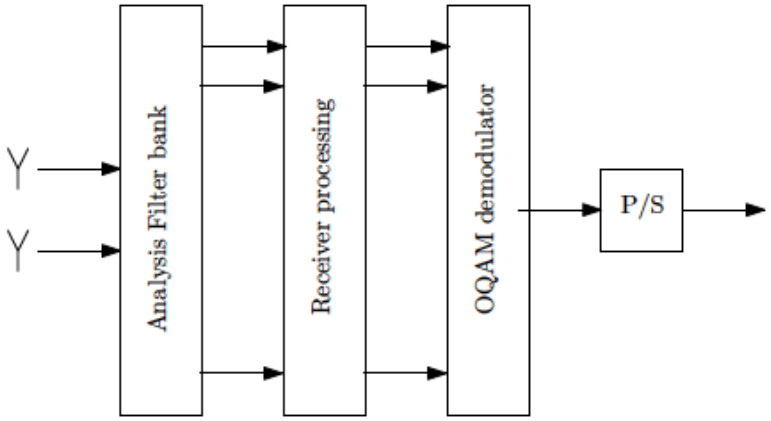

Figure 5-20: Receiver system model

SYSTEM MODEL

A simplified block diagram of the transmitter and receiver is given in Figure 5-19 and Figure 5-20, respectively. We use OQAM modulation.

The results in Figure 5-22 show the average BER when convolution code based forward error control (FEC) is used in conjunction with equalization and interference cancellation (EIC). We have evaluated performance with two different convolution codes of rates 2/3 and 1/2, and memory 3. For comparison, average BER without EIC is also presented.

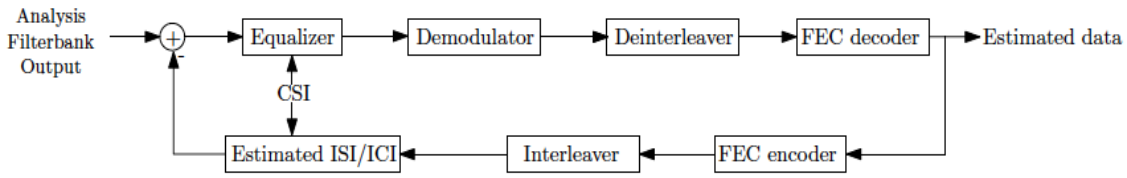

Figure 5-21: Receiver system model incorporating FEC with EIC

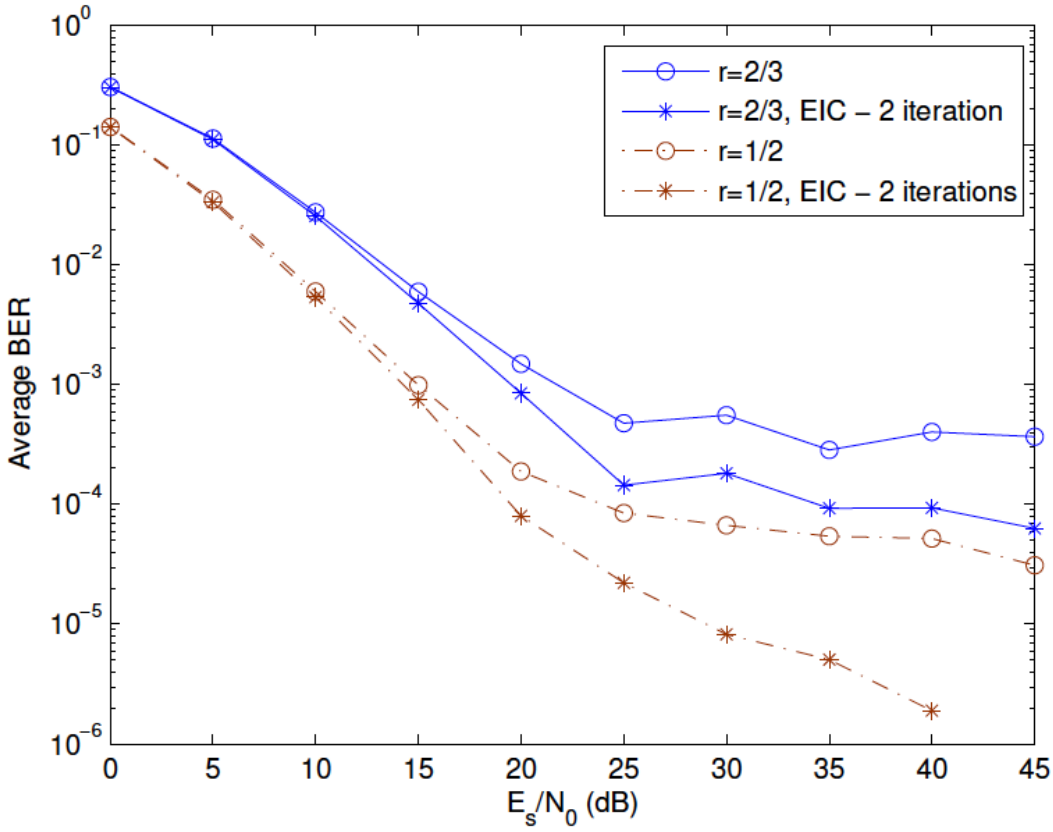

Figure 5-22: Average BER with EIC and FEC

Average BER with EIC and FEC ($\Lambda = 2, 2M = 16, L = 63, N_A = 2, \mathbb{E}\left[|h_{p,q}[1]|^2\right] = 0.2$)

5.9 Modulation & coding and new channel coding concepts

5.9.1 Constrained envelope coded modulation

In Figure 5-23 we illustrate the orthogonal frequency multiplexing of two users in CPM-SC-FDMA.

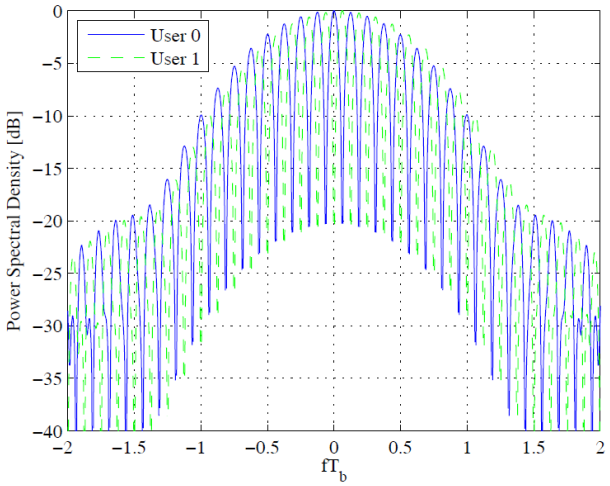

Figure 5-23: Illustration of two user orthogonal frequency multiplexing in CPM-SC-FDMA.

In Figure 5-24 and Figure 5-25 we summarize our current results on CPM-SC-FDMA, published in [WPS11]. As shown, CPM-SC-FDMA can outperform convolutionally encoded Quadrature Phase Shift Keying (QPSK) by up to 4 dB in end-to-end power efficiency, taking HPA power backoff into account.

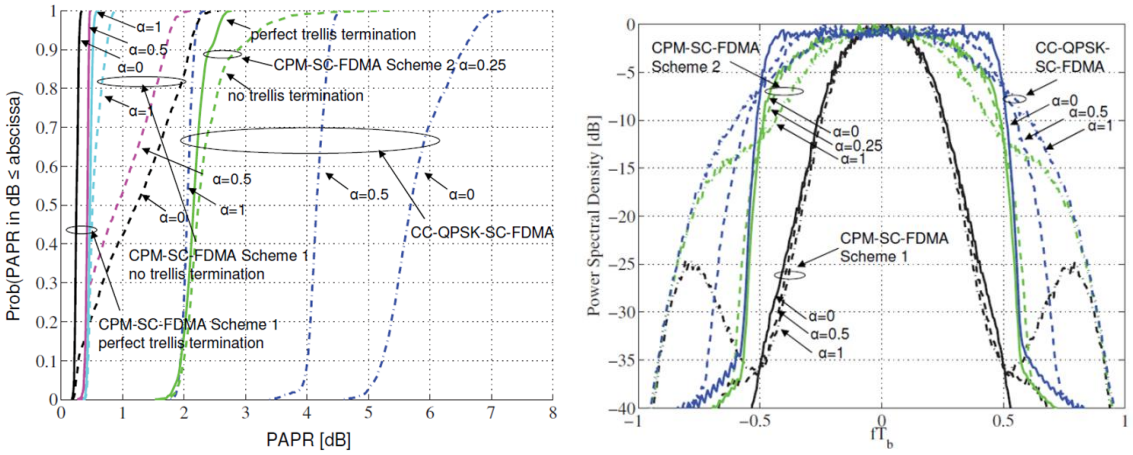

Figure 5-24: Performance overview of CPM-SC-FDMA. Left: The PAPR cumulative density function shows that CPM-SC-FDMA can be 7 dB better than convolutionally encoded QPSK modulated SC-FDMA (CC-QPSK-SC-FDMA). Right: Envelope of the multi-user power spectral density, showing that the spectrum is well confined and with equal data rate and spectrum efficiency as CC-QPSK-SC-FDMA.

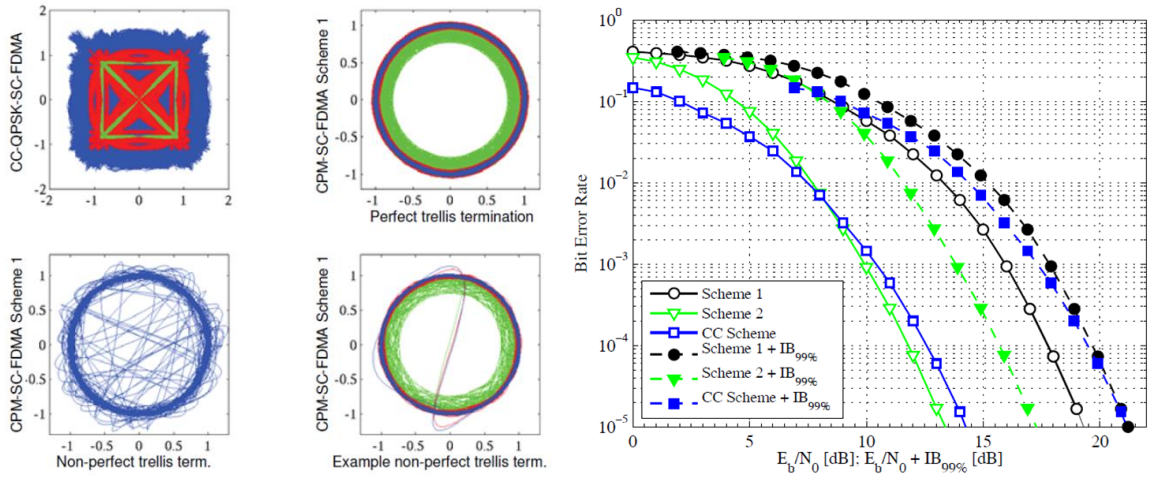

Figure 5-25: Performance overview of CPM-SC-FDMA. Left: CPM-SC-FDMA I/Q diagram shows that the signal is confined within two concentric rings. Right: The CPM-SC-FDMA schemes show equal or better Bit Error Rate (BER) versus energy per bit (Eb) over AWGN power spectral density (N0) than CC-QPSK-SC-FDMA including HPA backoff requirements.

5.9.2 Advanced coding and decoding

Introduction

Coded modulation schemes with multiple antennas offer a large number of parameters that need to be defined depending on the target application. Such parameters need to take into account input constraints related to KPIs such as intended throughput, error rate, signal-to-noise ratio, latency and resulting complexity.

Turbo decoding algorithms, reduced complexity MIMO detection, iterative algorithms at the receiver side and their corresponding quantization are investigated. Effect of coding rate, channel type, frame size, number of iterations are also taken into account. For a target performance, best set of parameters are chosen. Their resulting complexity in terms of number of quantized arithmetic operations and number of memory accesses is identified.

System model

The concept of turbo equalization shown in Figure 5-26 was first introduced in [DJB+95] to combat the detrimental effects of ISI for a transmission protected by a convolutional code. Then, it was extended to include turbo coded systems. It consists of taking advantage from the error correcting capability of the code to improve the soft information at the output of the equalizer. Therefore, extrinsic information is generated at the decoder output and fed back to the equalizer. This feedback loop introduces an iterative process between the decoder and the equalizer. In the case of using turbo codes, two levels of iterations can then be seen: inside the turbo decoder and between the decoder and the equalizer. Obtained error rates at the output of the decoder are sensitive to the scheduling of the two types of iterations. A prior work in [HAD12] has shown that one turbo decoder iteration for every decoder-detector iteration seems to provide the lowest error rates. Therefore such a schedule is considered in the rest of this work. Two different turbo codes are considered in this work: the single-binary 8-state turbo code adopted in the 3GPP LTE standard and the double-binary 8-state turbo code adopted in the WiMax standard. Simplified Max-Log-MAP algorithm with scaling factor is applied for decoding.

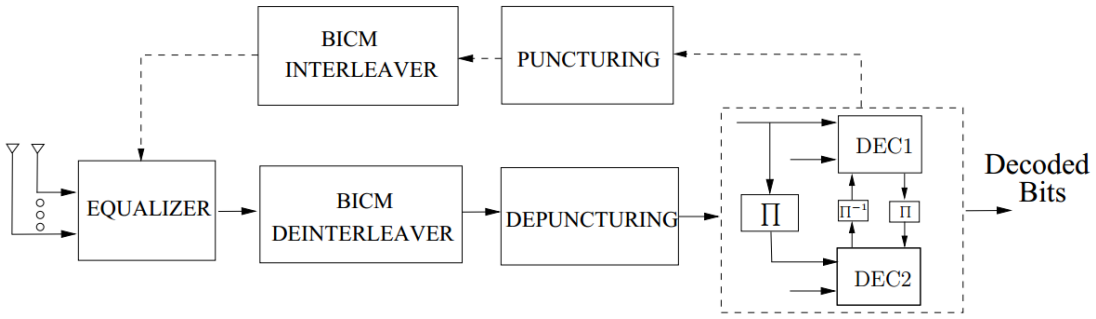

Figure 5-26: System-level receiver: turbo equalization with turbo decoding.

Multiple-Input Multiple-Output (MIMO) systems are recognized as a key enabling technology in high performance wireless communications, employed in many standards such as WiMax and 3GPP-LTE. In this context, several low-complexity sub-optimal MIMO detection algorithms can be proposed:

- The use of linear filtering based solutions like Minimum Mean-Squared Error (MMSE) linear equalizer considerably reduces the computational complexity of a Maximum Likelihood (ML) MIMO detector at the expense of BER performance degradation.
- The well-known List Sphere Decoding algorithm (LSD) achieves a reduced complexity with respect to ML, and excellent error-rate performance.
- The K-Best algorithm can show a near ML result for a reasonable range of SNR values with a reduced complexity.
- Other Performance/complexity trade-offs can be exploited between these detection algorithms in order to choose the most efficient configuration for each system parameters.

The Minimum Mean Squared Error (MMSE)-based detection algorithm

The MMSE equalizer uses channel information *Y* vector in addition to *a priori* information vector $\hat{X}$ provided by the turbo decoder to compute estimated vector $\tilde{X}$ corresponding to the transmitted vector *X* as shown in Figure 5-27.

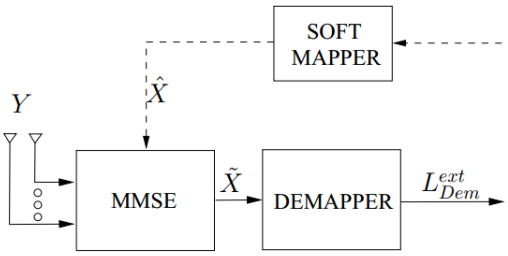

Figure 5-27: system model for iterative MMSE equalization.

After demapping, deinterleaving, depuncturing and turbo decoding, *a posteriori* information from the turbo decoder is punctured, passed through the BICM interleaver, and fed back to the equalizer (after soft mapping) as *a priori* information $\hat{X}$. Note that the entire *a posteriori* information is fed-back from the decoder to the equalizer. When considering MMSE turbo equalization of high-order modulation, significant performance degradation was noticed in [LLL05] and [WBS+02] when feeding-back only extrinsic information. The equalizer output $\tilde{X}$ is given in [TSK02], [Bid03] and [Mas05] as:

$$\tilde{X} = \lambda P^T (Y - H\hat{X}) + G\hat{X}$$

with

$$\lambda = \frac{\sigma_x^2}{1+\sigma_{\hat{x}}^2 \beta}, \quad G = \lambda \beta, \quad \beta = diag(P^T H)$$

where λ, β and G are real positive vectors which represent the MMSE equalization coefficients. P refers to the MMSE detection vector, it can be computed as follows:

$$P = [(\sigma_x^2 - \sigma_{\hat{x}}^2) HH^T + \sigma_w^2 I_{N_r}]^{-1} H$$

where σ_x^2 and $\sigma_{\hat{x}}^2$ are the variances of transmitted and decoded symbols, $(.)^T$ is the Hermitian operator. The variance vector σ_μ^2 of the additive distortion term taking into account the residual ISI and the filtered noise at the equalizer output can be expressed as by:

$$\sigma_\mu^2 = G(1-G)\sigma_x^2$$

These expressions exhibit three main computation steps:

- Detection vector computation referred by *P*,
- Equalization coefficients computation referred by λ, β and *G* followed by the estimate of σ_μ^2 ,
- Estimated symbols computation referred by $\tilde{X}$.

For the first equalization iteration where no *a priori* information is available, ($\tilde{X}$ is a null vector and $\sigma_{\hat{x}}^2$=0), the above expressions become:

$$\tilde{X} = \lambda P^T Y$$

where

$$\lambda = \sigma_x^2 \text{ and } P = [\sigma_x^2 HH^T + \sigma_w^2 I_{N_r}]^{-1} H$$

A typical fixed-point representation of channel inputs and various metrics is considered. Table 5-3 summarizes the total number of required quantization bits for every parameter of the MMSE equalizer [Jaf11]. Note that the number of considered quantization bits is computed for the worst case scenario of a 64-QAM constellation. Lower order constellations profit from increased accuracy.

Table 5-3: Summary of quantization precision levels for metrics required during MMSE equalization.

	Parameter	Number of bits
MMSE equalizer	Received complex symbol $y_l=\{y_l^I, y_l^Q\}$ from Y	{12,12}
	Complex Coeff. Fading symbol $h_{q,l}=\{h_{q,l}^I, h_{q,l}^Q\}$ from H	{12,12}
	Estimated complex symbol $\tilde{x}_q=\{\tilde{x}_q^I, \tilde{x}_q^Q\}$ from $\tilde{X}$	{16,16}
	A priori information complex symbol $\hat{x}_q=\{\hat{x}_q^I, \hat{x}_q^Q\}$ from $\hat{X}$	{16,16}
	Detection complex symbol $p_q=\{p_q^I, p_q^Q\}$ from P	{16,16}
	Bias symbol g_q from G	16
	Distortion variance symbol $\sigma_{\mu,q}^2$	16
	Equalization coefficient symbol λ_q from λ	16
	Equalization coefficient symbol β_q from β	16

Table 5-4: Summary of the computation complexity of MMSE equalization when *a priori* information is considered.

		Number and Type of operations per received vector per turbo equalization iteration	
MMSE equalization with *a priori* input	Computation units	2×2 MIMO SM	4×4 MIMO SM
	Detection vector	$10146Add(1,1) + load(193)$	$111017Add(1,1) + load(482)$
	Equalization coefficients	$5235Add(1,1)$	$16578Add(1,1)$
	Estimated symbol	$9913Add(1,1) + load(128) + store(64)$	$38030Add(1,1) + load(256) + store(128)$

Applying complexity evaluation, quantization and normalization for MMSE equalization with and without *a priori* information leads to the results summarized in Table 5-4 and Table 5-5 respectively.

Table 5-5: Summary of the computation complexity of MMSE equalization when *a priori* information is not considered.

		Number and Type of operations per received vector per turbo equalization iteration	
MMSE equalization without *a priori* input	Computation units	2×2 MIMO SM	4×4 MIMO SM
	Detection vector	$10130Add(1,1) + load(161)$	$111001Add(1,1) + load(450)$
	Equalization coefficients	$4332Add(1,1)$	$14772Add(1,1)$
	Estimated symbol	$5986Add(1,1) + load(64) + store(64)$	$24068Add(1,1) + load(128) + store(128)$

The List Sphere Decoder (LSD) detection algorithm

The LSD equalizer uses channel information Y vector in addition to *a priori* information vector $\hat{X}$ provided by the turbo decoder to compute estimated *a posteriori* vector $\tilde{X}$ and extrinsic vector $\tilde{X}^E$ of the transmitted vector x. After de-interleaving, de-puncturing and turbo decoding, a posteriori information from the turbo decoder is punctured, passed through the BICM interleaver, and fed-back to the equalizer as a priori information $\tilde{x}$.

The LSD algorithm was proposed as a straightforward extension of the sphere decoder. It finds not only the ML solution, but a list of *L* candidates which have the smallest distance from the received vector *Y*. Considering a block of transmitted vector *X*, the a posteriori information $\tilde{x}_q$ of $\tilde{X}$, with $q = MN_t$ (*M*: number of bits per modulated symbol, N_t number of transmit antennas), can be expressed by means of Log Likelihood ratio [HoT03] as:

$$\tilde{x}_q = \log\left(\frac{P[x_q = +1]|Y,H}{P[x_q = -1]|Y,H}\right)$$

$x_q = -1$ and $x_q = +1$ represent respectively the logical zero and the logical one. Using Bayes theorem, the *a posteriori* information $\tilde{x}_q$ can be written as:

$$\tilde{x}_q = \hat{x}_q + \tilde{x}_q^E$$

where $\hat{x}_q$ represents the q^{th} element of the *a priori* information $\hat{X}$, and $\tilde{x}_q^E$ the q^{th} element of the extrinsic information of $\tilde{X}$. By applying the Max-Log approximation, the extrinsic LLRs can be directly computed by the detector as:

$$\tilde{x}_q^E = \frac{1}{2}\max_{x_j \in L_q^{+1}}\left(-\frac{1}{\sigma_x^2}|Y - HS|^2 + X_{[q]}\hat{X}_{[q]}\right) - \frac{1}{2}\max_{x_j \in L_q^{-1}}\left(-\frac{1}{\sigma_x^2}|Y - HS|^2 + X_{[q]}\hat{X}_{[q]}\right)$$

where S denotes modulated symbols, $X_{[q]}$ denotes the subvector of x obtained by omitting q^{th} element x_q, and $\hat{X}_{[q]}$ denotes the vector of all $\hat{X}$ values omitting its $\hat{x}_q$. L_q^{-1} and L_q^{+1} denote respectively the subset of candidates in the whole list with bit $x_q = -1$ and the subset with bit $x_q = +1$. These simplified expressions exhibit three main computation steps [DCB00]:

- Partial Euclidean Distance (PED) computation referred by $-\frac{1}{2\sigma_x^2}|Y - HS|^2$,
- *a priori* adder operation referred by $\frac{1}{2}X_{[q]}\hat{X}_{[q]}$,
- maximum finder operation performed via *max* operations.

For a small number of antennas and a low modulation order, a short list is enough in order to achieve error rate performance not far from brute-force ML. On the contrary, if a short list is applied for a high number of antenna and/or a high modulation order, a problem of divergence [YSZ+04], [JiJ05] with respect to the ML solution is observed. It leads to a large performance penalty even when increasing the number of iterations between the decoder and the MIMO detector. Two methods addressing such a problem can be found in literature. The first method, introduced in [HoT03], consists in using the list obtained at the first iteration for all subsequent iterations. The second method updates the list for every iteration [JoW02]. As shown in \cite{problem_LSD2}, the latter method generates a long list at the first iteration. Then at the following iterations, this list is shortened depending on reliability information. This technique avoids iterative process divergence and achieves further improvements in terms of performance.

In fact, the size of the list is a key parameter having an important impact on latency and memory requirements. Therefore, it can be used to search for a proper trade-off between performance and complexity. The second key element of LSD is the LLR clipping technique [YSZ+04]. When one of the two sets L_q^{+1} and L_q^{-1} is empty, the LLR value for the bit under consideration should be set to a target value. This predefined value has an impact on

performance and convergence. Different choices are proposed in literature. These choices are in majority determined by Monte Carlo simulations such that the average mutual information at the detector output is maximized for the considered system configuration.

In this work, many simulations have been launched to carefully choose these values. Chosen values have shown best BER performance for WiMax and LTE parameters.

A typical fixed-point representation of channel inputs and various metrics is considered. Table 5-6 summarizes the total number of required quantization bits for each parameter of the LSD equalizer [Gam10].

Table 5-6: summary of quantization precision levels for metrics required during LSD detection and equalization.

	Parameter	Number of bits
LSD equalizer	Received complex symbol $y_l=\{y_l^I, y_l^Q\}$ from Y	{12,12}
	Complex Coeff. Fading symbol $h_{q,l}=\{h_{q,l}^I, h_{q,l}^Q\}$ from H	{12,12}
	Estimated complex symbol $\tilde{x}_q=\{\tilde{x}_q^I, \tilde{x}_q^Q\}$ from $\tilde{X}$	{16,16}
	A priori information complex symbol $\hat{x}_q=\{\hat{x}_q^I, \hat{x}_q^Q\}$ from $\hat{X}$	{16,16}

Performance comparisons

Performance comparisons between MMSE and LSD detection and equalization were performed with the LTE turbo code under various conditions. These were chosen to show the impact of the constellation size, the coding rate, the number of antennas and the error correcting power on performance of these two different algorithms.

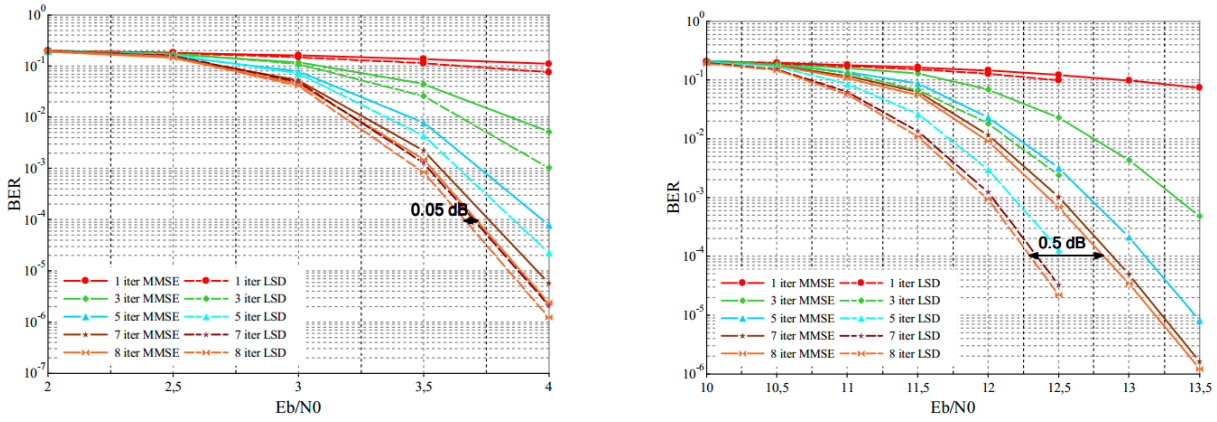

(a) QPSK, $R_c=\frac{1}{2}$, $N_t=4$, $F=1920$ Bits (b) QAM64, $R_c=\frac{1}{2}$, $N_t=4$, $F=1920$ Bits

Figure 5-28: Effect of constellation size (QPSK vs QAM64) on MMSE and LSD performance Comparison.

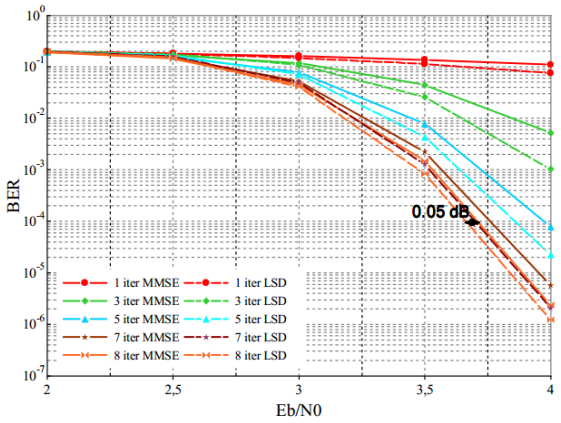

(a) QPSK, $R_c=\frac{1}{2}$, $N_t=4$, $F=1920$ Bits

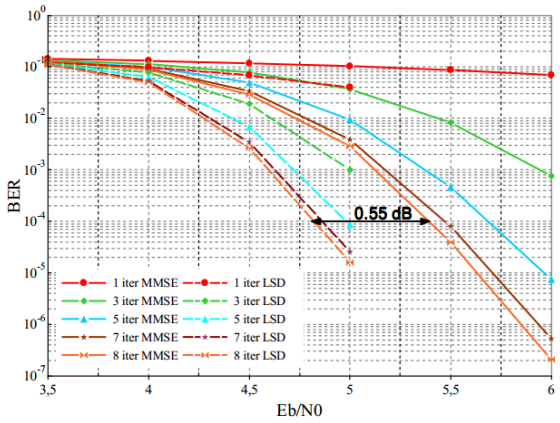

(b) QPSK, $R_c=\frac{2}{3}$, $N_t=4$, $F=1920$ Bits

Figure 5-29: Effect of coding rate (R=1/2 vs R=2/3) on MMSE and LSD performance Comparison.

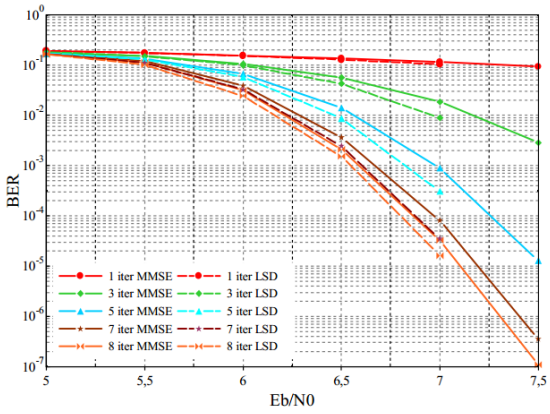

(a) QAM16, $R_c=\frac{1}{2}$, $N_t=2$, $F=1920$ Bits

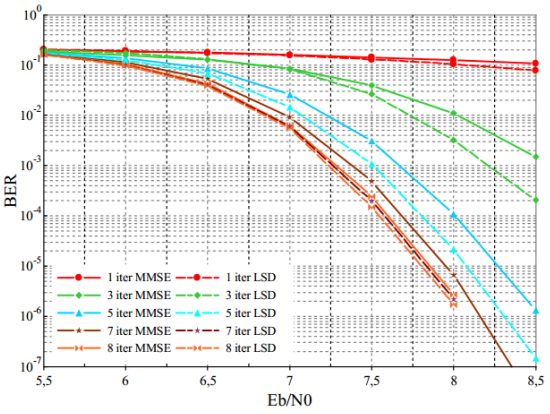

(b) QAM16, $R_c=\frac{1}{2}$, $N_t=4$, $F=1920$ Bits

Figure 5-30: Effect of number of antennas (2x2 vs 4x4) on MMSE and LSD performance Comparison.

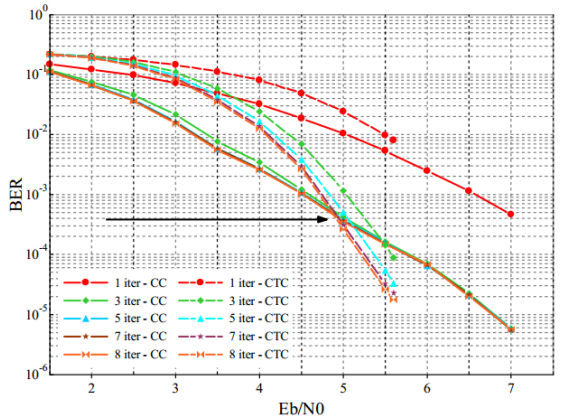

(a) QPSK, $R_c=\frac{1}{2}$, $N_t=4$, $F=30$ Bytes

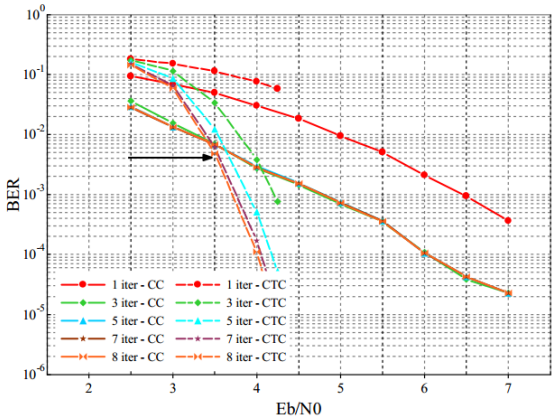

(b) QPSK, $R_c=\frac{1}{2}$, $N_t=4$, $F=120$ Bytes

Figure 5-31: Effect of error correcting power or FEC code type (convolutional vs turbo) and frame size (30 vs 120 Bytes) on MMSE and LSD performance Comparison.

5.10 Advanced transceiver design

5.10.1 Full-Duplex Communications

Almost all the current wireless communications technologies enable bidirectional communications using frequency division duplexing (FDD) or time division duplexing (TDD). This requires allocating orthogonal time (TDD) or spectral (FDD) resources for transmission (Tx) and reception (Rx). Although this mechanism has proved to be extremely successful, it may not be able to cater for the spectral efficiency requirements of future generation wireless communication technologies. Therefore, recently there has been a surge of interest on the systems where Tx and Rx is performed using the same time or spectral resources. These systems are commonly known as full-duplex (FD) systems, while conventional TDD and FDD systems are referred to as half-duplex (HD) systems. An inherent challenge of FD system is the interference on Rx by its own Tx. This is known as self interference (SI). Recent studies [DMK13] have proposed SI cancellation schemes that can achieve 110 dB isolation between the Tx and the Rx. Experimental results of [DDS12] have shown that FD systems are capable of achieving higher spectral efficiencies than HD systems for SI isolation above 74 dB. However, these gains have been observed in point-to-point FD systems with short distance between the nodes. Exploiting this fact, we aim to investigate the applicability of FD technique in device-to-device (D2D) networks, where the communications are generally short range.

Figure 5-32 shows the system sum rate comparisons for each mode as a function of the transmit power of D2D pair. The sum rate in the FD mode decreases with increasing transmit power due to the increase in SI. The ergodic rate of the HD mode remains almost constant and outperforms FD mode for SI cancellations below 75 dB. When the SI cancellation capability increases, the sum rate tends to improve with the increasing transmit power.

Figure 5-33 gives the sum rate performances with the distance between the D2D pair, with Pd = 20 dBm. It is clear that the FD mode outperforms the HD mode when the distance between the D2D pair is shorter. As the distance increases, FD with 80 dB SI cancellation results in lower sum rate than the HD mode. The performance of TWRN does not depend on the distance between the nodes, hence not considered for this comparison.

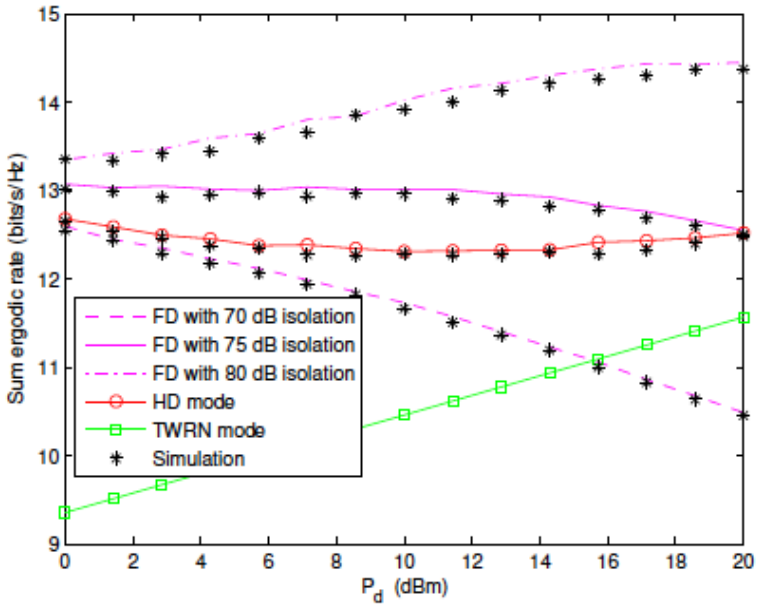

Figure 5-32: The sum ergodic rates of the system as a function of the transmit power of the D2D pair

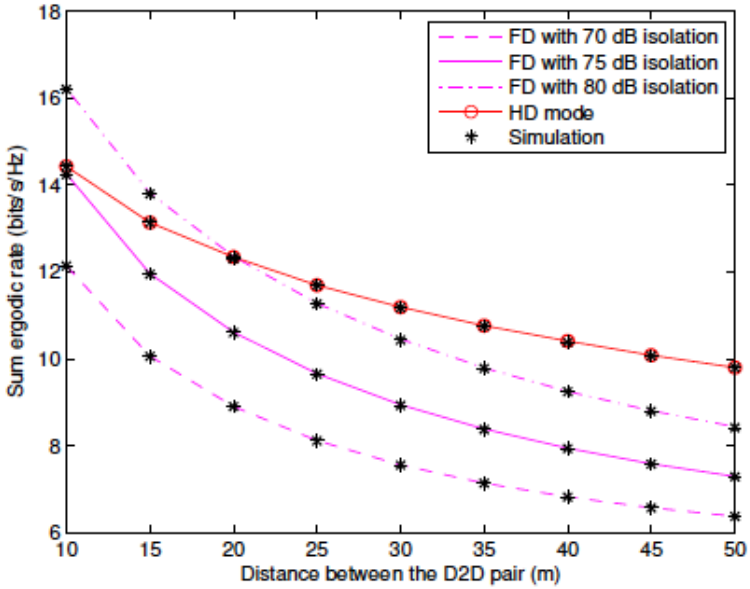

Figure 5-33: The sum ergodic rates of the system as a function of the distance between the D2D pair

5.10.2 Multi-rate Equalizer for Single-Carrier Communications

Numerical Results

In order to empirically observe the rate of convergence of parallel sub-channels to memoryless channels, we gathered empirical data about the root mean square (rms) delay spreads of the parallel channels obtained by decomposing an ISI channel. Figure 5-34 shows the expected value of the rms delay spreads of sub-channels averaged over all sub-channels versus M in a frequency selective Rayleigh fading channel of length 10 and with uniform power delay profile. This result indicates that the residual ISI in the parallel sub-channels converge to zero exponentially fast. We repeated this experiment for various fading scenarios with different power delay profiles. All these experiments yielded very similar results which indicate that this fast convergence behavior is not something specific to the given fading scenario but a general phenomenon.

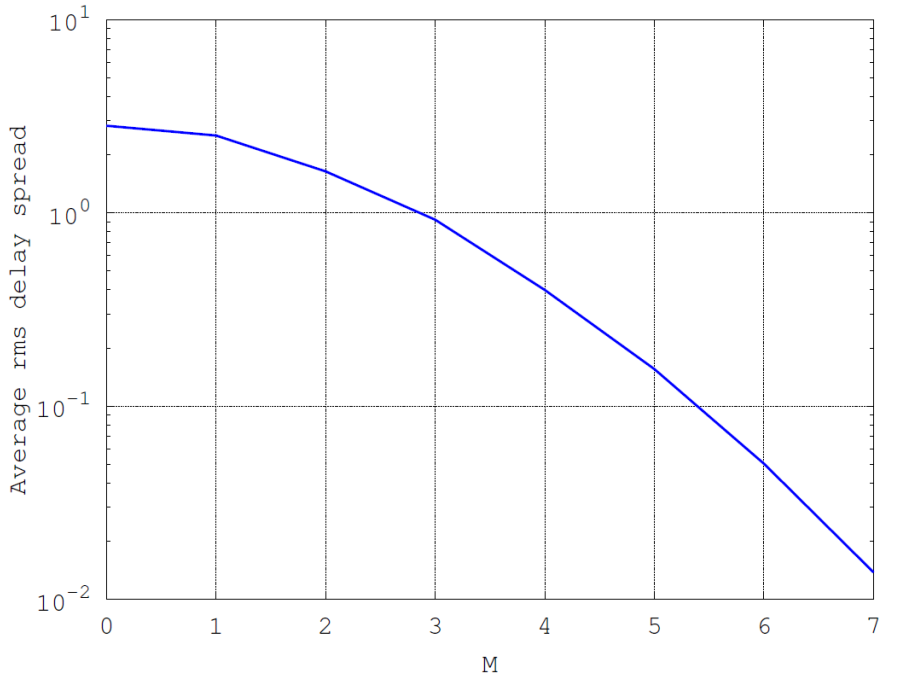

Figure 5-34: The expected value of the rms delay spreads versus M averaged over all sub-channels

The performance of the proposed MRE is numerically evaluated in terms of average reliable throughput. Since it is difficult to evaluate the average throughput using discrete input alphabets, we assumed that transmitted symbols are chosen from a continuous input alphabet which basically means that the input symbols are normal distributed complex variables.

Firstly, we compare the achievable rate to the limit, i.i.d. capacity, in a Rayleigh fading scenario of length 10 with uniform power delay profile. Figure 5-35 shows the ergodic achievable rate of MRE and the ergodic i.i.d. capacity of the channel at different SNR values. First of all, it can be observed that the throughput of the proposed transmission can get very close to the ergodic i.i.d. capacity of the channel. Note that achieving i.i.d. capacity requires using channel codes designed for a given channel impulse response, which is practically impossible for wireless communications, and at the receiver side decoder must work iteratively with a BCJR equalizer [KMM03]. On the other hand, the proposed MRE is capable of getting very close the i.i.d. capacity by using codes designed for AWGN channel and just using some linear signal processing blocks. Furthermore, it detects the whole transmission in a single pass. This is a very important property of the MRE.

Another observation that can be made from Figure 5-35 is that the throughput of the system increases with increasing M but saturates after $M = 4$. This indicates that in order to achieve the above mentioned throughput, it is sufficient to decompose the original channel to just 16 parallel sub-channels for this fading scenario. We repeated this simulation for many other fading scenarios and observed very similar results. In every scenario, throughput improves with increasing M and saturates after $M = \lceil \log_2 L \rceil$ where L is the channel memory and this asymptotic throughput always gets quite close to the i.i.d. capacity.

Secondly, we compare the achievable throughput of the proposed transmission system to that of the DFE. Since it is difficult to evaluate the throughput of the DFE while taking error propagation in to account, we assumed the feedback filter of the DFE is fed by correct decisions. In other words, we compared the throughput of MRE to that of the so called genie aided DFE. The throughput of an actual DFE would be significantly lower. The results for the same fading scenario mentioned above are shown in Figure 5-36. It can be observed that the

proposed transmission system can achieve slightly higher rates than a genie aided DFE which is a quite important achievement for a practical transmission scheme.

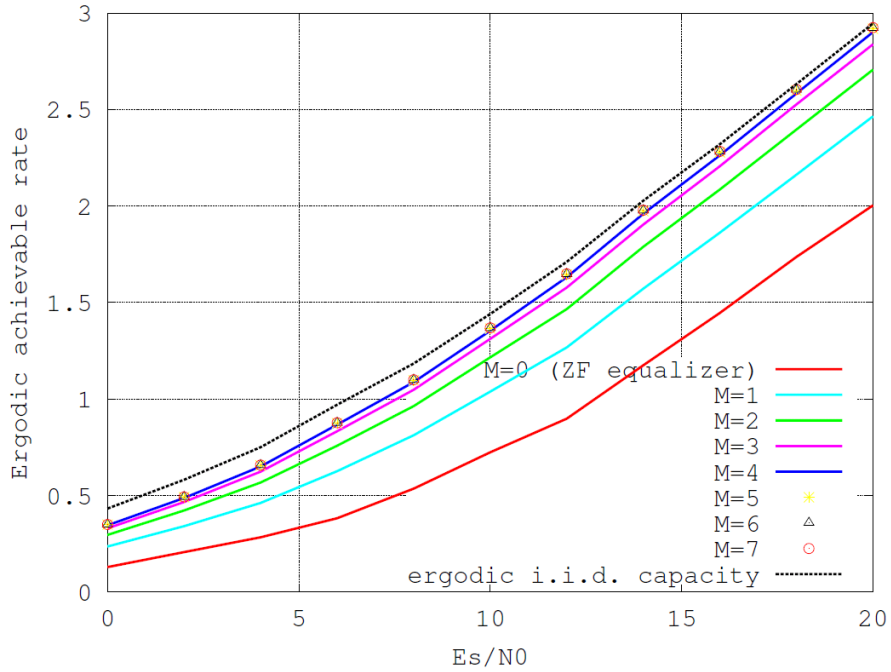

Figure 5-35: Ergodic achievable rates of MRE for different M compared to the i.i.d. capacity of the channel

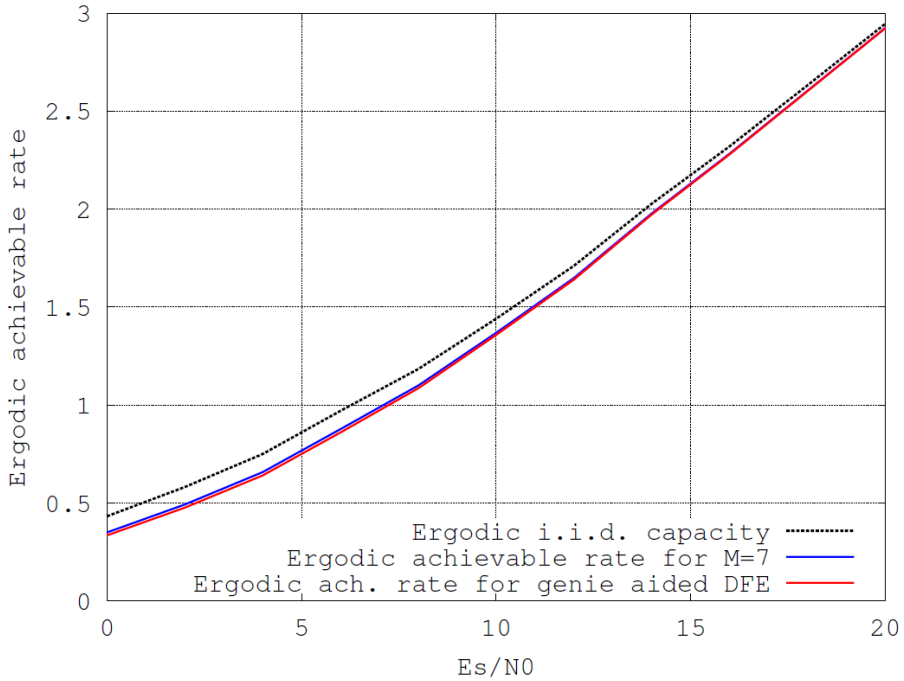

Figure 5-36: Ergodic achievable rate of MRE for M=7 compared to the ergodic achievable rate for genie aided DFE

5.11 Multiple Access

5.11.1 Non- and quasi-orthogonal multiple access allowing spectrum overload

UL SCMA Random Access

To evaluate UL random access, 200 users are randomly dropped in each cell of a 57-cell network layout. In each cell, every OFDMA user can randomly select one out of 4 available RBs in each TTI, while every SCMA user randomly selects one out of 6 available SCMA codebooks. SCMA codewords are distributed over 4 RBs shared among SCMA users. RB or codebook collision is the nature of these contention based access modes. In OFDMA case, two or even more UE might collide over the same randomly selected RB. For the SCMA case, users always share the same RBs but they are separated in the codebooks domain. Two or more users may select the same codebook for transmission but the SCMA multiuser detector relies on the channel variation across the users to extract the original data streams of the SCMA multiplexed users even if some users use exactly the same codebook set.

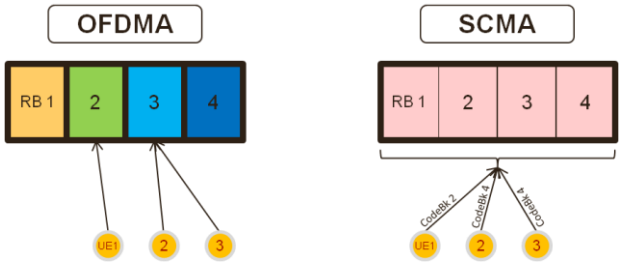

Figure 5-37. Resource allocation for SCMA and OFDMA

Further details of the simulation parameters are listed in Table 5-7.

Table 5-7 Simulation parameters

Parameter	Setting
Network layout	57 cells with centre cell as desired hot cell
ISD	500 m
Channel	Flat Rayleigh fading
Antenna configuration	SIMO 1x2, uncorrelated antennas
Modulation and coding	Fixed, QPSK ½ per layer, or 4-point SCMA codebooks with code rate ½
Channel Estimation	Perfect
Resources	4 RBs and 6 codebooks with spreading factor 4
System traffic load	200 users per cell with varying inter-arrival times per user (below)
Traffic pattern	Poisson arrival with varying mean IATs
Power control	□ = 1.0 (full PL compensation), P_0 = -95 dBm
Detection	ML multi-user detection
HARQ	Disable
ARQ	Enable
ACK feedback time	T_{ack} = 2 ms
ARQ backoff time	A uniform random number between 0 and T_{ack}

5.12 Medium Access Control

5.12.1 Contention based massive access

Coded Random Access:

In [SP13a] it was shown that a simple criterion for contention termination based on the monitoring of the fraction of resolved users F_R and instantaneous throughput T_I, coupled with an optimized slot access probability p_a, yields expected throughput T that is the highest in the reported literature for low to moderate number of contending users, i.e., when the number of users N is in the range 50 – 1000. In Table 5-8 is shown a sample of the obtained results.

Table 5-8 Coded random access results

N	50	100	500	1000
T	0.82	0.84	0.87	0.88
p_a	$\frac{2.68}{N}$	$\frac{2.83}{N}$	$\frac{2.99}{N}$	$\frac{3.03}{N}$
Threshold on F_R	0.83	0.87	0.88	0.89
Threshold on T_I	1	1	1	1

Further discussion on the obtained results as well as detailed analysis of the considered scenarios is found in [SP13a] and [SP13b].

Coded Access Reservation:

Discussion on the baseline and Random Coded Access Mode is available in [PTS+12, TPS+13b]. The research on defining the load operating ranges and code length for a given population size, so to formalize an Adaptive Switching Mode (ASM) is currently underway.

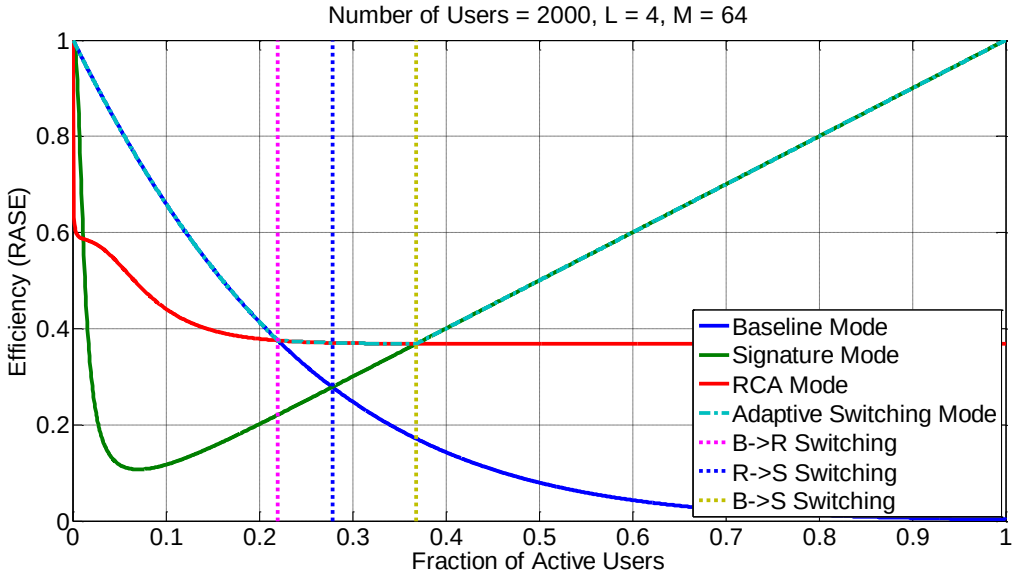

Figure 5-38 - Different modes available with Adaptive Coded Reservation and respective switching points, when the population size is 2000 users.

Initial results show that the ASM does not always requires access to the three modes, as example compare Figure 5-38 and Figure 5-39. While in the case depicted in Figure 5-38 the ASM includes the three modes, in the case depicted in Figure 5-39 only the baseline and signature mode are considered.

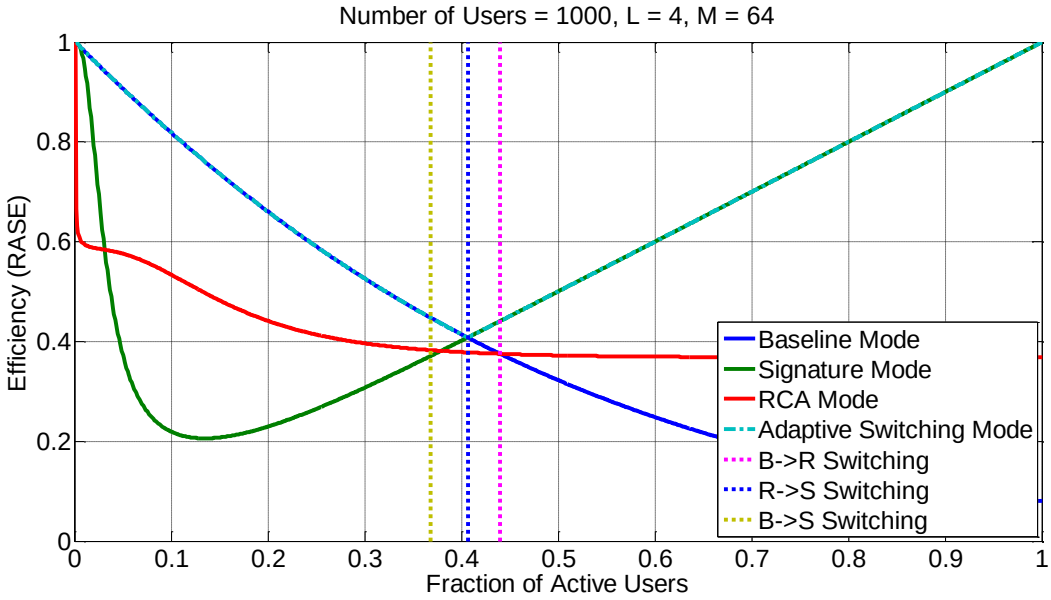

Figure 5-39 - Different modes available with Adaptive Coded Reservation and respective switching points, when the population size is 1000 users.

Advanced physical layer processing for enhanced MAC:

Joint detection of node activity and data

Current systems like LTE have been designed for large data rates and a limited number of connected devices, which is contrary to the envisioned requirements of MMC. To keep the massive number of nodes with small payloads manageable, the signalling overhead required to communicate with those nodes has to be kept as low as possible. Furthermore, most MMC devices are expected to be only sporadically active, which leads to a communication setup, where a large number of devices are associated with a base station, but only a fraction is actually transmitting data at a given time. In order to identify these active nodes without further signalling, and to jointly estimate the transmitted payload, novel detection schemes at the base station are required. To this end, the recently emerging compressive sensing (CS) theory provides theoretical bounds and algorithms applicable to the joint activity and data detection problem arising in MMC scenarios.

In a communications context CS methods have to be evaluated and adapted in terms of

- error rate behaviour,
- incorporation of channel coding,
- channel estimation and synchronization,

which will be the focus of the results section below.

Machine Type Communication Setup

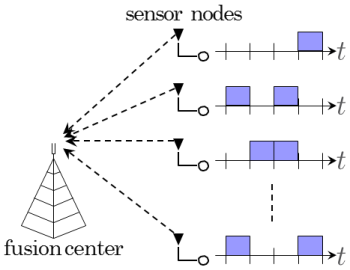

Figure 5-40: Machine Type Communication setup with fusion center.

The basic machine type communication setup that is assumed here is illustrated in Figure 5-40. Several sensor nodes transmit their data to a central aggregation node, whenever a transmission is required, e.g. event-driven or periodically. Due to the sporadic nature of this communication, only a subset of all nodes is active at any given time, as indicated by the time scales for each node. Furthermore, message sizes are expected to be very small, which necessitates very low control overheads for efficient communication. Here, the goal is to reduce or avoid the control signalling required for the initiation of the sensor node communication, such that each sensor can just transmit its payload data even after long periods of inactivity without additional call setup.

The described setup can be summarized in an abstract input-output relationship as

$$\boldsymbol{y} = \boldsymbol{A}\boldsymbol{x} + \boldsymbol{n}$$

The transmit vector $\boldsymbol{x} \in \mathbb{C}^{KL}$ encompasses the signals of all K nodes. Active nodes transmit messages of L symbols from a modulation alphabet $\mathcal{A}$, inactive nodes are modelled as transmitting L zeros. In general, a service dependent traffic model determines the activity behaviour of the nodes. Due to the expected sporadic nature of the communication, the stacked vector of all nodes $\boldsymbol{x}$ is block-sparse. Moreover, the system matrix $\boldsymbol{A} \in \mathbb{C}^{M \times KL}$ summarizes all influences on the transmitted symbols, e.g. the channel and the multiple access scheme, whereas $\boldsymbol{n} \in \mathbb{C}^{M}$ summarizes the noise as AWGN. Depending on the number of observations M, the detection problem may be under-determined, i.e. $M < KL$, which is usually the case when efficient resource exploitation is targeted.

A specific example of this general model is a CDMA system, which will be used to demonstrate results. Here, the system equation describes the chip-rate model with $M = NL + L_h - 1$, where N denotes the length of the PN spreading sequences and L_h is the number of taps for a frequency selective channel with exponential decaying power. Thus, the detection problem is under-determined, if the spreading sequence length is smaller than the number of users $N < K$ (overloaded CDMA system). A simplified activity model is chosen, determining active users randomly with a probability of p_a.

The goal is to reconstruct $\boldsymbol{x}$, i.e. the symbols of active nodes as well as the zero entries describing inactive nodes, from the observations $\boldsymbol{y}$, given the system matrix $\boldsymbol{A}$ (perfect CSI) and the activity probability p_a. Two approaches have been investigated in this context: activity error event control through Bayes Risk detection and low complexity Greedy CS algorithms with channel coding. Furthermore, an extension of Greedy algorithms to asynchronous communication and channel estimation has been investigated.

Control of error rate behaviour by Bayes-Risk detection

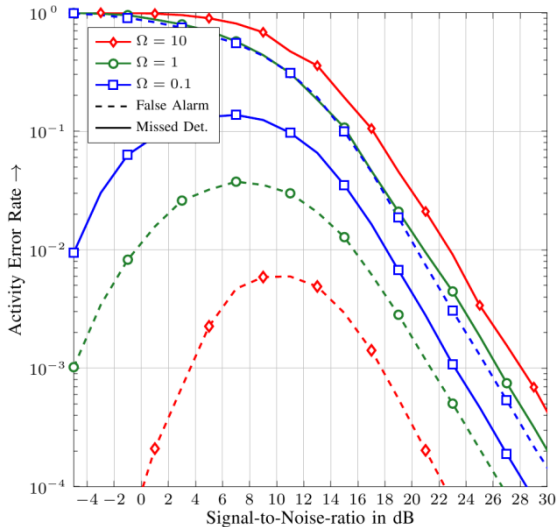

Figure 5-41: Activity Error Rates for Bayes Risk Minimization.

In typical compressive sensing applications, the activity estimation errors (false alarms / missed detections) that occur are of symmetric importance: either error is equally bad. However, in communication systems false alarms and missed detections are of asymmetric importance. A missed detection of an active node is fundamentally worse than a false alarm of an inactive node, which may be corrected at higher layers. Thus, an extension of optimal MAP detection to Bayes risk minimization has been developed in [MBW13] as an approach to control the impact of activity errors in a system context by an additional cost term defined through an activity control variable Ω. Figure 5-41 shows the performance curves for an under-determined CDMA system with variable Ω involving $K = 20$ nodes. The nodes transmit their data over an frequency selective Rayleigh fading channel with 3 taps and with an activity probability of $p_a = 0.2$. As can be clearly seen, the detection performance in terms of missed detections and false alarms can be controlled by proper choice of Ω to fit the PHY performance to system needs, where $\Omega = 1$ is the MAP detector performance.

The main results of this work are:

- Even highly under-determined detection problems can still be solved efficiently for sporadic communication. Consequently, resources can be used very efficiently even for a large number of nodes, i.e. in terms of CDMA the spreading factor may be much lower than the number of nodes
- The detection performance in terms of the trade-off between missed detections and false alarms can be tuned to any behaviour. Essentially, this allows a trade-off between the packet error rate (PER) at the MAC layer and the added computational complexity of sorting out garbage data.

Exploitation of channel coding towards genie-aided performance

The application of greedy algorithms to communication systems has been shown in a CDMA context [SD11] and further extended to channel coded systems in [BSD13]. The performance of these methods, however, still incurs a substantial loss compared to the genie case of known activity, i.e. in scheduled access.

In communication systems, FEC is usually employed to enhance the bit and frame error rates.

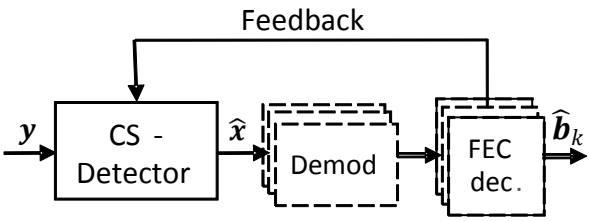

Figure 5-42: Iterative Feedback from FEC to CS-MUD

This provides additional structure that can be exploited to additionally enhance the performance of the activity detection. To facilitate the exploitation of side information about the activity of nodes, greedy algorithms need to be modified in such a way, that the activity decision is weighted by a node-dependent factor to favour activity (high value) or inactivity (low value). Thus, a weighted Group-Orthogonal Matching Pursuit (wGOMP) [SBD13a] has been developed to exploit knowledge about the coding structure of node message in an iterative feedback process to enhance the activity detection. To this end, reliability information about the activity of nodes has to be extracted from the coding structure to be fed back to the wGOMP in terms of weights as indicated by Figure 5-42.

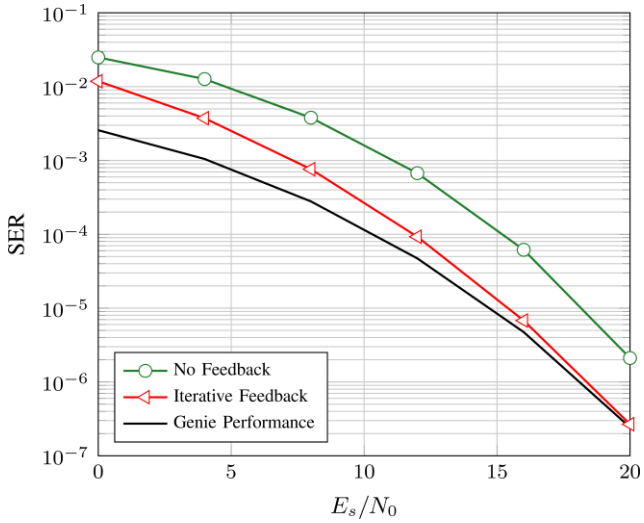

Figure 5-43: Symbol Error Rate (SER) performance of the iterative joint activity and data detection for an exemplary CDMA system.

Figure 5-43 depicts results for an exemplary CDMA system with $K = 128$ nodes and a spreading factor of $N = 32$ (i.e. 4 times overloaded) communicating over a frequency selective Rayleigh fading channel with $L_h = 6$ taps. The nodes are sporadically active with a probability of $p_a = 0.02$. These results clearly show that the wGOMP with iterative feedback asymtotically achieves the same performance as a genie aided detection that knows the active nodes as for example in scheduled access.

The main results of this work are:

- Greedy algorithms are a low complexity solution for joint detection of activity and data in a sporadic MMC setup.
- Exploitation of all available side information (frame activity, FEC, etc.) allows asymptotic performance near the boundary of perfectly known node activity.

Extension to asynchronous communication and channel estimation

Asynchronous communication can be easily introduced by adding delay hypotheses up to a maximum assumed delay τ_{hyp} to the synchronous model. To exploit this asynchronous detection model the GOMP has to be modified by a restriction of the eligible group indices to one active delay hypotheses per node. Once any delay hypothesis has been estimated as active, all other hypotheses belonging to the same node have to be deleted from the eligible set. With this simple modification the restricted GOMP (rGOMP) solves the activity and delay estimation problem for the asynchronous case [SBD13b].

Similarly the joint data and activity detection can be modified towards a joint channel and activity estimation facilitated by inserting a pilot frame separate from the data , which allows to nearly achieve perfect CSI. Figure 5-44 illustrates the impact of the pilot frame length F_P in the context of an exemplary system with spreading and a data frame of length $F = 512$ chips. The SNR loss incurred by the separate pilot frame is included in the E_S/N_0 to achieve a fair comparison. The best compromise is achieved at $F_P = 128$, which is an overhead of 1/4th of the data frame length. Depending on the working point even lower overheads may be possible [SBD13c].

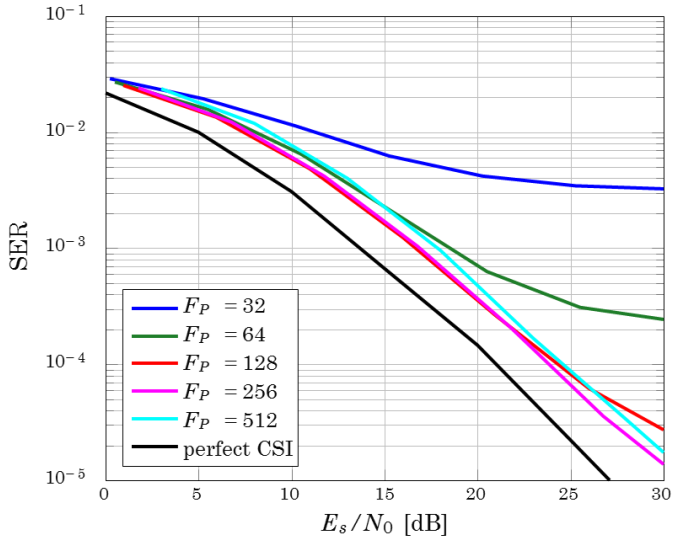

Figure 5-44: Influence of the pilot frame length F_P on the channel estimation quality.

The main results of these works are:

- Asynchronous communication can be solved by compressive sensing based joint activity and data detection without additional signalling requirements. Basically, synchronization is not required and can be considered by the signal processing at the base station.
- Pilot-aided joint channel estimation and activity detection followed by standard data detection schemes is able to achieve error rate performances near perfect CSI with an additional overhead in the order of ¼ of the data sequence length.

5.12.2 Distributed network synchronization

Each node in the network is equipped with a physical clock that has its frequency and offset. The physical clock of node i is $T_i(t) = f_i t + \theta_i$, where t is the perfect time, f_i indicate the physical clock frequency, and θ_i denotes the physical clock offset. Note that f_i and θ_i are both determined by the physical clock and cannot be measured or adjusted. Besides, each node i also maintains a logical clock, whose value is denoted by $C_i(t)$ and can be modified. The

logical clock $C_i(t)$ represents the synchronized time of node i, which is c function of the current physical clock value $T_i(t)$. Here we use an affine model for $C_i(t)$: $C_i(t) = a_i T_i(t) + b_i = \hat{f}_i t + \hat{\theta}_i$, where a_i and b_i are control parameters, and $\hat{f}_i = a_i f_i$ and $\hat{\theta}_i = a_i \theta_i + b_i$ represent the logical clock frequency and logical clock offset. In this way, the goal is to synchronize the clocks in the entire network such that the logical clocks of different have the same (or very close) values for any instant of perfect time t.

In this work, rather than synchronizing all clocks to a real reference clock, we aim at attaining an internal consensus between logical clocks through local interactions between nodes. Namely, we say that is achieved if the following two consensus equations are satisfied: $\lim_{t\to\inf} \hat{f}_i = f_v$ and $\lim_{t\to\inf} \hat{\theta}_i = \theta_v$, where f_v and θ_v, the frequency and offset of some virtual clock. In fact, the values of f_v and θ_v are not important, since what really matters is that all clocks converge to one common value.

We propose a novel Random Broadcast based Distributed consensus clock Synchronization (RBDS) scheme, which is fully distributed in the sense that all the nodes independently execute the same algorithm without the need of a network hierarchy, and is thus robust to node failures and changing topologies. In the proposed RBDS scheme, the logical clock is adjusted by partial updates or complete updates to achieve the consensus. More specifically, the control parameters a_i and b_i are updated by the received timing messages and different update rules, which will then adjust f_i and θ_i jointly automatically. By distinguishing partial update and complete update for different situations, both convergence and error decrease speed are taken into account in the RBDS scheme.

In the RBDS scheme, at time t_l, assume node i receives the timing message : $C_{j(l)}(t_l)$ from node $j(l)$. Then the conditions and operations of the two updates are as follows.

1) Partial update rule.

It is clear that node i can not make any meaningful update of a_i before receiving at least two timing messages from the same node, since $\hat{f}_i$ basically represents the slope of the linear logical clock model. Therefore node i will only update the contral perameter b_i as

$$b_i^+ = b_i + (C_{j(l)}(t_l) - C_i(t_l))/2.$$

Also node i will define a parameter $\Delta_i^l = (C_{j(l)}(t_l) - C_i(t_l))/2$, which captures the logical clock adjustment of node i.

2) Complete update rule

Suppose node i receives the timing message : $C_{j(l)}(t_l)$ from node $j(l)$ at time t_l. Furthermore, suppose the last time node i received a timing message from node $j(l)$ was t_n. Hence, $t_n < t_l$ and $j = j(l) = j(n)$. Then, node i will perform a complete update if the following two conditions are satisfied.

a) Node j has not performed a partial or complete update in the interval $(t_n, t_l]$.
b) Node i has not performed a complete update in the interval $(t_n, t_l]$.

The complete update rule is

$$a_i^+ = \frac{1}{2} a_i^+ (1 + \frac{\hat{f}_j}{\hat{f}_i^{(l)}})$$

$$b_i^+ = \frac{1}{2}(C_j(t_l) - \frac{\hat{f}_j}{\hat{f}_i^{(l)}} C_i(t_l)) + \frac{1}{2}(1 + \frac{\hat{f}_j}{\hat{f}_i^{(l)}}) b_i$$

where

$$\frac{\hat{f}_j}{\hat{f}_i^{(l)}} = \frac{C_j(t_l) - C_j(t_n)}{C_i(t_l) - \sum_{m=n}^{l-1} \Delta_i^m - C_i(t_n)}$$

In the absence of transmission delays, the convergence of the RBDS scheme can be theoretically proved. Moreover, by utilizing a threshold for clock update, i.e., the partial or complete update is implemented only when $|C_{j(l)}(t_l) - C_i(t_l)|$ is larger than the threshold value, the RBDS scheme reveals robustness even when transmission delays are present.

For performance evaluation, we simulate the 90th percentile of synchronization errors versus time evolution, where the number of nodes is 50. The following four synchronization schemes are compared.

1) Average TimeSynch (ATS) in [SF+11], which synchronizes the clock offset and frequency separately but not jointly .
2) Modified Automatic Selftime-correcting Procedure (MASP) in [PTM+10], which follows the converge-to-max principle.
3) Consensus based clock Synchronization (CoSyn) in [SGS+13], which uses different conditions for partial updates and complete updates.

The results are shown in Figure 5.45 for the scenario without delay and in Figure 5.46 when the mean value of delays is 3 microseconds.

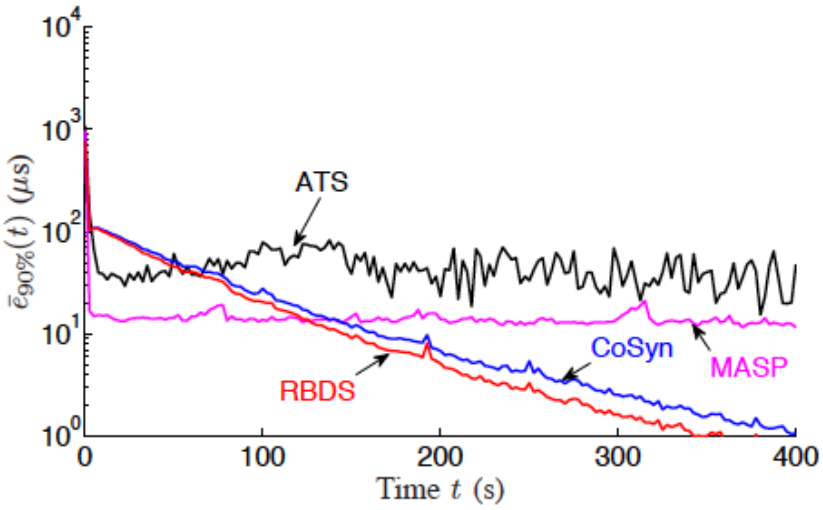

Figure 5.45: 90th percentile of synchronization errors versus time evolution when there is no transmission delay.

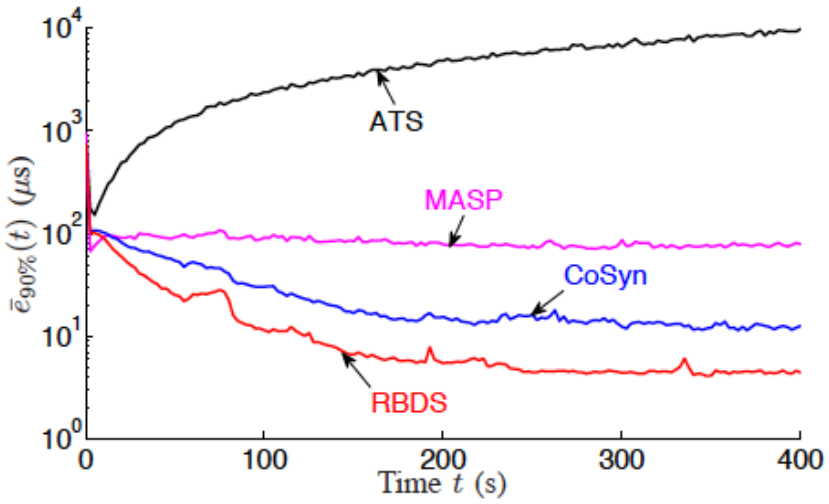

Figure 5.46: 90th percentile of synchronization errors versus time evolution when the mean value of transmission delays is 3 microseconds.

From the simulation results, in the absence of delay (Figure 5.45), even though ATS and MASP exhibit less synchronization errors in the first 140s, there are floor effects for both of them. These are because of the problem of over-adjusted logical frequencies in ATS, as well as the contradiction between the fastest node asynchronism and the time partitioning in MASP. On the other hand, CoSyn and RBDS present similar trends regarding the decrease of synchronization errors. Nevertheless, RBDS shows faster convergence due to its increased opportunities of complete updates. Furthermore, the effects of delays are considered in Figure 5.46. It is depicted that the error of ATS is boosted with time, which implies that ATS becomes ineffective under the scenario with delays. Also, the error decrease is very small in MASP. When it comes to CoSyn and RBDS, they both show robustness against delays, where RBDS outperforms CoSyn.

5.12.3 MAC for UDN and mmW

A scheduled MAC approach for UDN in mmW frequencies is under evaluation. The MAC approach uses template-frame assignment for each link with an optional mode/feature which uses template-frame assignment to clusters of nodes with contention based access inside the cluster. The details and results of the scheduled approach will be shown below. The optional mode/feature with template-frame in cluster level and contention based approach inside the cluster is still under study.

The scheduled MAC and it's relation to other protocol layers are shown in Figure 5-47 below. As mentioned in chapter 2.12.3, the spectrum controller operating is slowest (>1000 x12.5µs) and determines resources a UDN may use (the left block). The UDN Resource Coordination functionality determines communication routes for wireless self-backhaul and performs resource assignment in form of template-frame for each link (the middle block) with green-OK to use, yellow-shared resource, and red-prohibited resource (type 1 of red: not allowed to use; type 2 of red: allocated to other links which may turn yellow). The MAC in a node plans and schedules the transmission in a shared (yellow) resource (if no green UL resources are available).

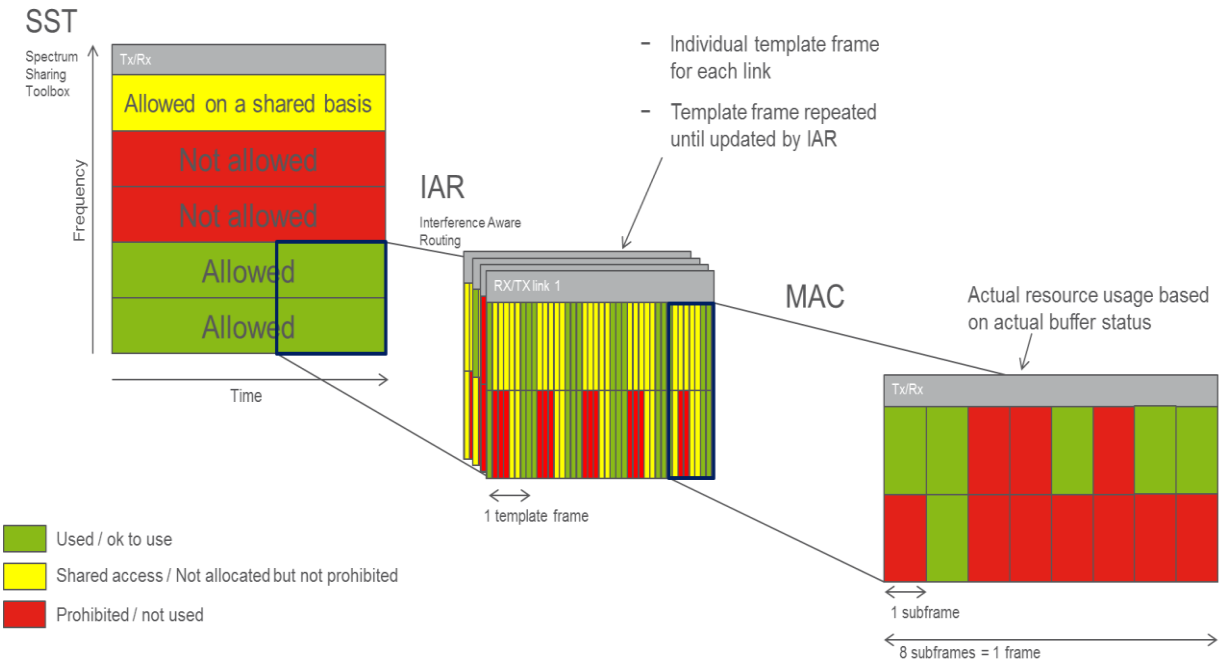

Figure 5-47: Scheduled MAC with template-frame assignment for each link

When the MAC layer in a node intends to access a shared resource it has to announce the intent to the other nodes. This announcement is done via flooding using the regular high capacity data channels to the other nodes in the UDN as shown in Figure 5-48.

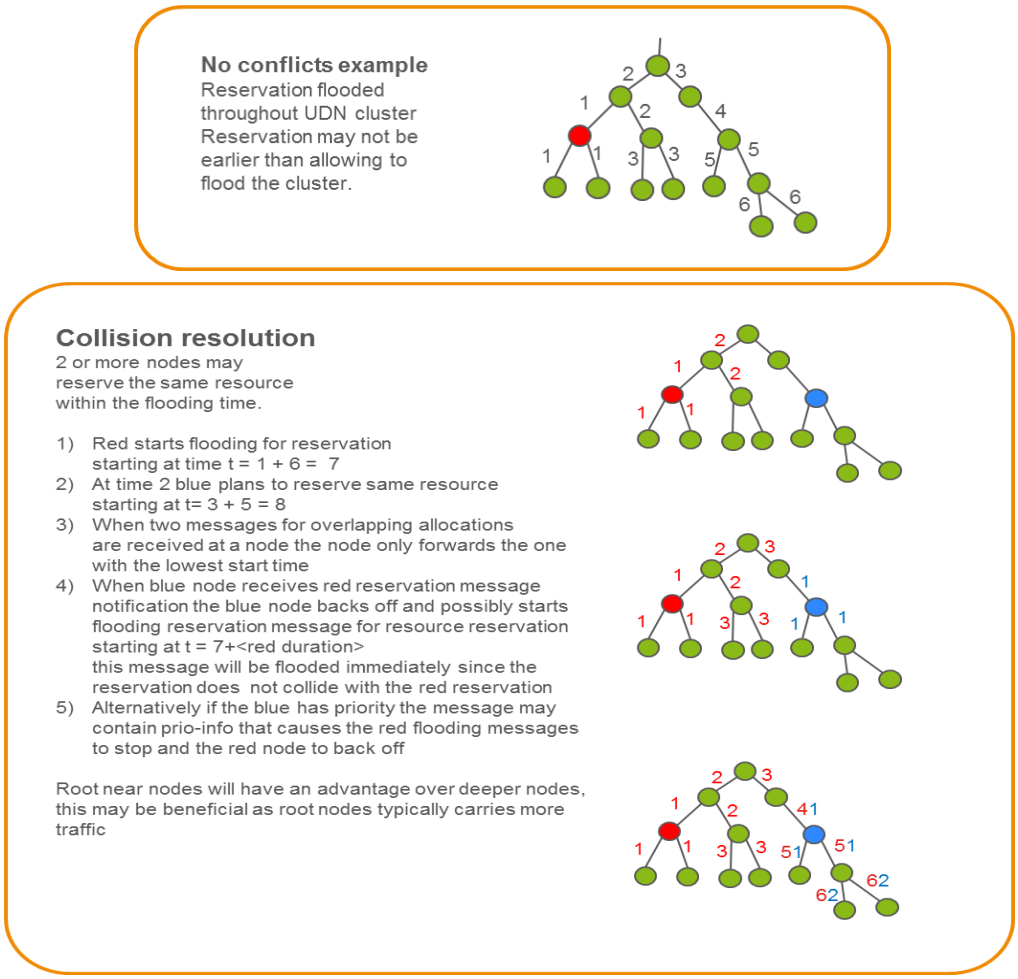

Figure 5-48: Resource reservation flooding

A performance comparison of opportunistic scheduling using any non-prohibited resource versus fixed scheduling for which only the allocated resources is shown in Figure 5-49. The floor plan consists of one corridor with 3 rooms at each side. There are in total ten access nodes, one access node in each room and four in the corridor. Three routing cases are simulated, with all 10 access nodes connected to the fixed backhaul (i.e. N AgN is 10), and with only 1 or 2 access node(s) connected to the fixed backhaul (i.e. N AgN is 1 or 2). The simulation uses bandwidth of 184.32 MHz on 60 GHz frequency with max Tx power of 2 mW and 7 antenna elements in each access node; max Tx power of 1 mW and 2 antenna elements in each UE. The results show substantial gains in total system throughput with the proposed approach (dashed curves) over the fixed scheduling approach (solid curves) for all three cases.

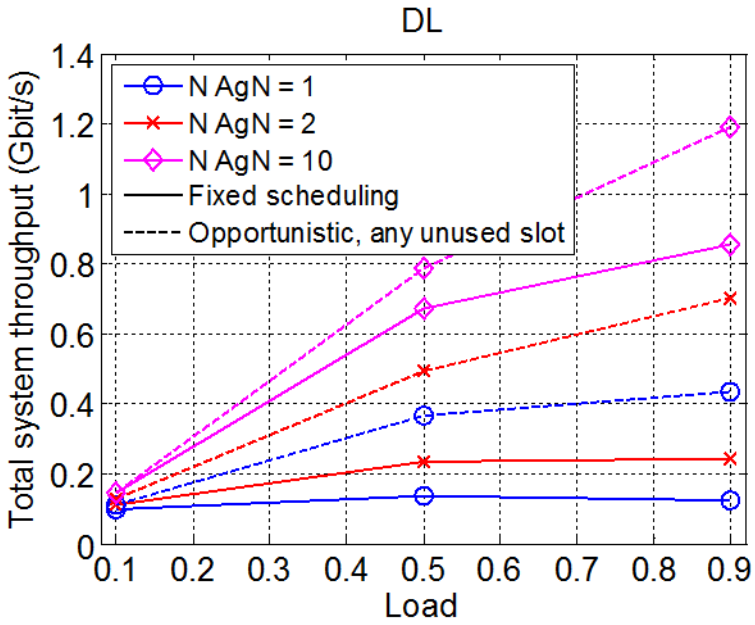

Figure 5-49: Performance comparison, opportunistic scheduling vs. fixed scheduling

5.13 Hybrid Automatic Repeat Request (HARQ)

Further details on Incremental Redundancy with Backtrack Retransmission can be found in [Pop14], and further details on reliability-based HARQ with 2bit ACK/NACK for the reliability feedback can be found in [WWD+14].

5.14 Radio link enablers for Radio Resource Management (RRM)

Figure 5-50 shows the system performance of above introduced signalling schemes. A standard Macro scenario defined in [TR36.814] is used here to set up simulation assumption. And in the case where partial CSI are presented in BS, RRM algorithm neglects the interference level for D2D links. As we can see from this figure, due to lack of interference information, a relative small performance deterioration gap occurs in between the RRM scheme with partial awareness of CSI and the one with full awareness of CSI. We also show the performance where there is no CSI at all. In this case, BS randomly selects one cellular user and one D2D link and assigns them the same resource block. As a conclusion drawn from this performance comparison, signalling scheme with partial CSI has a good performance compared with the case where no CSI is available, meanwhile its performance deterioration compared with optimal case is small.

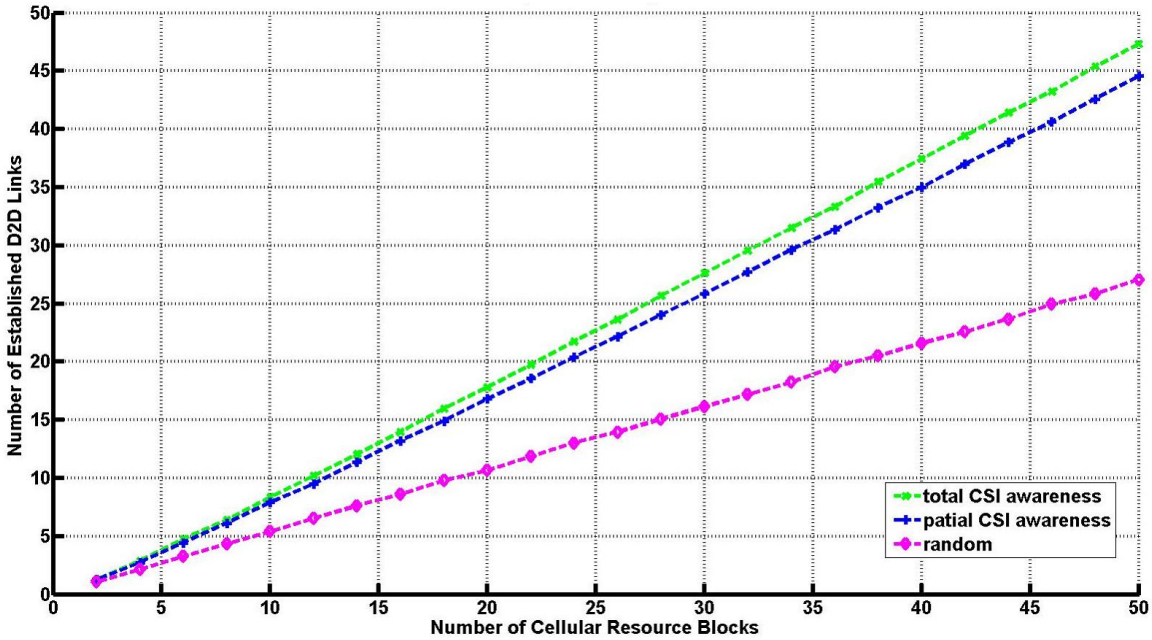

Figure 5-50: Performance comparison among different schemes